



Olena Artiushenko

Silica-based Adsorbents with Immobilized Derivatives of Phosphonic, Hydroxamic and Pyridinecarboxylic Acids for Dispersive Solid Phase Extraction and Separation of Rare Earth Elements

Tese de Doutorado

Thesis presented to the Programa de Pós-graduação em Química of PUC-Rio in partial fulfillment of the requirements for the degree of Doutor em Química.

Advisor: Prof. Volodymyr Zaitsev

Rio de Janeiro
Novembro de 2019



Olena Artiushenko

Silica-based Adsorbents with Immobilized Derivatives of Phosphonic, Hydroxamic and Pyridinecarboxylic Acids for Dispersive Solid Phase Extraction and Separation of Rare Earth Elements

Thesis presented to the Programa de Pós-graduação em Química of PUC-Rio in partial fulfillment of the requirements for the degree of Doutor em Química. Approved by the Examination Committee.

Prof. Volodymyr Zaitsev

Advisor

Departamento de Química – PUC-Rio

Prof. Ricardo Erthal Santelli

Universidade Federal do Rio de Janeiro (UFRJ)

Prof.^a Christiane Béatrice Duyck Pinto

Universidade Federal Fluminense (UFF)

Prof. Jefferson Rodrigues de Souza

Universidade Federal do Espírito Santo (UFES)

Prof.^a Tatiana Dillenburg Saint Pierre

Departamento de Química – PUC-Rio

All rights reserved.

Olena Artiushenko

Graduated in Chemistry at Taras Shevchenko National University of Kyiv in 2011 and obtained her M.Sc. Degree in Analytical Chemistry from Taras Shevchenko National University of Kyiv in 2012.

Bibliographic data

Artiushenko, Olena

Silica-based adsorbents with immobilized derivatives of phosphonic, hydroxamic and pyridinecarboxylic acids for dispersive solid phase extraction and separation of rare earth elements / Olena Artiushenko ; advisor: Volodymyr Zaitsev. – 2019. 138 f. : il. color. ; 30 cm

Tese (doutorado)–Pontifícia Universidade Católica do Rio de Janeiro, Departamento de Química, 2019.
Inclui bibliografia

1. Química – Teses. 2. Adsorventes à base de sílica gel. 3. Extração em fase sólida. 4. Separação. 5. Elementos terras raras. I. Zaitsev, Volodymyr. II. Pontifícia Universidade Católica do Rio de Janeiro. Departamento de Química. III. Título.

CDD: 540

“My only advice is to stay aware, listen
carefully, and yet for help if you need it”.

Judy Blume

Acknowledgments

To my research advisor Prof. Volodymyr Zaitsev, for his endless patience and inspiration and for all the skills he has cultivated in me. I could not have imagined better advisor for my Ph.D. research. With his excellent guidance and continuous support, immense knowledge and perceptiveness I reached this point.

To my parents for showing me the right path and supporting me unconditionally on it.

To Dr. Tatiana Kovalchuk, my lovely and best professor ever at Taras Shevchenko National University of Kyiv. You were the first who believed in me and made me love Chemistry.

To Prof. Tatiana Dillenburg Saint´Pierre, Prof. Jiang Kai and Prof. Renato da Silva Carreira, who gave me access to their laboratories and research facilities. Without provided materials and equipment it would not be possible to conduct this research.

To Prof. Nicolás A. Rey and Prof. Ricardo Queiroz Aucélio and their laboratories staff for FT-IR, CHN and TGA analysis.

To Mauricio for spending endless hours with me doing ICP OES analysis, Álvaro and Bia for their help with advice, reagents, glassware, and equipment.

To Wendy and Gabriel for giving me fresh ideas and assistance on their realization.

To Mikhail Nazarkovsky for always being ready quickly analyze my samples, whether SEM in Rio or XPS in Rio Grande do Sul.

To the staff of the Chemistry Department of PUC-Rio that I haven't mentioned personally, professors, secretaries, technicians, co-workers, students, and labmates. Thank you all for your open hearts, help, and acceptance.

To all my Russian and Brazilian friends. Katia, Alena, Lera, Dasha, Lucas and others, you are the best! I'm very lucky to have met you here, guys! Wherever we will be later, count on me!

To Sveta and Lesha for being in my life.

To my tango family. Alice and Andre, and all others, those who taught me to dance, who practiced with me my first steps, who share with me the pleasure of tango now. Tango has changed my life and you all were part of it. My endless thanks for that!

To Programa de Pós-graduação de Química da PUC-Rio for the opportunity to do and defend my thesis.

To CAPES, CNPq and FAPERJ for given financial support, my scholarship, and all provided resources.

This study was financed in part by the Coordenação de Aperfeiçoamento de Pessoal de Nível Superior - Brasil (CAPES) - Finance Code 001.

Abstract

Artiushenko, Olena; Zaitsev, Volodymyr (Advisor). **Silica-based Adsorbents with Immobilized Derivatives of Phosphonic, Hydroxamic and Pyridinecarboxylic Acids for Dispersive Solid Phase Extraction and Separation of Rare Earth Elements**. Rio de Janeiro, 2019. 138 p. Tese de Doutorado - Departamento de Química, Pontifícia Universidade Católica do Rio de Janeiro.

Rare earth elements (REEs) have been increasingly used in modern industry as essential components of many catalysts, high-performance magnets, superconductors, telecommunication systems. Clean energy development will further boost the demand for REEs since they are used in the production of batteries and solar panels. Environmentally sustainable production process shall substitute or supplement current ore sources. Thus, separation and recycling of REEs are of great importance to diversify the sources of REEs. Most existing technologies for enrichment of REEs are based on solvent extraction and ion exchange. They are not sustainable and are not applicable to electronic waste (e-waste) treatment. One of the first selective adsorbent for REEs SPE extraction was proposed recently (Callura *et al.*, 2018). The research proposed demonstrates other organo-silica adsorbents (OSAd) with covalently immobilized fragments of N-Benzoyl-N-phenylhydroxylamine (BPHA), 2,6-pyridinedicarboxylic acid (PdCA) and amino-di(methylene-phosphonic) acid (AdMPA) can be successfully used both for preconcentration and separation of REEs. This research demonstrates high affinity of the adsorbents to REE (La^{3+} - Lu^{3+}), Sc^{3+} and Y^{3+} . Competitive adsorption of REEs from multielement solution and pH dependence, isotherm and kinetics studies, metal ion recovery and desorption, as well as the adsorbent reusability have been investigated. The research is accomplished with qualitative and quantitative characterization of the adsorbent, physical and chemical properties using Fourier transform infrared spectroscopy, high-resolution X-ray photoelectron spectroscopy, solid-state NMR, BET measurements, elemental and thermogravimetric analysis. It has been demonstrated that the proposed OSAd can be successfully used to remove REE ions from aqueous solution within 10 min. Sharp changes of REEs recovery has been observed in a narrow range of the pH that allows developing a methodology for removal of REEs from solution. The adsorbents demonstrate an essential difference in REE affinity that allows utilization of the OSAd for various purposes, including pre-concentration for determination of REE traces in natural waters, separation of REE from color and other metals in e-waste, separation of individual REE. It is demonstrated that SiO_2 -BPHA can recover all REE from solution with $\text{pH} \geq 5.0$ and release them to solution under treatment with 0.1 M HNO_3 with efficiency more than 95%. Additionally, OSAd - SiO_2 -PdCA and SiO_2 -AdMPA are the only adsorbents that can remove REE ions from aqueous solution with $\text{pH} \geq 2$. Because of this SiO_2 -PdCA and SiO_2 -AdMPA can be used for the

recycling of rare earth elements from electronic waste. It was demonstrated that SiO₂-PdCA can be used for selective recovery of rare earth elements (Y, Eu, Tb) from waste fluorescent lamps. SiO₂-PdCA demonstrates high selectivity that allows complete (>95%) recovery of all REE in the presence of 50-fold excess of Ba²⁺ ions that is used for analytical determination of REE traces by ICP-MS. Also, SiO₂-PdCA is useful for selective adsorption of REE from environmental objects since 200-fold excess of such ions as Fe³⁺, Cu²⁺, Ca²⁺, Mg²⁺, Na⁺, K⁺ and Al³⁺ which are predominate in environmental objects cause little interference on the adsorbent removal efficiency. SiO₂-BPHA demonstrates higher selectivity towards heavy REEs. In optimal conditions selectivity factor is about 80 (for Lu/La and Yb/La pairs) and about 60 (for Tm/La pair), which demonstrates the high potential of SiO₂-BPHA in separation of individual REEs. Reusability test demonstrates that SiO₂-BPHA can be used for quantitative adsorption of almost all REEs (average adsorption of Ce and Pr ions is about 90%) from multielement solution with pH=5.0 without lost in adsorption capacity and selectivity for at least five consecutive cycles. It is demonstrated that adsorption of metals on the OSAd takes place due to complex formation between immobilized ligand and metal ions. For example, adsorption of Eu³⁺ and Tb³⁺ ions on SiO₂-PdCA and SiO₂-AdMPA generates strong red and green luminescence, respectively. Adsorption of Fe³⁺ on SiO₂-BPHA leads to development of red color of the adsorbent which intensity is proportional to metal loading. Immobilized metal complexes are very stable in water and organic media that can be used for further development of optical sensors for REE and stationary phases for ligand-exchange chromatography.

Keywords

Silica-based Adsorbent; Solid Phase Extraction; Separation; Rare Earth Elements.

Resumo

Artiushenko, Olena; Zaitsev, Volodymyr. **Adsorventes à Base de Sílica Gel Modificada com Derivados de Ácido Fosfônico, Hidroxâmico e Piridinocarboxílico para Extração em Fase Sólida Dispersiva e Separação dos Elementos Terras Raras**. Rio de Janeiro, 2019. 138 p. Tese de Doutorado - Departamento de Química, Pontifícia Universidade Católica do Rio de Janeiro.

Os elementos terras raras (ETRs) têm sido cada vez mais utilizados na indústria moderna como os componentes essenciais de catalisadores, ímãs de alto desempenho, supercondutores, sistemas de telecomunicações. O desenvolvimento da energia limpa aumentará ainda mais a demanda, pois ETRs são usados na produção de baterias e painéis solares. O processo de produção ambientalmente sustentável substituirá ou complementarará as fontes atuais. Assim, a separação e a reciclagem de ETRs são de grande importância para diversificar as fontes dos ETRs. A maioria das tecnologias atuais para o enriquecimento de ETRs é baseada na extração de solventes e troca iônica. Elas não são sustentáveis e não são aplicáveis ao tratamento de lixo eletrônico. Um dos primeiros adsorventes seletivos para extração em fase sólida dos ETRs foi proposto recentemente (Callura *et al.*, 2018). A presente pesquisa estudou 3 adsorventes organo-sílicas (OSAd) com fragmentos imobilizados covalentemente de N-Benzoil-N-fenil-hidroxilamina (BPHA), ácido 2,6-piridinodicarboxílico (PdCA) e ácido amino-di(metileno-fosfônico) (AdMPA). Foi mostrado que os adsorventes podem ser utilizados com sucesso para separação e preconcentração dos elementos terras raras das soluções aquosas. A pesquisa demonstrou a alta afinidade dos adsorventes aos ETRs (La^{3+} - Lu^{3+}), Sc^{3+} e Y^{3+} . A adsorção competitiva dos ETRs da solução multielementar, sua dependência de pH, isothermas e estudos de cinética, recuperação e dessorção de íons metálicos, bem como a reutilização de adsorventes foram investigados. A caracterização qualitativa e quantitativa dos adsorventes foi estudada por espectroscopia no infravermelho por transformada de Fourier, espectroscopia de fotoelétrons de raios-X de alta resolução, análise RMN no estado sólido, medições BET, análise elementar e termogravimétrica. Foi demonstrado que os OSAd propostos podem ser utilizados com sucesso para remover íons ETR da solução aquosa em 10 minutos. Os adsorventes demonstram diferenças essenciais na afinidade para ETRs que permitem a utilização dos OSAd para vários fins, incluindo pré-concentração para determinação de traços de ETRs em água natural, separação de ETRs dos outros metais em lixo eletrônico, e a separação individual dos ETRs. A pesquisa demonstra que o SiO_2 -BPHA pode recuperar todos os ETRs de solução com $\text{pH} \geq 5.0$ e liberá-los após eluição de $0.1 \text{ mol L}^{-1} \text{ HNO}_3$ com eficiência superior a 95%. Outros OSAd - SiO_2 -PdCA e SiO_2 -AdMPA são os únicos adsorventes que podem remover os íons ETRs da solução aquosa em $\text{pH} \geq 2$. Devido a isso, SiO_2 -PdCA e SiO_2 -AdMPA podem ser usados para a reciclagem dos ETRs do lixo eletrônico. Foi demonstrado que o SiO_2 -

PdCA pode ser utilizado para a recuperação seletiva de elementos de terras raras (Y, Eu, Tb) dos resíduos de lâmpadas fluorescentes. SiO₂-PdCA demonstra alta seletividade que permite recuperação completa (> 95%) de todos os ETRs na presença de excesso (50 vezes) de íons Ba²⁺ que é útil para determinação analítica de traços dos ETRs por ICP-MS. Além disso, SiO₂-PdCA é útil para a adsorção seletiva dos ETRs de amostras ambientais, pois o excesso de 200 vezes de íons Fe³⁺, Cu²⁺, Ca²⁺, Mg²⁺, Na⁺, K⁺ e Al³⁺ predominantes em amostras ambientais, causa pouca interferência na eficiência do adsorvente. SiO₂-BPHA demonstra maior seletividade para ETRs pesados. Em condições ótimas, o fator de seletividade é cerca de 80 (para pares Lu/La e Yb/La) e cerca de 60 (para o par Tm/La), que demonstra alto potencial do SiO₂-BPHA na separação individual dos ETRs. Estudos de reusabilidade demonstram que SiO₂-BPHA pode ser usado para adsorção quantitativa de quase todos os ETRs (adsorção média de Ce e Pr é cerca de 90%) de uma solução multielementar com pH=5.0 sem perda na capacidade de adsorção e seletividade por pelo menos cinco ciclos. Foi demonstrado que a adsorção de metais por OSAd ocorre devido à formação de complexos entre o ligante imobilizado e os íons metálicos. Por exemplo, a adsorção de íons Eu³⁺ e Tb³⁺ por SiO₂-PdCA e SiO₂-AdMPA gera luminescência forte de cor vermelha e verde, respectivamente. A adsorção de Fe³⁺ em SiO₂-BPHA leva ao desenvolvimento da cor vermelha do adsorvente cuja intensidade é proporcional à concentração de metal adsorvido. Os complexos metálicos imobilizados são muito estáveis em água e meios orgânicos e podem ser usados para o desenvolvimento de sensores ópticos dos ETRs e fases cromatográficas de troca de ligante.

Palavras-chave

Adsorventes à Base de Sílica Gel; Extração em Fase Sólida; Separação; Elementos Terras Raras.

Summary

1 Introduction	20
1.1. Uses of the Rare Earth Elements	22
1.2. Global Rare Earth Elements production	24
1.3. Alternative sources of REEs	25
1.4. Instrumental methods for REEs determination	28
1.5. Modern approaches in extraction and separation of REEs	30
1.6. Chelating organo-silica adsorbents	35
2 Objectives	43
3 Experimental procedure	45
3.1. Materials and methods	45
3.2. Synthesis of reagents	47
3.2.1. Synthesis of <i>N</i> -phenylhydroxylamine	47
3.3. Functionalization of materials	47
3.3.1. Cleaning and activation of silica gel	47
3.3.2. Synthesis of amino-functionalized silica gel	48
3.3.3. Synthesis of silica gel with immobilized aminophosphonic acids	48
3.3.4. Synthesis of silica gel with immobilized 2,6-pyridinecarboxylic acid	51
3.3.5. Synthesis of silica gel with immobilized hydroxamic acid	53
3.4. Determination of the concentration of functional groups	54
3.5. Preparation of hybrid luminescent materials	56
3.6. Adsorption of metal ions by functionalized adsorbents	56
3.6.1. Effects of pH	57
3.6.2. Effect of contact time	57
3.6.3. Adsorption capacity of functionalized materials	58
3.6.4. Adsorption isotherms	58
3.6.5. Evaluation of extraction capacity and selectivity	59
3.6.6. Metal desorption optimization and reusability test	60
3.6.7. Interference effect of competing ions on adsorption of REEs	60
3.6.8. Recovery of REEs from waste fluorescent lamps	61
4 Results and discussion	62
4.1. Quantitative characterization of the adsorbents	62
4.1.1. Adsorption capacity of functionalized materials	62

4.1.2. Elemental analysis	65
4.1.3. Thermogravimetric analysis	66
4.1.4. Concentration of immobilized groups	67
4.2. Spectroscopic characterization of the adsorbents	67
4.2.1. FT-IR characterization	67
4.2.2. X-ray photoelectron spectroscopy	69
4.2.3. NMR characterization	73
4.3. Morphological characteristics of the adsorbents	75
4.3.1. The pore size and morphology of synthesized materials	75
4.3.2. Scanning electron microscopy	77
4.4. Spectroscopic characterization of the immobilized complexes	78
4.4.1. Luminescent properties of REE complexes with immobilized ligands	78
4.4.2. Diffuse reflectance spectroscopy of Fe(III) complexes with SiO ₂ -BPHA	81
4.5. Adsorption and separation of REEs	82
4.5.1. The adsorption kinetics and adsorption isotherms	82
4.5.2. REEs adsorption from multi-component solution	89
4.5.3. Desorption study	90
4.5.4. Reusability of adsorbents	96
4.5.5. Statistical analysis of desorption data	99
4.5.6. Application of the adsorbents for removal and separation of REE ions from complex metal-containing solution	106
4.5.7. Separation of REEs on SiO ₂ -BPHA	111
4.5.8. Recovery of REEs on SiO ₂ -PdCA and SiO ₂ -AdMPA from waste fluorescent lamps	113
5 Conclusion	123
6 Perspectives	125
7 References	126

List of abbreviations

Acac	Acetyl acetone
AIBN	2,2'-Azobisisobutyronitrile
AmSA	Aminosulfonic acid
APT	Attapulgite
APTES	(3-Aminopropyl)triethoxysilane
APTMS	(3-Aminopropyl)trimethoxysilane
AsA	Ascorbic acid
BET	Brunauer–Emmett–Teller theory
BJH	Barrett–Joyner–Halenda method
BPG	Bis(phosphonomethyl)glycine
CiA	Citric acid
CNTs	Carbon nanotubes
CRT	Cathode ray tubes
DGA	Diglycolamide
DGAA	Diglycolamic acid
DIGLYME	Diethylene glycol dimethyl ether
DIPEA	N,N-Diisopropylethylamine
DMF	N,N-dimethylformamide
dMNP	Double-coated magnetic nanoparticle
DSPE	Dispersive solid phase extraction
DTPA	Diethylenetriaminepentaacetic acid
DTPADA	Diethylenetriaminepentaacetic dianhydride
EDTA	Ethylenediamine tetraacetic acid
EGDMA	Ethylene glycoldimethacrylate
FT-IR	Fourier-transform infrared spectroscopy
GONS	Graphene oxide nanosheets
HBA	α -Hydroxyisobutyric acid
HPC	Hydroxypropyl cellulose
ICP AES	Inductively coupled plasma atomic emission spectroscopy
ICP-MS	Inductively coupled plasma mass spectrometry
ICP OES	Inductively coupled plasma optical emission spectrometry
IIP	Ion imprinted polymers
LED	Light-emitting-diode
Ln	Lanthanides

MAA	Methacrylic acid
MAS-NMR	Magic-angle spinning nuclear magnetic resonance
MWCNTs	Multi-walled carbon nanotubes
MS	Mesoporous silica
NAA	Neutron activation analysis
NMR	Nuclear magnetic resonance
NP	Nanoparticle
OSAd	Organo-silica adsorbent
OxA	Oxalic acid
PAA	Phosphonoacetic acid
PAN	1-(2-Pyridylazo) 2-naphthol
REE	Rare earth element
REM	Rare earth metal
REO	Rare earth oxide
SEM	Scanning electron microscopy
SPE	Solid phase extraction
SSA	5-Sulfosalicylic acid
TGA	Thermogravimetric analysis
TMCS	Trimethylchlorosilane
TMS-EDTA	N-[(3-trimethoxysilyl)propyl]ethylenediamine triacetic acid
TXRF	Total reflection X-ray fluorescence spectrometry
UV-vis	Ultraviolet–visible spectroscopy
XPS	X-ray photoelectron spectroscopy
XRF	X-ray fluorescence spectrometry

List of figures

Figure 1. The estimated distribution of REEs by end use in 2018.	22
Figure 2. Adsorption capacity of functionalized materials.	64
Figure 3. TGA thermograms of functionalized silica gels.	66
Figure 4. FT-IR spectra of SiO ₂ (pure) and SiO ₂ -NH ₂ .	68
Figure 5. FT-IR spectra of functionalized silica gels.	69
Figure 6. XPS low-resolution spectra of SiO ₂ -PdCA (a), SiO ₂ -BPHA (b), SiO ₂ -AdMPA (c).	71
Figure 7. XPS high-resolution N1s spectra of functionalized silica gels. Partially reproduced from (Artiushenko <i>et al.</i> , 2019).	72
Figure 8. XPS high-resolution C1s spectra of SiO ₂ -BPHA and SiO ₂ -NH ₂ . Partially reproduced from (Artiushenko <i>et al.</i> , 2019)..	73
Figure 9. Solid state ²⁹ Si MAS-NMR spectra of SiO ₂ -AdMPA (a) and SiO ₂ -AdEPA (b).	73
Figure 10. Q _n type (n=2,3,4) and T _n type (n=1,2,3) Si local environments. Adapted from (Topel <i>et al.</i> , 2014).	74
Figure 11. Solid state ¹³ C MAS-NMR spectra of SiO ₂ -AdMPA (a) and SiO ₂ -AdEPA (b).	74
Figure 12. Solid state ³¹ P MAS-NMR spectra of SiO ₂ -AdMPA.	75
Figure 13. N ₂ adsorption–desorption isotherms of silica materials.	76
Figure 14. Pore size distribution obtained by BJH method.	76
Figure 15. SEM images of unmodified and functionalized silica gels. Partially reproduced from (Artiushenko <i>et al.</i> , 2019).	77
Figure 16. Luminescent hybrid materials a) SiO ₂ -PdCA pure; b) SiO ₂ -PdCA-Eu, λ = 365 nm; c) SiO ₂ -PdCA-Tb, λ = 254 nm.	78
Figure 17. 3D mapping around the optical band gap of luminescent hybrid materials – SiO ₂ -PdCA-Eu ³⁺ (a), SiO ₂ -PdCA-Tb ³⁺ (b), SiO ₂ -AdMPA-Eu ³⁺ (c), SiO ₂ -AdMPA-Tb ³⁺ (d).	80
Figure 18. Luminescence emission spectra of SiO ₂ -PdCA-Eu ³⁺ (a) and SiO ₂ -PdCA-Tb ³⁺ (b).	80
Figure 19: UV-Vis diffuse reflectance spectra of SiO ₂ -BPHA with different metal loading.	81
Figure 20. Effect of contact time on the removal of metal ions.	83
Figure 21. Adsorption isotherm of Eu ³⁺ by SiO ₂ -PdCA (1) and SiO ₂ -AdMPA (2).	85
Figure 22. Adsorption isotherm of Eu ³⁺ (1) and Tb ³⁺ (2) by SiO ₂ -BPHA. Reproduced from (Artiushenko <i>et al.</i> , 2019).	85
Figure 23. Effects of pH on adsorption of REEs by SiO ₂ and SiO ₂ -NH ₂ .	87
Figure 24. Effects of pH on adsorption of REEs by adsorbents.	88
Figure 25. Effects of pH on adsorption of REEs by SiO ₂ -BPHA. Adapted from (Artiushenko <i>et al.</i> , 2019).	89

Figure 26. Distribution coefficients (K_d) values for REEs adsorption. Partially reproduced from (Artiushenko <i>et al.</i> , 2019).	90
Figure 27. Chemical formulas of chelating agents.	92
Figure 28. Desorption of REEs from SiO ₂ -PdCA. Adapted from (Artiushenko <i>et al.</i> , 2018).	93
Figure 29. Desorption of REEs from SiO ₂ -AdMPA.	94
Figure 30. Desorption of Eu ³⁺ from adsorbents. Adapted from (Artiushenko <i>et al.</i> , 2018).	95
Figure 31. Desorption of REE from adsorbents using 0.01 mol L ⁻¹ EDTA at pH 8. Adapted from (Artiushenko <i>et al.</i> , 2018).	95
Figure 32. Desorption of REEs from SiO ₂ -BPHA with HNO ₃ . Adapted from (Artiushenko <i>et al.</i> , 2019)	96
Figure 33. Adsorption recovery (R,%) and desorption efficiency (E,%) of REEs on SiO ₂ -PdCA in five adsorption/desorption cycles. Adapted from (Artiushenko <i>et al.</i> , 2018).	97
Figure 34. Adsorption recovery (R,%) and desorption efficiency (E,%) of REEs on SiO ₂ -AdMPA in five adsorption/desorption cycles.	98
Figure 35. Adsorption recovery (R,%) and desorption efficiency (E,%) of REEs on SiO ₂ -BPHA in five adsorption/desorption cycles.	98
Figure 36. A general distribution of the recovery data over the entire group of lanthanides from SiO ₂ -PdCA.	99
Figure 37. The violin plots on the recovery of lanthanides from SiO ₂ -PdCA.	100
Figure 38. Linear plots of standard deviations for desorption from SiO ₂ -PdCA.	101
Figure 39. General distribution of the recovery data over the entire group of lanthanides from SiO ₂ -AdMPA.	102
Figure 40. The violin plots on the recovery of lanthanides from SiO ₂ -AdMPA.	103
Figure 41. The violin plots on the recovery of lanthanides with HNO ₃ .	104
Figure 42. The violin plot on the recovery over the lanthanide ions group from SiO ₂ -BPHA.	105
Figure 43. General distribution of the recovery data over the entire group of lanthanides from SiO ₂ -BPHA.	106
Figure 44. Effects of pH on adsorption of different metals by SiO ₂ (a), SiO ₂ -PdCA (b), SiO ₂ -AdMPA (c) and SiO ₂ -BPHA (d).	107
Figure 45. Interference effect Fe ³⁺ and Cu ²⁺ ions on REEs recovery from SiO ₂ -PdCA and SiO ₂ -AdMPA.	109
Figure 46. Interference effect of 22 metal ions on REEs recovery from SiO ₂ -PdCA and SiO ₂ -AdMPA.	109
Figure 47. Interference effect of Na ⁺ , K ⁺ , Ca ²⁺ , Mg ²⁺ ions on REEs recovery from SiO ₂ -BPHA. Adapted from (Artiushenko <i>et al.</i> , 2019).	110
Figure 48. Adsorption of REEs on SiO ₂ -BPHA from multi-element solutions. Reproduced from (Artiushenko <i>et al.</i> , 2019).	112

Figure 49. Separation factor for pairs Ln/La. Reproduced from (Artiushenko <i>et al.</i> , 2019).	112
Figure 50. Composition of leaching solution #1 (A) and the concentrate obtained after desorption of metals from SiO ₂ -PdCA (B).	116
Figure 51. Distribution (%) of REEs in the leaching solution #1 (A) and in the concentrate (B) obtained after desorption of metals from SiO ₂ -PdCA.	117
Figure 52. Composition of leaching solution #2 (A) and the concentrate (B) obtained after desorption of metals from SiO ₂ -PdCA.	118
Figure 53. Distribution (%) of REEs in the leaching solution #2 (A) and in the concentrate (B) obtained after desorption of metals from SiO ₂ -PdCA.	119
Figure 54. Distribution (%) of REEs in the leaching solution #2 (A) and in the concentrate (B) obtained after desorption of metals from SiO ₂ -AdMPA.	122

List of schemas

Scheme 1. Synthesis of N-phenylhydroxylamine.	47
Scheme 2. Surface functionalization of silica gel with APTES.	48
Scheme 3. Surface functionalization of silica gel with aminophosphonic acids.	49
Scheme 4. Surface functionalization of silica gel with 2,6-pyridinedicarbonyl dichloride.	51
Scheme 5. Surface functionalization of silica gel with N-Benzoyl-N-phenylhydroxylamine.	53
Scheme 6. Metal adsorption process on adsorbents.	63

List of tables

Table 1. The adsorbent systems used for SPE of REEs.	31
Table 2. Examples of ligands coordinating through N-atom.	37
Table 3. Examples of ligands coordinating through N- and O-atoms.	38
Table 4. Examples of ligands coordinating through O-atom.	38
Table 5. Results of elemental analysis of organo-silica samples.	65
Table 6. The estimated concentration of grafted functional groups.	67
Table 7. Concentration of immobilized groups.	67
Table 8. The morphological characteristics of obtained materials.	76
Table 9. Kinetic parameters for metal adsorption.	84
Table 10. Adsorption isotherm parameters.	85
Table 11. Statistical parameters of desorption from SiO ₂ -PdCA.	101
Table 12: Statistical parameters of desorption from SiO ₂ -AdMPA.	104
Table 13. The descriptive statistics summary on the recovery of lanthanides from SiO ₂ -BPHA.	105
Table 14. Interference effect of Fe ³⁺ and Cu ²⁺ ions on REEs recovery.	108
Table 15. Interference effect of 22 metal ions on REEs recovery.	108
Table 16. Interference effect of Na ⁺ , K ⁺ , Ca ²⁺ , Mg ²⁺ ions on REEs recovery.	110
Table 17. Composition of the leaching solution #1, supernatant and desorbing solutions received after DSPE with SiO ₂ -PdCA, and corresponding adsorption, desorption, and overall recovery degrees.	115
Table 18. Composition of the leaching solution #2, supernatant and desorbing solutions received after DSPE with SiO ₂ -PdCA, and corresponding adsorption, desorption, and overall recovery degrees.	120
Table 19. Composition of the leaching solution #2, supernatant and desorbing solutions received after DSPE with SiO ₂ -AdMPA, and corresponding adsorption, desorption, and overall recovery degrees.	121

1 Introduction

Rare earth elements (REEs) are defined by IUPAC as a group of 17 transition metals. This group consists of 15 lanthanides (Ln) (elements with atomic numbers from 57 to 71), as well as scandium and yttrium, that have atomic numbers 21 and 39, respectively, but are considered rare-earth elements because of exhibit similar physical and chemical properties to lanthanides, including low solubility and immobility in the terrestrial crust.

Recently, Rare Earth Elements attract much attention due to their wide use in high-tech and sustainable technologies. From 2010, REEs group is considered by European Commission one of the 14 critical mineral raw materials (metals or group of metals) that are a crucial part of high tech and every-day consumer products (European Commission, 2010).

The demand for REEs is constantly growing since they are used in high-tech and sustainable technology (high-performance magnets, rechargeable NiMH batteries, fluorescent lamps, etc.) (Gutfleisch *et al.*, 2002; Lucas *et al.*, 2015; Tanaka *et al.*, 2006; Zhuang *et al.*, 2004), but their availability is increasingly under pressure (European Commission, 2010). For the REEs, their high supply risk is mainly due to the monopoly in mining operations (mainly in China), compounded by low substitutability and low recycling rates.

Due to the recent high-tech boom, the amount of electronic waste (e-waste) products, containing REEs is growing proportionately. In the search of alternative sources of REEs recycling from e-waste REEs products already attracts considerable attention from scientists and engineers. In long-term global REE demand, an environmentally sustainable production process shall substitute or supplement current ore sources (Dutta *et al.*, 2016). Effective technologies for processing of e-waste for REEs extraction and recovery are still under investigation. Several methods have been developed and are currently under the attempt of being optimized, such as liquid-liquid extraction, extraction with ionic liquids, ion-exchange resins or novel adsorbent materials with high affinity towards REE.

The present work focuses on the solid phase extraction (SPE) technique, having the aim of developing organo-silica adsorbent (OSAd) highly efficient and selective for the extraction and separation of REE in solution.

Among other separation and pre-concentration techniques, SPE has several important advantages, such as less use of solvents, high enrichment factors, rapid recovery and phase separation and good compatibility with different detection techniques. Moreover, application of technologies for enrichment of REEs based on solvent extraction and ion exchange to electronic waste (e-waste) treatment is questionable since they are environmentally hazardous (extraction) and not sufficiently selective (ion exchange), because of the low concentrations of REEs in waste sources (Binnemans, Jones, *et al.*, 2013; Binnemans, Pontikes, *et al.*, 2013; Gambogi, 2016). Due to the easier procedure, high adsorption capacities and rapid phase separation, solid-phase extraction can be an essential substitution for solvent extraction in REEs separation and purification from recyclable sources, such as e-waste. Also, SPE is cost-effective and more environmentally friendly, thus can reduce the costs and environmental impacts.

Nanostructured materials, such as organo-silica adsorbent (OSAd) are widely used in SPE. Compared to bulk materials, OSAd possess high specific surface area, resulting in higher surface activity and larger possibility of surface functionalization with adequate and adsorption-efficient organic ligands.

1.1. Uses of the Rare Earth Elements

Due to their unique physical and chemical properties, magnetic and optical, REEs have diverse applications. In 2018, 120.000 tons (t) of rare earth oxides (REOs) were consumed worldwide (U.S. Geological Survey, 2018). REEs are used as components in high technology devices, including smartphones, digital cameras, computer hard disks, fluorescent and light-emitting-diode (LED) lights, flat-screen televisions, computer monitors, and electronic displays (Baba, Hiroshige e Nemoto, 2013; Fifarek, Veloso e Davidson, 2008; G.B. Haxel, J.B. Hedrick, 2010; Popov *et al.*, 2018; Sergo, Schmid e Meriani, 1992). Large quantities of some REEs are used in clean energy and defense technologies. REEs are used individually or in combination to make phosphors (substances that emit luminescence). Yttrium, europium, and terbium phosphors are the red-green-blue phosphors used in many light bulbs, panels, and monitors (Chen, Chu e Liu, 2012; Ekambaram e Patil, 1995; Hao *et al.*, 2018; He e Yan, 2011; Jia e Hunter, 2006; Lee e Seo, 2002; Leskelä e Niinistö, 1992; Luo e Cao, 2007; Yeo, Cho e Huh, 2016).

Mature applications (catalysts, glass industry, metallurgy excluding battery alloy, and phosphors) consume about 60% of the total amount of REE, and the remaining 40% is consumed in developing, high-tech technologies (battery alloys, ceramics, magnets, etc.) (Goonan, 2011). Thus, the estimated distribution of rare earths by end-use in 2018 was: catalysts (60%), ceramics and glass (15%), metallurgical applications and alloys (10%), polishing (10%), and other (5%), Figure 1 (U.S. Geological Survey, 2019).

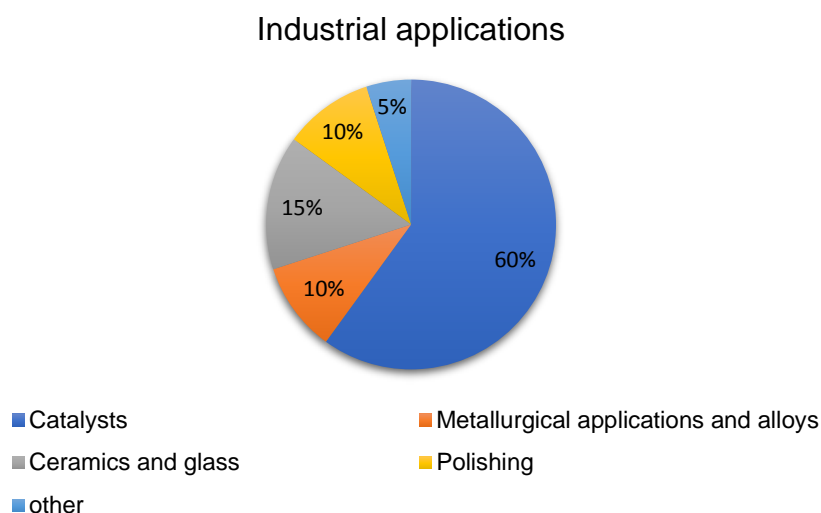


Figure 1. The estimated distribution of REEs by end use in 2018.

The mature market sector consumes mainly lanthanum and cerium constitute about 80% of rare earth elements used, and in new market segments, dysprosium, neodymium, and praseodymium account for about 85% of rare earth elements used (Charalampides *et al.*, 2015).

Catalysts. Fluid cracking is the conversion process in petroleum refining. REOs are used as catalysts for fluid cracking and automobile catalytic converters (Sanchez-Castillo, Madon e Dumesic, 2005; Tang e Zhang, 2010; Voolapalli *et al.*, 2013). In 2008, 27 400 t of REOs were used as catalysts for fluid cracking and automobile catalytic converters (Charalampides *et al.*, 2015). Mainly lanthanum (66%), cerium (32%), neodymium (0.8%) and praseodymium (0.6%) oxides are used for this purpose. Used catalysts are generally considered to be hazardous wastes. However, REOs are not recovered due to high disposal costs.

Ceramics and glass. REOs (mainly La_2O_3 , Y_2O_3 , and Gd_2O_3) are added to glass to perform such properties like absorbing ultraviolet light, altering the refractive index, colorizing or decolorizing. High purity REOs are used in special optical glasses of lenses of cameras, binoculars or microscopes. The one-year total world production of optical glasses is about 20 000 t (Humphries, 2011). REEs are added to ceramic glazes for color control. Barium titanite powder, which is used in electronic applications, is doped with lanthanides to modify the properties. Yttrium is used to make ferrites for high frequencies and to stabilize zirconia in oxygen sensors.

Metallurgical applications and alloys. In metallurgy, REEs are added to aluminum, iron, steel, and other alloys to improve their physical properties. Mainly cerium, lanthanum, neodymium and praseodymium oxides are used for this purpose. Because of their superior magnetic flux density neodymium-iron-boron (NdFeB) and samarium-cobalt alloys (SmCo) are used in permanent magnets. The negative electrode of nickel-metal-hydride (NiMH) rechargeable batteries comprises of a mixture of light rare earth elements (mischmetal) (Müller e Friedrich, 2006).

For other applications mainly used cerium, lanthanum, yttrium, neodymium, and fewer quantities of praseodymium, samarium and gadolinium oxides and other REOs (about 1%). This application includes the use of REEs in chemicals, military weapons, and satellite systems.

1.2. Global Rare Earth Elements production

Contrary to their name, REEs are more abundant in the Earth's crust than many other valuable elements. All REEs, except promethium, are more abundant on average in the Earth's crust than silver, gold, or platinum. For example, the rarest rare earth, thulium, is 125 times more common than gold and least-rare rare earth, cerium, is 15 000 times more abundant than gold (Zepf, 2013). However, they are rarely found in easy-to-mine minerals and are often unfavorably distributed in common ores/minerals (Chen, 2011).

There are about 200 rare earth content minerals of different classes, such as halides, carbonates, oxides, phosphates, silicates, etc. (Kanazawa e Kamitani, 2006). Due to their radius and oxidation state, REE ions in minerals have large coordination numbers (6-10). Light rare earth elements (LREEs) tend to concentrate in carbonates and phosphates, while heavy rare earth elements (HREEs) are abundant in oxides and a part of phosphates. Silicates include both REEs. However, due to strong chemical bonds in the structure that requires high energy for their breaking, only a few minerals, such as bastnaesite (Ce,La)CO₃(F,OH), monazite (Ce,La,Nd,Th)PO₄, xenotime YPO₄, and RE-bearing clay are processed for commercial production. Bastnaesite deposits in the United States and China account for the largest concentrations of REEs, while monazite deposits in Australia, South Africa, China, Brazil, Malaysia, and India account for the second largest concentrations of REEs (Humphries, 2011). REEs are also often found associated with uranium/thorium mineralization and uranium ores often contain REEs. This co-deposition with radionuclides plays a significant role in REE mining and end in high costs thorium disposal from radioactive waste after monazite processing.

Until 1990s almost all REE mining and production was done in the U.S. Since 1990 there is a decrease in U.S REEs production. By 2000, the REE market was dominated by China and nowadays it provides 85–95 percent of the world's REEs (Chen, 2011). Currently, China has effective control of global REE mining, beneficiation, and separations. Despite the risks of the monopoly control of the REE market, there is no effective competition exists worldwide. Moreover, Chinese manufacturers have the first call on available REE.

In addition to the problems of monopolistic production, mining rare earth metal ores in China have many negative effects on the environment (Ali, 2014). Solvent extraction is mostly used nowadays; beneficiation of concentrated leaching solutions has low selectivity for the individual REE that results in many separation

stages and generation of a lot of waste. Also, solvent extraction separation methods, generally, require the use of many corrosive and toxic chemicals. Moreover, extraction of HREEs from bastnaesite and monazite causes the excessive production of LREEs and the harmful accumulation of radioactive waste (Lee, 2012).

In a future perspective of global REEs production, driven by global population increase, increased affluence of the global population, need to replace end-of-life products containing REE, and production of new products containing REE, the demand for selected members of the REE family is expected to grow. Thus, recycling of produced waste could be an effective approach for replenishment. Significant amounts of REEs are lost during the multistep purification process and additional material could be potentially recovered from what is now waste. As well, since rare earth elements do not degrade during the lifetime of their products, used products could also become an alternative source of REEs.

1.3. Alternative sources of REEs

Due to the inefficient collection, technological problems and lack of incentives, nowadays commercial recycling of REEs is extremely low, only about 1% of all REEs used in different applications are recycled (Binnemans e Jones, 2015; Jowitt *et al.*, 2018). Recycling of REEs from waste have the potential to become an alternative source of REEs and in a monopoly market is an absolute necessity, especially in countries with no or few rare-earth deposits. Also, the recycling of REEs is important in view of the efficient use of natural resources and balance maintaining. As regards to the “balance problem”, mentioned by Falconnet and coworkers the demand and supply of the individual rare-earth elements have to be equal at any time for not to generate shortages or excesses of some elements (Falconnet, 1985). For example, mining of REE ores for neodymium produces large amounts of lanthanum and cerium that are more abundant, but their excess is unusable. Compared with the primary extraction of REEs from ores, the recovery of REEs from waste has the advantage that the composition of the obtained REE concentrate is less complex.

There are three major applications of REEs, that represent more than 80% of the rare-earth element market: permanent magnets (38%), lamp phosphors (32%) and nickel-metal hydride batteries (13%) (Binnemans, Jones, *et al.*, 2013). So, they are more promising alternative source of REEs. Other rare earth-

containing materials (cathode ray tubes (CRT) phosphors, catalysts, polishing powders, glasses) are of less interest.

Permanent magnets. The most common REE magnets are based upon neodymium-iron-boron (NdFeB) alloys (Coey, 2012). These magnets are made with NdFeB matrix, covered by neodymium-rich grain boundary phase, with some additions of praseodymium, gadolinium, terbium, dysprosium, as well as cobalt, vanadium, titanium, zirconium, molybdenum or niobium (Binnemans, Jones, *et al.*, 2013). The grain boundary phase contains copper, aluminum or gallium. The other, a less popular type of rare earth magnets are based upon samarium-cobalt alloys (SmCo). Such magnets may contain different transition metals, such as Fe, Zr, and Cu. The most beneficial approach to recycling of REE magnets would be direct re-use of the magnets in their current form/shape. Unfortunately, direct re-use is only relevant for the large magnets, used in wind turbines, large electric motors, and generators and in hybrid and electric vehicles. However, large magnets are not currently available in large quantities in waste due to their long lifetime. Most of the current NdFeB waste material is present in electronics devices, such as loudspeakers, mobile phones, and hard disk drives.

Computer hard disk drives (HDDs) are probably the most important source of REE (each HDD contains between 10 and 20 g of NdFeB). For such REE source, it is recommended to separate the rare earths from the transition metals and other elements (e.g. boron) present in the magnet alloys (Binnemans, Jones, *et al.*, 2013). There are several routes for recovery of REEs from magnets: hydro- and pyrometallurgy and gas-phase extraction (Kim *et al.*, 2015; Tunsu, 2018). In the traditional method of hydrometallurgy, the magnet alloys are dissolved in strong mineral acids and the REEs are precipitated as double sulfates, oxalates or fluorides. This approach requires large amounts of chemicals and is lack of selectivity. The magnets contain on average 72 wt% of iron. And leaching cannot avoid that unwanted elements, such as iron, nickel, copper, boron, enter to the solution. Pyrometallurgical route and gas-phase extraction have also some disadvantages. Larger energy input, generation of large amounts of solid waste, consumption of large amounts of chlorine gas are some of them.

Lamp phosphors. According to recent estimates, REE use in phosphors is about 11-19% of total REE market demand. About 90% of all phosphors are used in energy-efficient lamps, 10% in TVs and screens and 11% are used by various phosphors using applications (Machacek *et al.*, 2015). Usually, concentrated REE products (oxides or compounds) are used by phosphor manufactures. REE-based phosphor powders have a wide variety of powder compositions and varying

amounts of REE. Mostly lamp phosphors in End-of-Life fluorescent lamps are a rich source of the heavy rare earth's elements europium, terbium, and of yttrium. Five rare-earth phosphors are often encountered in fluorescent lamps: the red phosphor $Y_2O_3:Eu^{3+}$ (YOX), the green phosphors $LaPO_4:Ce^{3+},Tb^{3+}$ (LAP), $(Gd,Mg)B_5O_{12}:Ce^{3+},Tb^{3+}$ (CBT), $(Ce,Tb)MgAl_{11}O_{19}$ (CAT) and the blue phosphor $BaMgAl_{10}O_{17}:Eu^{2+}$ (BAM) (Ronda, Jüstel e Nikol, 1998). Almost all global supply of Eu, about 85% of Tb and close to 77% of Y are used for phosphors. Linear tube lamps are more promising to recycle by cutting off the ends of the tube and blowing the phosphor powder out, while other shapes of lamps are more problematic for recycling. There are three options for recycling phosphors: (1) direct re-use of powder in new lamps, (2) recycling of the individual phosphor components and their re-use in new lamps and (3) recover pure REE content (Binnemans, Jones, *et al.*, 2013). However, the recycled phosphor powder has less quality than the original product, due to deteriorating over the lifetime of a lamp and changing particle size of the powder during recycling processes. Thus, the third way to recover pure REE content is preferred. Usually, for REEs recovery from lamp phosphors, strong acids are used. The recycled lamp phosphor fraction contains mainly six rare-earth elements: La, Ce, Eu, Gd, Tb, Y, and many non-REE elements are present: Al, Si, P, Ca in relatively large concentrations, and Ba, Sr, Mg, Mn, Sb, Cl, F, Hg, Pb, Cd in small to trace concentrations.

Nickel-metal-hydride batteries. The active components of a rechargeable NiMH battery in the charged state consist of positive electrode made from nickel hydroxide ($Ni(OH)_2$) and negative electrode that is hydrogen storing metal alloy as well as an alkaline electrolyte. $LaNi_5$ based alloys are ideal hydrogen storage alloys but the use of pure lanthanum increases the price. In order to reduce the price of the alloy, mischmetal (a mixture of light rare earth elements (La, Ce, Pr, Nd)) is used to replace pure lanthanum. The composition of mischmetal depends on the origin of the rare earth minerals and its processing. Nickel also can be substituted by other elements (Al, Mn, Cr, Fe, Co, Cu, and Si). Nowadays are widely used NiMH batteries with composition $La_{0.8}Nd_{0.2}Ni_{2.5}Co_{2.4}Si_{0.1}$, $La_{0.8}Nd_{0.2}Ni_{2.5}Co_{2.4}Al_{0.1}$, $MischmetalNi_{3.55}Co_{0.75}Mn_{0.4}Al_{0.3}$ or $MischmetalNi_{3.5}Co_{0.7}Al_{0.8}$ instead of $LaNi_5$. Hybrid electric cars represent 57% of the usage of all NiMH batteries. Every Toyota Prius contains about 2.5 kg of REEs in the form of mischmetal in its battery pack (Buchert *et al.*, 2012). Mainly the industrial recycling of NiMH batteries was their use in stainless steel production as a cheap nickel source, and the rare earths were lost (Müller e Friedrich, 2006). There are hydro- and pyrometallurgy routes for recovery of REEs from NiMH batteries, but as it was

mentioned above this process has a lot of very important disadvantages, like large consumption of chemicals, needs of further REEs separation, etc.

Glass polishing powders could be considered as a source of cerium: a slurry of cerium oxide in water is the best polishing agent for glasses. *Fluid catalytic cracking catalysts*, used in the petrochemical industry, contain about 3.5 wt% rare-earth oxides, mainly lanthanum (50% of the world production of lanthanum) and smaller amounts of cerium, praseodymium, and neodymium (Zhao *et al.*, 2017). Special *optical glasses* used in lenses of cameras, microscopes, binoculars or microscopes contain more than 40 wt% of very high purity La_2O_3 (Jiang *et al.*, 2005). Some optical glasses also contain Y_2O_3 and Gd_2O_3 . The total world production of optical glass is about 20 000 tons per year, which means about 1600 tons of rare-earth oxides per year could be recycled.

1.4. Instrumental methods for REEs determination

Due to increased interest in these elements, accurate and precise analytical methods are needed for their determination (Zawisza *et al.*, 2011a). Nowadays the most used analytical methods for REEs determination are: inductively coupled plasma mass spectrometry (ICP-MS) (Dupont *et al.*, 2014; Fisher e Kara, 2016; Iftekhar, Srivastava e Sillanpää, 2017a; Li, W. *et al.*, 2016; Moussa *et al.*, 2017; Su *et al.*, 2014; Tu *et al.*, 2010; Yan *et al.*, 2017; Zhang *et al.*, 2008; Zhang, Q. *et al.*, 2016; Zhao *et al.*, 2016), inductively coupled plasma optical emission spectrometry (ICP OES) (Ashour *et al.*, 2017; Moussa *et al.*, 2017; Yan *et al.*, 2017; Zhang, Q. *et al.*, 2016), x-ray fluorescence spectrometry (XRF) (Zawisza *et al.*, 2011a), and neutron activation analysis (NAA) (Tu *et al.*, 2010; Yan *et al.*, 2017; Zhang *et al.*, 2008; Zhang, Q. *et al.*, 2016). ICP OES and ICP-MS are very powerful techniques because of their high sensitivity, large dynamic linear range, multi-element analysis and possibility to perform isotopic measurements in case of ICP-MS. However, the concentration of REE in samples is usually much lower than the detection limits of ICP OES, thus determination frequently involves preconcentration and separation steps to reduce matrix effects. ICP-MS analysis of trace and ultra-trace (ppb) amounts also requires preconcentration and spectral interferences are still one of the problems to be solved in ICP-MS. NAA and XRF give a possibility of direct determination of these materials. NAA is a very sensitive technique. However, it suffers from serious interferences from the main elements and from a long irradiation time usually used in the determination of REE. Spectral interferences are also representative of XRF analysis. XRF is widely used for multi-element

determination and plays an important role in metal, ceramic and heavy industries, in mineral and geological exploration or in environmental monitoring (Zawisza *et al.*, 2011b) because it does not require any treatment of the material, but since detection limits for REE are in the ppm range, analysis of environmental or biological samples is restricted.

To *inductively coupled plasma mass spectrometry (ICP-MS)* method are dedicated about half of all publication of REEs determination. It's related to the high potentialities of the method. For example, high-resolution ICP-MS have been used for REEs determination in basalt, andesite, and ultrabasite standards (Robinson *et al.*, 1999). The linear range was 0.8–50 ng g⁻¹ without previous preconcentration. Simple, accurate and specific ICP-MS method for simultaneous direct quantification of 15 REEs in human urine has been developed (Li, Y. *et al.*, 2016) with limits of detection and quantification in the range of 0.009–0.010 µg L⁻¹ and 0.029–0.037 µg L⁻¹. ICP-MS method was used to REEs determination in high purity samarium oxide (Zhang *et al.*, 2007). Ce, Eu, Gd, La, Lu, Nd, Pr, Tb, and Y, were determined without separation since samarium does not have any interfering influence. To determine Dy, Er, Ho, Tm, and Yb, it was used extraction chromatography for matrix separation. Another method with detection limits between 0.2–8 pg mL⁻¹ for 16 REEs was applied to the quantification of trace amounts of rare earth elements in high purity gadolinium oxide (Pedreira *et al.*, 2004).

Inductively coupled plasma optical emission spectrometry (ICP OES) is the second in importance technique for the determination of REEs. The method allows a rapid multielement analysis in a wide range of content with moderate absolute detection limits, excellent reproducibility, and low systematic errors. However, the sensitivity of ICP OES can be insufficient sometimes. Without preconcentration and matrix separation, trace contents of the REEs can be determined within detection limits on the order of ppb. Preconcentration can reduce the detection limits to ppt.

The ICP OES method of REEs determination after their on-line preconcentration was used to analyze the pig liver and various mushrooms as well as standards of soils, sedimentary rocks, and tea leaves. The detection limits were in ng L⁻¹ (Zhang *et al.*, 2007). In another research, authors developed a rapid method for ICP OES determination of La, Ce, Nd, Sm, Eu, Gd, Dy, Yb, and Lu in the granitic rocks and pure apatite after separation on Dowex 50W-X8 cation-exchange resin (Gásquez *et al.*, 2005). Authors (Yenisoy-Karakaş *et al.*, 2004) developed an analytical method for direct determination of Y, La, Ce, Pr, Nd, Sm,

Eu, and Yb by ICP OES in bastnasite ores. The proposed method enables determination of REE with 0.18 (Yb) - 74 (Nd) ng g⁻¹ limits of detection without their separation or preconcentration. Using of reversed-phase high performance liquid chromatography (HPLC) separation before ICP OES determination of La, Ce, Pr, Nd, Sm, Eu, Gd, Dy, Ho, Er, Yb, Sc, Y in red mud and bauxite samples allowed to achieve detection limits for this elements up to 10 ng (Tsakanika, Ochsenkühn-Petropoulou e Mendrinou, 2004).

Neutron activation analysis (NAA) have detection limits at the level of mg/g to µg/g and is widely used to determine the REEs in geological samples and objects of extraterrestrial origin, as well as in environmental, soil, and water samples. NAA analysis was used to determine La, Ce, Nd, Sm, Eu, Yb, and Lu in the granite rocks. Detection limits were in the range from 0.5 pg g⁻¹ for Eu to 10 ng g⁻¹ for Nd (El-Taher, 2007, 2012). Due to the use of solvent extraction with N-1923 reagent and extraction chromatography before NAA analysis of La, Ce, Nd, Sm, Eu, Tb, Yb, Lu in geological reference samples, olivine crystals separated from pallasite meteorites and the limits of detections achieved 0.003 (Eu) to 1.0 (Ce, Nd) µg g⁻¹ (Minowa, Takeda e Ebihara, 2007).

X-ray fluorescence analysis (XRF) has the major disadvantage its low sensitivity (ppm) that does not allow application of this technique to direct determination of REEs in trace amounts. Moreover, a serious problem in XRF is the spectral interference L lines of REE and overlap of these lines with the K series of matrix medium-Z elements (Zawisza *et al.*, 2011b). However, TXRF method was used for determination of La, Pr, Nd, Sm, Gd, Tb, Dy, Ho, Er, Yb, Lu amount adsorbed by TMS-EDTA/Fe₃O₄, SiO₂, TiO₂ nanoparticles (Dupont *et al.*, 2014). Sm, Eu, Gd were determined in Granite GS-N, andesite AGV-1 by XRF after preconcentration using chemofiltration and thorin as a complexing agent, with limits of detection in the range between 23 (Sm, Eu) and 49 (Gd) µg g⁻¹ (Vito, De, Olsina e Masi, 2000).

1.5. Modern approaches in extraction and separation of REEs

As it was discussed in the section above, even such powerful techniques, like ICP-MS, can require previous preconcentration and matrix separation step. The most commonly used techniques for the separation and recovery of REEs are precipitation, liquid-liquid extraction, and ion exchange (Ashour *et al.*, 2017).

There are different modern preconcentration and matrix elimination methods that have been used to reduce the matrix effect prior to REE determination. Among

them: classical liquid-liquid extraction (LLE) (Hoogerstraete, Vander *et al.*, 2013; Hoogerstraete, Onghena e Binnemans, 2013; Hoogerstraete, Vander, Onghena e Binnemans, 2013; Rout e Binnemans, 2014) solid-phase extraction (SPE) (Hennebrüder *et al.*, 2004; Patra *et al.*, 2017; Zhang, Q. *et al.*, 2016; Zhang e Wu, 2015), and their more modern modifications - liquid-liquid-liquid micro-extraction (Xuejuan e Zhefeng, 2009), dispersive liquid-liquid micro-extraction (Çelik *et al.*, 2015; Leme *et al.*, 2018), cloud point extraction (Li, X. *et al.*, 2017; Li e Hu, 2010; Lian *et al.*, 2012; Varbanova *et al.*, 2017) and solidified floating organic drop micro-extraction (Chen *et al.*, 2013; Fisher e Kara, 2016; Song, Zhang e Li, 2018).

Separation methods for REEs based on liquid-liquid extraction utilize toxic and corrosive organic solvents, have low selectivity and generate large amounts of waste. Damage to the environment, caused by solvent extraction, is not accounted for in the cost of producing rare earth products (Izatt *et al.*, 2016). Among other separation and pre-concentration techniques, solid-phase extraction (SPE) is free from these disadvantages. SPE is an easy and rapid operation and has high adsorption capacities. Also, SPE is more cost-effective and more environmentally friendly. This makes SPE one of the most popular methods for REEs recovery from water samples (Fisher e Kara, 2016). Table 1 summarizes the adsorbents recently used for solid-phase extraction of REEs.

Table 1. The adsorbent systems used for SPE of REEs.

Adsorbent system	Metals	Adsorption capacity (mg g ⁻¹)	Technique	Ref
DTPADA, PAA, BPG/SiO ₂	Nd, Gd, Ho	-	ICP-MS	(Callura <i>et al.</i> , 2018)
TMS-EDTA/ Fe ₃ O ₄ , SiO ₂ , TiO ₂	11 REEs	100-400	TXRF	(Dupont <i>et al.</i> , 2014)
Activated carbon modified with KMnO ₄	Y, Yb, Sc, Lu, Eu, La	0.05-0.1	ICP AES	(Kano <i>et al.</i> , 2017)
dMNP-DTPA	10 REEs	-	ICP-MS	(Zhang, H., McDowell, Rocklan G., <i>et al.</i> , 2016)
DTPA, DTPADA, PAA, BPG/SiO ₂	Nd, Gd, Ho	-	ICP-MS	(Noack <i>et al.</i> , 2016)
APTES, APTMS, TMCS/SiO ₂	La, Sc, Er, Eu and Y	-	ICP	(Ramasamy, Khan, <i>et al.</i> , 2017)
Zn/Al Layered double hydroxide intercalated cellulose	Y, La, Ce	102.25 (Y), 92.51 (La), 96.25 (Ce)	ICP OES	(Iftekhar, Srivastava e Sillanpää, 2017b)
PAN/Acac modified silica-chitosan hybrid adsorbents	La, Sc, Y	120.7 (La), 175.2 (Sc), 158.8 (Y)	ICP OES	(Ramasamy, Wojtuś, <i>et al.</i> , 2017)

Gum Arabic grafted polyacryl-amide based silica nanocomposite	Eu, La, Nd, Sc	10.11 (Eu), 7.9 (La), 12.24 (Nd), 11.05 (Sc)	ICP OES	(Iftekhar <i>et al.</i> , 2018)
PAN/Acac modified MS	La, Er, Sc, Eu, Y	-	ICP	(Ramasamy, Repo, <i>et al.</i> , 2017)
Bidentate phthaloyl diamide ligands grafted on MS	15 REEs	8.57 (Lu)	ICP-MS/MS	(Hu <i>et al.</i> , 2017)
Cellulose based silica (CLx/SiO ₂) nanocomposite	Eu, La, Sc	24.27(Eu), 29.48 (La), 23.76 (Sc)	ICP OES	(Iftekhar, Srivastava e Sillanpää, 2017a)
Flowerlike Nano-Mg(OH) ₂	Eu, Tb, Dy, Yb	1827 (Tb)	ICP AES	(Li <i>et al.</i> , 2013)
Kenaf cellulose-based poly(hydro-xamic acid) ligand grafted cellulose	La, Ce,Pr, Gd, Nd, Eu, Sm	192 (Sm) - 260 (La)	ICP OES	(Rahman <i>et al.</i> , 2017)
Thiourea functionalized cellulose	Eu, Nd	27 (Eu), 73 (Nd)	ICP-MS	(Negrea <i>et al.</i> , 2018)
EDTA-cross-linked b-cyclodextrin (EDTA-b-CD) biopolymer	La, Ce, Eu	~48-55	ICP OES	(Zhao <i>et al.</i> , 2016)
Diglycolamic-acid modified chitosan sponges (CSs-DGAA)	Eu, Y	79.0 (Eu) 40.7 (Y)	ICP OES	(Bai <i>et al.</i> , 2018)
IIP with Nd, MAA, EGDMA, AIBN	La, Ce, Nd, Sm, Er, Gd, Dy, Er, Lu	~8-30	ICP-MS	(Moussa <i>et al.</i> , 2017)
DGA, FDGA, NDOODA on KIT-6	15 REEs	-	ICP-MS	(Florek <i>et al.</i> , 2015)
Di(2-ethylhexyl)-phosphoric acid grafted Fe ₃ O ₄ @TiO ₂ NPs	15 REEs	7.75 (Y) – 12.9 (Tm)	ICP-MS	(Yan <i>et al.</i> , 2017)
Saussurea tridactyla Sch-Bip	15 REEs	62.2 (Y) – 153 (Tm)	ICP OES	(Zhang, Q. <i>et al.</i> , 2016)
Anion resin (AG1-X8) and the TRUspec ion-exchange resin	16 REEs	-	ICP-MS	(Li, W. <i>et al.</i> , 2016)
Silica gel modified with diglycolamic acid	14 REEs	~7 (La) – 25 (Dy)	ICP	(Ogata, Narita e Tanaka, 2015)
4-(2-morinyldiazenyl)-N-(3-(trimethylsilyl)propyl)benzamide modified silica gel	Sc	~27	ICP AES	(Zhang <i>et al.</i> , 2008)
1-(2-aminoethyl)-3-phenylurea-modified silica gel	Sc	32.5	ICP AES	(Tu <i>et al.</i> , 2010)
Fe ₃ O ₄ @SiO ₂ @polyaniline graphene oxide composite	15 REEs	8.1 (Y, Ho) – 16 (Dy)	ICP-MS	(Su <i>et al.</i> , 2014)
Granular hybrid hydrogel HPC-g-PAA/APT	La, Ce	199.26 (Ce), 264.17 (La)	UV-vis	(Zhu, Zheng e Wang, 2015)
2-ethylhexyl phosphonic acid mono-2-ethylhexyl ester-	La	55.9 (La)	UV-vis	(Wu, Sun e Wang, 2013)

grafted magnetic silica nanocomposites				
Carbonized polydopamine nano carbon shells	14 REEs	-	ICP AES	(Sun <i>et al.</i> , 2016)
Fe ₃ O ₄ NPs with citric acid or L-cysteine	La, Nd, Gd, Y	52-98	ICP OES	(Ashour <i>et al.</i> , 2017)
L-cysteine Fe ₃ O ₄ NPs	La, Nd, Gd, Y	13.6 (Y) - 145.5 (Nd)	ICP OES	(Ashour <i>et al.</i> , 2016)
Phosphorus functionalized nanoporous carbon	Nd, Dy	335–344	UV-vis	(Saha <i>et al.</i> , 2017)
DTPA modified silica gel	La, Ce, Pr, Nd and Dy	-	ICP OES	(Ashour <i>et al.</i> , 2018)
Bis(2-ethylhexyl)-phosphoric acid/SiO ₂ -P	Gd	~50	ICP AES	(Shu <i>et al.</i> , 2018)
Tridentate diglycolamide ligand silica gel	16 REEs	-	ICP OES	(Li, F. K. <i>et al.</i> , 2017)
Multi-Walled Carbon Nanotubes Coated Cellulose Acetate Membrane	Y, La, Ce, Nd, Sm, Gd and Dy	23 (Ce) – 41 (Sm)	ICP OES	(Zolfonoun e Yousefi, 2016)
Silica/polyvinyl imidazole/H ₂ PO ₄ -coreshell NP	Sm, Dy	160 (Sm), 150 (Dy)	ICP OES	(Ettahadi <i>et al.</i> , 2017)

Ion-exchange resins and organo-mineral materials are the most important types of REE-selective SPE adsorbents. *Ion-exchange resins*. Successful application of commercially available ion-exchange resins, such as XAD-4, Tulsion CH-90 and Tulsion CH-93 (Dave, Kaur e Menon, 2010; Radhika *et al.*, 2012), Chelex-100 (Rahmi *et al.*, 2007), Toyopearl AF-Chelate (Willie e Sturgeon, 2001) and Meta SEPME-2 (Iwashita *et al.*, 2011), were reported for matrix separation and/or REEs pre-concentration studies. With their high metal capacity, ion-exchange resins fulfill the needs of REEs separation from technological solutions. However, they have a significant lack of selectivity, and they hardly applicable for removal of REEs from solutions with large amounts of alkaline and alkaline earth metal ions, which normally occur in high concentrations in different kinds of natural water samples.

Chelating sorbents. The lack of ion-exchange resins selectivity has driven the development of SPE adsorbents, where the extraction of metal ions is assisted by complexing agents. Organo-mineral adsorbents with immobilized chelating groups ensuring high affinity towards REEs can be a good alternative. Commonly silica is used in SPE as a support because it provides mechanical stability, high surface area (300 - 1000 m² g⁻¹), high pore volume (>1 cm³ g⁻¹) large pore diameter (3-10 nm) and good adsorption kinetics. Since REEs form strong complexes with

O-donor ligands, such type of ligands is used for immobilization. For example, diglycolylamide modified mesoporous silica was used for the recovery and enrichment of REEs (Florek *et al.*, 2014). It was demonstrated that the affinity of silica-based adsorbent towards REEs is about 8 times higher than for the resin with identical functional groups. In fact, immobilized fragments of the reported adsorbent belong to the class of N,O-donor ligands (rather than O-donor as it was suggested in the publication), as well as other silica-based adsorbents with immobilized EDTA (Dupont *et al.*, 2014) and diethylenetriaminepentaacetic acid (Zhang, H., McDowell, Rocklan G., *et al.*, 2016). In contrast to O-donor ligands, N,O-donor ligands demonstrate high affinity towards many metal ions and so no sharp selectivity to f-elements can be expected. At the same time, in most solvent extraction systems for REEs separation, O-donor chelating compounds are used as collectors. For example, hydroxamate-based collectors demonstrated very good efficiency regarding of rare earth elements (Jordens, Cheng e Waters, 2013). The enhanced selectivity of hydroxamic acid derivatives in REEs extraction was also noted in other studies and has been explained by formation of chelates with the rare earth ions (Zhang e Wu, 2015).

The *ion imprinted polymers (IIPs)* are less commonly used for REEs sorption. A novel IIP was reported for Sc(III) removal based on metal complex with 8-hydroxyquinoline as the template molecule and methacrylic acid and ethylene glycol dimethacrylate as the functional monomer and cross-linking agent (Liu *et al.*, 2013). Also, the IIPs for removal Lu(III) as Lu(III)-4-vinylpyridine-acetylacetonate complex and Nd(III) ions with N-methacryloylamido folic acid were described (Dolak *et al.*, 2015; Lai *et al.*, 2012).

Carbon nanostructures. Carbon nanoparticles, nanotubes (CNTs) or nanofibers are widely used recently in solid-phase extraction. The nature of the surface of carbon nanostructures is complex, depend on the raw material and on the method of production, commonly has a larger number of oxygen-containing functional groups (–OH, –C=O and –COOH), which respond for sorption of ionic species, as rare earth element ions, by electrostatic forces (Pyrzynska, Kubiak e Wysocka, 2016). Oxidized multi-walled carbon nanotubes (MWCNTs) were used for on-line preconcentration of scandium before its ICP OES determination in acid mine drainage (Jerez *et al.*, 2014). Analysis of rare earth elements in seawater by ICP OES was performed after their pre-concentration by highly dispersive MWCNTs (Cho *et al.*, 2012). In this work (Liang, Liu e Guo, 2005) MWCNTs were used for preconcentration of some REEs traces (La, Sm, Eu, Gd, Tb, Yb Ho) from water samples. As shown in the works above, REEs are poorly adsorbed onto

CNTs at low pH, different pH values were reported as optimal for preconcentration of REEs – from 1.5 up to 4.0. A novel two-dimensional structure carbon nanomaterial - graphene oxide nanosheets (GONS) were used for Eu(III) adsorption (Sun *et al.*, 2012). The maximum adsorption capacity of Eu(III) on GONS was found much higher than any currently reported (175.44 mg g⁻¹).

Core/shell nanoparticles. Core/shell nanoparticles attract attention mainly because the different properties can be combined in one material by adjusting the composition of the core and shell. Zhang and coworkers used microcolumn packed with TiO₂-graphene composite in on-line flow injection system for preconcentration of La, Tb, and Ho (Zhang *et al.*, 2011). Magnetic core/shell sorbent composed of activated carbon and Fe₂O₃ nanoparticles has been used for the preconcentration of La, Sm, Nd, and Pr and their further determination in soil (Tajabadi, Yamini e Sovizi, 2013). Fe₃O₄@SiO₂@polyaniline-graphene oxide adsorbent has been proposed for magnetic solid-phase extraction of trace REEs before their determination in tea leaves and environmental water (Su *et al.*, 2014).

1.6. Chelating organo-silica adsorbents

Immobilizing organic reagents on the surface layers or in the bulk of a solid phase (matrix) is the most popular direction of creation of new adsorbent materials for SPE and are introduced into the practice of chemical analysis, in combination with a variety of analytical methods. The organic active components can be fixed on the surface by physical or chemical interactions. The latter is preferable, since they allow to achieve significantly greater stability of obtained materials to various environmental influences and, consequently, greater stability of action of surface-modified materials.

Both polymers and mineral matrices are used as carriers for grafting various compounds. The advantages of the mineral matrix include chemical resistance, mechanical strength, non-swelling in various solvents, thermal stability, radiation resistance, and high mass transfer rate. Silica gel received widespread use as a mineral matrix for chemical modification due to the availability of their various forms, which possess the required structural characteristics - granulation, particle shape, pore size, and specific surface. Silicagel-based materials demonstrate good adsorption kinetics, high surface area (up to 800 m²/g). Additional advantage of silica-based materials is good hydrolytic stability in a wide pH range (from 0.0 to 8.5) and well-developed surface chemistry. Analysis of literature using the Scopus database shows that over the past 15 years, the interest of researchers in modified

silica gels has grown steadily, new types of materials with grafted functional groups have been developed, suitable for extraction and separation of different analytes, methods for their fabrication are being improved, and the previously described applications are being expanded.

For the preparation of new modified silica gels exotic reagents - calixarenes, fullerenes, macrocycles, and well-known analytical reagents from spectrophotometric methods of analysis are used. The requirements for the nature of organic reagents are determined by the analytical method in which it is used. For example, widely used in analytical chemistry for separation and metal concentrations found chelating covalently modified silica gels (Ramasamy, Khan, *et al.*, 2017; Repo, Kurniawan, Warchol e Sillanp, 2009; Repo, Kurniawan, Warchol e Sillanpää, 2009; Zhang, H., McDowell, Rocklan G, *et al.*, 2016). The determination of organic compounds requires that the reagent molecule contained specific groups able to react with functional groups of determined compounds with the formation of easily detected products. That's why the nature of the organic reagent is one of the key factors defining the selectivity of the method.

Thus, one of the most promising ways of obtaining new materials is the chemical grafting of various compounds on solid substrates. Indeed, highly selective sorbents, immobilized enzymes, sensors, heterogeneous metal complex catalysts, stationary phases for liquid and gas chromatography, polymer fillers, emulsion stabilizers and many other materials received by chemisorption of one or another active component on a suitable matrix. The chemical properties of such materials are determined by the nature of the fixed compound, while the mechanical ones are determined by the nature of the matrix.

It is not possible to cover all areas of application of chemically modified silica gels. Thus, this section will be dedicated to chemically modified silica gels mostly with chelating properties toward transition metals.

Chelating covalently modified silicas can be classified according to classification of ligands in the chemistry of coordination compounds (Vladimir N. Zaitsev, 1997). According to this classification, silicas can bind metal ions: due to the formation of donor-acceptor bond; by ion-exchange mechanism; due to the formation of complexes with charge transfer; forming associates according to the guest – host mechanism (Vladimir N. Zaitsev, 1997). The most numerous groups of chelating covalently modified silica gels are with grafted electron-donor atoms. The property of chelating sorbent to bind metal ions under certain conditions is determined by the nature of functional groups and/or donor atom. The largest and most important groups of chelating silica gels contain N,O,S- donor atoms.

Generally, N,O-containing ligands have selectivity towards transition metals and sulfur-containing ligands towards heavy or low-charge metals (such as Pd, Pt, Au, Ag). Several organo-silicas with immobilized N,O-donor ligands have been applied for REE adsorption (Dupont *et al.*, 2014; Zhang, H., McDowell, Rocklan G., *et al.*, 2016) and demonstrated great potential. But, in fact, no one from known adsorbent demonstrated high enough selectivity towards REEs. Essential difficulties exist for separation of REEs on individual elements.

Some examples of the structure of chemically modified silica gels with ligands coordinating mostly through N-atom, N,O-atoms and O-atom are presented in the Table 2-Table 4.

Among the vast variety of N,O-containing silica gels by type of functional group on the surface, the most common classes of materials contain amino- and imino-, aminocarboxy-, aminophosphonic-, ureido-, azo-groups, or fragments with nitrogen-containing heterocycles.

Table 2. Examples of ligands coordinating through N-atom.

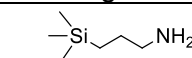
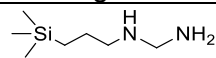
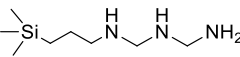
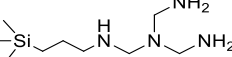
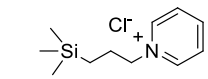
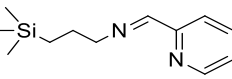
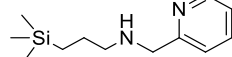
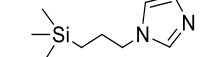
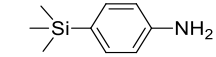
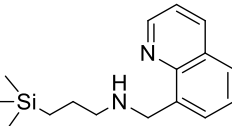
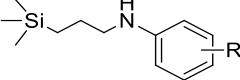
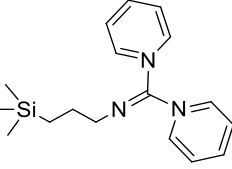
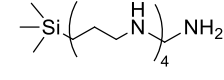
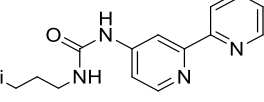
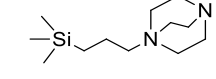
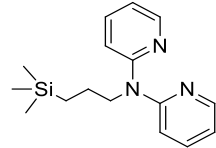
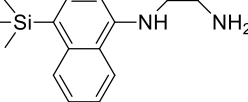
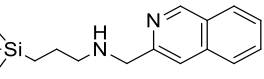
n	Ligand	n	Ligand
1.		11.	
2.		12.	
3.		13.	
4.		14.	
5.		15.	
6.		16.	
7.		17.	
8.		18.	
9.			
10.			

Table 3. Examples of ligands coordinating through N- and O-atoms.

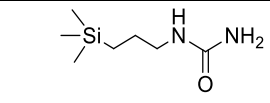
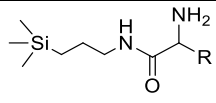
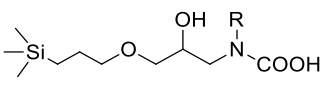
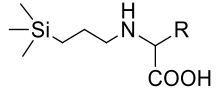
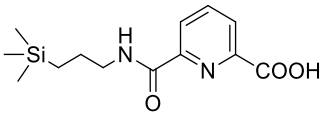
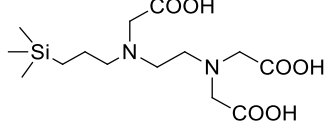
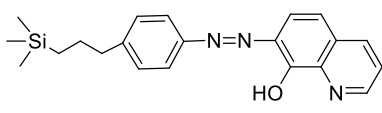
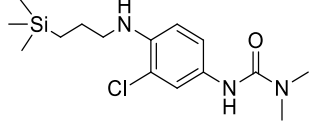
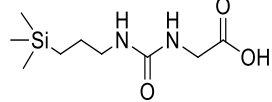
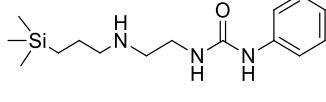
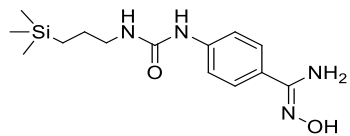
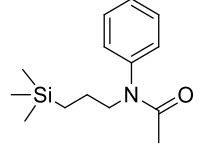
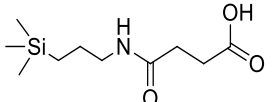
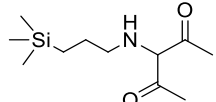
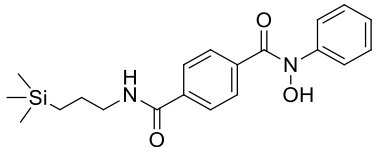
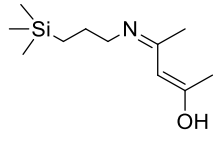
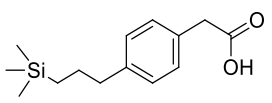
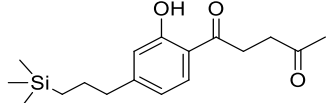
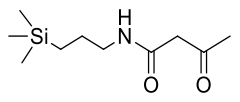
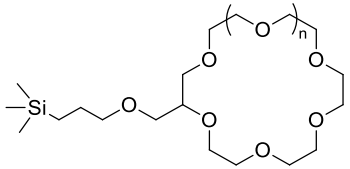
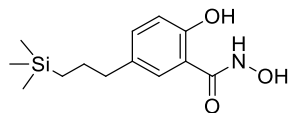
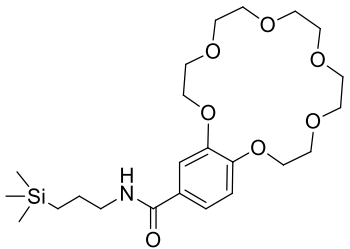
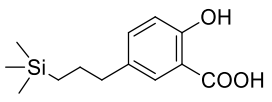
n	Ligand	n	Ligand
1.		7.	
2.		8.	
3.		9.	
4.		10.	
5.		11.	
6.		12.	

Table 4. Examples of ligands coordinating through O-atom.

n	Ligand	n	Ligand
1.		7.	
2.		8.	
3.		9.	
4.		10.	
5.		11.	
6.			

Analysis of the structures in Table 2-Table 4 leads to an important conclusion: the variety of surface-modified silica gels is inexhaustible. Indeed, by the end of the twentieth century, from 12 to 15 million chemical compounds were known; and there is no limit in the synthesis of new substances. Consequently, the set of grafted surface compounds is open. In addition, a wide range of parameters of surface-modified materials can vary: the chemical nature of the fixed substance, the morphology and chemical nature of the matrix, the structure and length of the spacer leg and, finally, the structure of the grafted layer. The grafted layer can be monomeric or polymeric, dense or loose, mono- and polyfunctional. The distribution of grafted molecules may also be different: statistically erratic, islet or regular. It is possible to design a structure when the inner surface of the pores (in the porous matrix) is modified by groups of the same nature, and the outer surface of the particles is different.

Extraction of metal ions using chelating sorbents has several advantages (Zougagh, Cano Pavón e Garcia De Torres, 2005): 1) selectivity is achieved using a chelating sorbent with ligand processing high selectivity to the targeted metal ion; 2) phase separation is facilitated in comparison with conventional liquid-liquid extraction method; 3) the application of chelating sorbents is more cost-effective since it uses only a small amount of ligand, and free from difficult phase separation; 4) metals can be concentrated on the solid phase, which significantly increases the sensitivity of the method; 5) the technique is eco-friendly, the use of carcinogenic organic solvents is minimized.

8-Hydroxyquinoline immobilized on silica gel is one of the most famous chelating sorbent used for separation of trace metals (Bernal *et al.*, 2000; Esser *et al.*, 1994; Fazaeli *et al.*, 2019; Jezorek e Freiser, 1979; Kotlyar, Yanishpol'skii e Tertykh, 1989; Ryabchenko *et al.*, 2013; Slebioda *et al.*, 1994; Sturgeon *et al.*, 1981, 1983; Yanovska *et al.*, 2006). This chelating sorbent has been used for preconcentration of trace elements, since early 80 (Sturgeon *et al.*, 1981) and until 2019 (Fazaeli *et al.*, 2019), the interest is not lost. Sturgeon and coworkers have used this chelating sorbent for preconcentration of Cd^{2+} , Pb^{2+} , Zn^{2+} , Cu^{2+} , Fe^{2+} , Mn^{2+} and Ni^{2+} from seawater (Sturgeon *et al.*, 1981). This sorbent was found to permit large enrichment factor, rapid processing of large volume samples, quantitative recovery and matrix-free concentrate. This adsorbent also was used (Lührmann, Stelter e Kettrup, 1985) for sorption of Cu^{2+} , Ni^{2+} , Co^{2+} , Fe^{3+} , Mn^{2+} , Cd^{2+} , Pb^{2+} , Cr^{3+} , Zn^{2+} , and Hg^{2+} .

Metal adsorption on modified silicas mainly depends on the nature of immobilized groups and composition of complexes. But due to the multifunctional

nature of the surface, it also depends on additional interaction of metal ions with residual aminopropyl and silanol groups. Therefore, it is varied from sample to sample and must be studied for every case. For example, in the study of the adsorption properties of the 3-aminopropylated materials (Table 2, №1), Tong and coworkers have found that adsorbent able to remove quantitatively Au^{3+} , Pt^{4+} and Pd^{2+} from solution in the pH range 3-5 in the presence of Cu^{2+} and Fe^{3+} interfering ions (Tong, Akama e Tanaka, 1990). At the same time, Erdem and coworkers have obtained a material with the same functional group and used it for separation and determination of V^{5+} and V^{4+} (Erdem *et al.*, 2011).

Phosphonates - effective chelating agents, which process chelating due to coordinate more than one pair of donor ligand to a central metal atom. And the stability of metal complexes increases with an increasing number of phosphonic groups. Alkyldiphosphonic acids are under significant interest because demonstrate higher specificity of interaction with a number of cations (Knepper, 2003). Cation exchangers, with immobilized aminodiphosphonic groups have been obtained (Kingdom *et al.*, 1999; Kostenko, S.A. Ahmedov e V.N. Zaitsev, 2006). Such silica gels (SG-AdPA) form stable complexes with metals (for complex with Cu^{2+} $\beta_1 = 10.03$), have perspectives in selective separation and concentration relative to the cations Fe^{3+} , Cu^{2+} , Pb^{2+} , Cd^{2+} and Zn^{2+} . These compounds have a donor function of amine nitrogen atoms and oxygen atoms phosphonic group capable of chelating lock loops form different relationships and take various conformations in accordance with the configuration of metal ions.

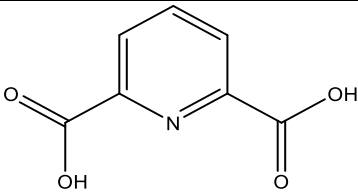
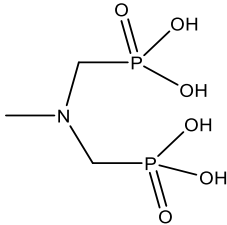
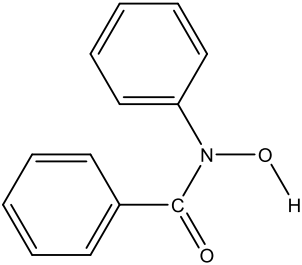
In the reaction of 3-chloropropyl-silica with N-(2-pyridyl)acetamide material with functionalization $1.57 \cdot 10^{-4} \text{ mol g}^{-1}$ has been obtained (Airoldi e Alcantara, 1995). This material has a great ability to chemisorb cations from propanonic or ethanolic solutions. The sequence of the maximum capacity is $\text{Cu}^{2+} > \text{Co}^{2+} > \text{Zn}^{2+}$ in propanone and $\text{Hg}^{2+} > \text{Cd}^{2+} > \text{Zn}^{2+} > \text{Co}^{2+} > \text{Cu}^{2+} > \text{Ni}^{2+}$ in ethanol. Silica gels with covalently immobilized fragments of amide of isonicotinic acid were obtained by silylation of mesoporous silica MCM-48 and SBA-15 with N-[3-(Triethoxysilyl)propyl]isonicotinamide (Sadeghi *et al.*, 2011). Pyridine-functionalized silica gels were used for the extraction, pre-concentration, and electrothermal atomic absorption spectrometric determination of nickel and lead in food samples at ppm levels.

2,6-Pyridinedicarboxylic acid has been covalently immobilized through the formation of the acid chloride, which is acylated with 3-aminopropyl silica gel (Zhang *et al.*, 2010). It has been shown that this adsorbent has the highest affinity for the Hg^{2+} ; the maximum capacity has been 92 mg g^{-1} . Sorption conditions of

Hg²⁺ has been optimized in static and dynamic mode. Quantitative desorption was possible with 2 mL of 0.1 mol L⁻¹ HCl and 3% thiourea.

The popularity of EDTA arises from its strong metal chelating ability, local availability, and low price. Single-stage production of EDTA-silica gel (Ohshima, Watanabe e Haraguchi, 1986) has been carried out by treating commercially available silica with N-[(3-trimethoxysilyl)propyl]ethylenediamine triacetic acid trisodium salt in ultrasonic activation reactions and subsequent continuous stirring for 3 hours. The content of chelating groups in the resulting material calculated from elemental analysis has been 161 μmol g⁻¹. The adsorption properties were studied with respect to Cu²⁺, Ni²⁺, Pb²⁺, Zn²⁺, Co²⁺, Cd²⁺, Ca²⁺, Mn²⁺. From immobilization of 3-aminopropyl silica with anhydrides of ethylenediamine-tetraacetic and diethylenetriamine-pentaacetic acids were obtained silica gels suitable for the separation of mixture of Cu²⁺, Ni²⁺, VO²⁺, Zn²⁺, Co²⁺, Mn²⁺ and recovering Co²⁺ and Ni²⁺ from aqueous samples (Repo, Kurniawan, Warchol e Sillanpää, 2009; Shiraishi *et al.*, 2002).

In this work among various O-donor chelating ligands, derivatives of next three were selected for immobilization:

1	2,6-pyridinedicarboxylic acid	
2	aminobis(methylene phosphonic) acid	
3	phenylhydroxamic acid	

Derivatives of 2,6-pyridinedicarboxylic acid are widely used in chemistry of REE and give very stable complexes with high quantum yield of fluorescence (Barja *et al.*, 2011). Derivatives of aminophosphonic acids are well known as P-containing analog of aminopolycarboxylic acids. In contrast to the latter,

aminophosphonic acids form strong complexes only with large highly charged metal ions (Queffélec *et al.*, 2012). Hydroxamate derivatives recently demonstrated higher selectivity in beneficiation of rare earth elements from concentrate (Jordens, Cheng e Waters, 2013; Wanhala *et al.*, 2019).

2 Objectives

The main objective of the research is focused on the development of reusable adsorbents for selective recovery and separation of REEs from complex metal-containing solution.

To reach the main project goal, the next specific objectives will be investigated:

- The following silica-based adsorbents will be synthesized:
 - silica gel with covalently immobilized 2,6-pyridinedicarboxylic acid (SiO₂-PdCA);
 - silica gels with covalently immobilized amino-di(methylene phosphonic) acid (SiO₂-AdMPA) and amino-di(ethylene phosphonic) acid (SiO₂-AdEPA);
 - silica gel with covalently immobilized N-benzoyl-N-phenylhydroxylamine (SiO₂-BPHA).
- The materials will be characterized by various methods including FTIR, X-ray photoelectron spectroscopy, solid-state NMR spectroscopy.
- Concentration and chemical nature of immobilized groups will be determined from elemental analysis, thermogravimetric analysis, pH-metric analysis.
- Adsorption properties of the adsorbents towards REEs ions will be investigated in pH range of the adsorbent stability (0.5-8.5) and, particularly, the next characteristics will be studied:
 - The adsorbent total adsorption capacity;
 - Metal adsorption isotherms;
 - REEs adsorption kinetics;
 - Adsorption characteristics of the organo-silicas as function of the solution acidity;
 - Influence of concentration of matrix ions of the adsorbent's analytical characteristics (recovery degree).
- Conditions of metal desorption will be studied in order to optimize REEs desorption and the metals recovery.

- Reusability of the adsorbents will be analyzed in optimum conditions.
- The adsorbents will be applied for dispersive solid-phase extraction (DSPE) and separation of the REEs.
- The proposed adsorbents will be used for selective recovery of REEs from waste of fluorescent lamps.

3 Experimental procedure

3.1. Materials and methods

Chemicals and reagents

Silica gel (technical grade, pore size 60 Å, 40-63 µm particle size), silica gel (high-purity grade, pore size 90 Å, 63-200 µm particle size), (3-Aminopropyl)triethoxysilane (APTES, ≥98%), Phosphorous acid (99%), Paraformaldehyde (reagent grade), Formaldehyde solution (ACS reagent, 37 wt.% in H₂O), Acetaldehyde (≥99.0%), 2,6-pyridinedicarbonyl dichloride (≥97%), N,N-Diisopropylethylamine (diPEA, 99.5%), Pyridine (≥99.0%), Ninhydrin (ACS reagent), Terephthaloyl chloride (>99%), Zinc (PA), Ethylenediaminetetraacetic acid disodium salt dihydrate (EDTA, 99%), Nitric acid (ACS reagent, 70%), Hydrochloric acid (reagent grade, 37%), Acetic acid (HPLC, 98%), 5-Sulfosalicylic acid (SSA, ACS reagent, ≥99%), Citric acid (CiA, 99.5%), Aminosulfonic acid (AmSA, 98%), α-hydroxyisobutyric acid (HBA, 98%), Oxalic acid (OxA, ACS reagent, ≥99%), Ascorbic acid (AsA, reagent grade) all were purchased from Merck, as well as Toluene (99.9%), Ethanol (99.8%), Acetonitrile (for HPLC, ≥99.9%), N,N-dimethylformamide (DMF, 99.8%), Dipropylene glycol (99%), Diethylene glycol dimethyl ether (DIGLYME, 99%), Dichloromethane (≥99.5%), Nitrobenzene (≥99%). Toluene and N,N-dimethylformamide were used after distillation with CaH₂. Nitrobenzene and nitric acid - after distillation, the other reagents were used without further purification.

Copper(II) sulfate pentahydrate (≥98%), Iron(III) nitrate nonahydrate (≥98%), Europium(III) chloride hexahydrate (≥99.9%), Terbium(III) chloride hexahydrate (≥99.9%), Lanthanum(III) oxide (≥99.9%) and ICP multi-element standard solution IV (1000 mg L⁻¹: Ag, Al, B, Ba, Bi, Ca, Cd, Co, Cr, Cu, Fe, Ga, In, K, Li, Mg, Mn, Na, Ni, Pb, Sr, Tl, Zn in 2% nitric acid), ICP Copper standard solution (Cu(NO₃)₂ in HNO₃, 1000 mg L⁻¹ Cu), ICP Iron Standard solution (Fe(NO₃)₃ in HNO₃, 1000 mg L⁻¹ Fe), Barium ICP standard (Ba(NO₃)₂ in HNO₃, 1000 mg L⁻¹ Ba), Rare earth element mix for ICP (100 mg L⁻¹ each: Sc, Y, La, Ce, Pr, Nd, Sm, Eu, Gd, Tb, Dy, Ho, Er, Tm, Yb and Lu in 2% nitric acid) were also purchased from Merck. Stock solutions of metals with concentration of 1000 mg L⁻¹ were prepared by dissolving required amount of their salts or oxide in water or nitric acid, respectively. The

working solutions of desired concentration were prepared by dilution of the stock solution. Ultrapure water was used in all experiments.

The lamp phosphor residue was obtained from an authorized waste repository for discarded lamps at Pontifical Catholic University of Rio de Janeiro, Brazil.

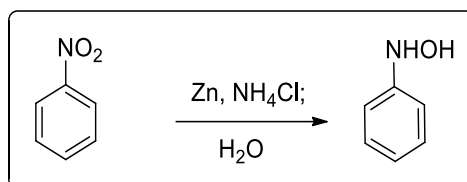
Equipment

FT-IR spectra were obtained on FTLA-2000 spectrometer (ABB), covering the range 400 a 4000 cm^{-1} . Specific surface area of the silica was determined using nitrogen adsorption on ASAP 2020 (Micrometrics). The determination of carbon, hydrogen, and nitrogen (CHN) content was performed on elemental analyzer PE-2400 (Perkin Elmer). Thermogravimetric analyses were performed on Pyris 1 TGA (Perkin Elmer) in temperature range 25-800 $^{\circ}\text{C}$ and the heating rate of 10 $^{\circ}\text{min}^{-1}$. X-ray photoelectron spectra (XPS) were measured on Escalab 250Xi x-ray photoelectron spectrometer (Thermo Scientific). The concentrations of metal ions in solution were determined on Optima 7300 DV Inductively Coupled Plasma Optical Emission Spectrometry, ICP OES (Perkin Elmer) or Nexlon 300X Inductively Coupled Plasma Mass Spectrometry, ICP-MS (Perkin Elmer). Luminescent properties of functionalized materials were studied using TGM (Toroidal Grating Monochromator) beam line with energy range of 3 to 330 eV (400 to 4 nm) in the Brazilian Synchrotron Light Laboratory. ^1H and ^{13}C NMR spectra were recorded on a Bruker DPX-400. ^1H NMR spectrum was referenced to CDCl_3 (7.26 ppm) and ^{13}C NMR spectra were referenced to CDCl_3 (77.0 ppm). The ^{13}C spectrum was measured with complete proton decoupling. Solid-state NMR spectroscopy was carried out on Bruker Avance III HD spectrometer (7.05 T). ^{31}P , ^{29}Si , and ^{13}C NMR experiments were performed at Larmor frequency of 121.00, 59.6 and 75.00 MHz, respectively. The surface morphology of neat and modified silica gel particles was observed with scanning electron microscopy, SEM (JEOL JSM 6490 LV). Measurements of the pH of solutions were performed by a laboratory ion-meter PHS-3E combined with Hamilton Minitrode pH electrode. Measurements of electric conduction of chemically modified silicas suspensions were performed on HI 8633 conductivity meter (HANNA instruments).

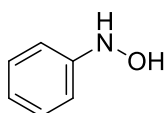
3.2. Synthesis of reagents

3.2.1. Synthesis of *N*-phenylhydroxylamine

N-phenylhydroxylamine was synthesized by the reduction of nitrobenzene by zinc dust, Scheme 1 (Oliver Kamm, 1925). In reaction flask, equipped with mechanical stirrer ammonium chloride (1.25 g; 23.5 mmol) in water (40 mL) and nitrobenzene freshly distilled (2.5 g, 20.5 mmol) were added. Activated zinc dust (3.1 g, 47.7 mmol) was slowly added while maintaining the temperature between 60-65 °C under mechanical stirring. After 1 hour, the reaction mixture was filtered while still warm and the solid was washed with hot water (2 x 10 mL). The filtrate was saturated with NaCl and cooled to 0 °C and the resultant solid was collected and dried. This crude *N*-phenylhydroxylamine was recrystallized from hexane-petroleum ether. The deposited colorless crystals of *N*-phenylhydroxylamine were filtered, and, without washing, were dried in vacuum (50% of yield).



Scheme 1. Synthesis of *N*-phenylhydroxylamine.



The product was obtained as white crystals (250 mg). ¹H NMR (400 MHz, CDCl₃) δ: 7.34-7.30 (m, 2H), 7.04-7.00 (m, 3H), 6.15 (s, 1H). ¹³C NMR (100 MHz) δ: 149.6, 129.0, 122.4, 114.7. IR (KBr, cm⁻¹): 3245, 3102, 3060, 2846, 1604, 1521, 1497, 1091.

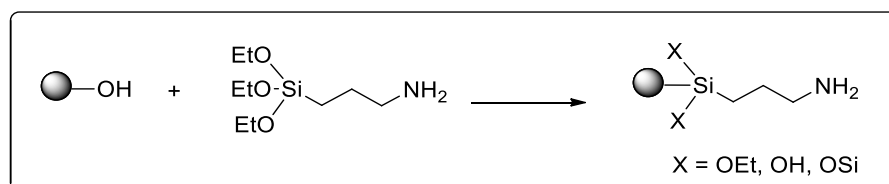
3.3. Functionalization of materials

3.3.1. Cleaning and activation of silica gel

Before utilization in synthesis, silica gels were treated to hydroxylate the surface and remove impurities, trace metals and organic compounds adsorbed during storage. In a round bottom flask were dispersed 50 g of each silica gel in HNO₃ solution (300 mL, 3 mol L⁻¹). The formed suspension was refluxed under stirring for 2 h. Then the silica gels were filtered and washed several times with deionized water until neutralization (minimum value of electrical conductivity) and dried at 120 °C under vacuum for 6 h and activated at 500 °C for 6 h.

3.3.2. Synthesis of amino-functionalized silica gel

Amino-functionalized silica gel ($\text{SiO}_2\text{-NH}_2$) was obtained according to the Scheme 2. A 15 g of silica gel, activated according to paragraph 3.3.1, was suspended in absolute toluene (100 mL) and placed in a round bottom flask equipped with a magnetic stirrer and a reflux condenser protected from atmospheric action with a calcium chloride tube. Then, there was added 3-aminopropyltriethoxysilane (3.6 mL) in absolute toluene (100 mL), the reaction mixture was heated to 100 °C and kept under constant stirring for 12 h. After cooling, the solid phase of amino-functionalized silica gel was filtered and washed in a Soxhlet apparatus with absolute toluene until negative reaction on amine with 1% solution of ninhydrin in ethanol. Then, the solution was dried under vacuum at 120 °C before use.

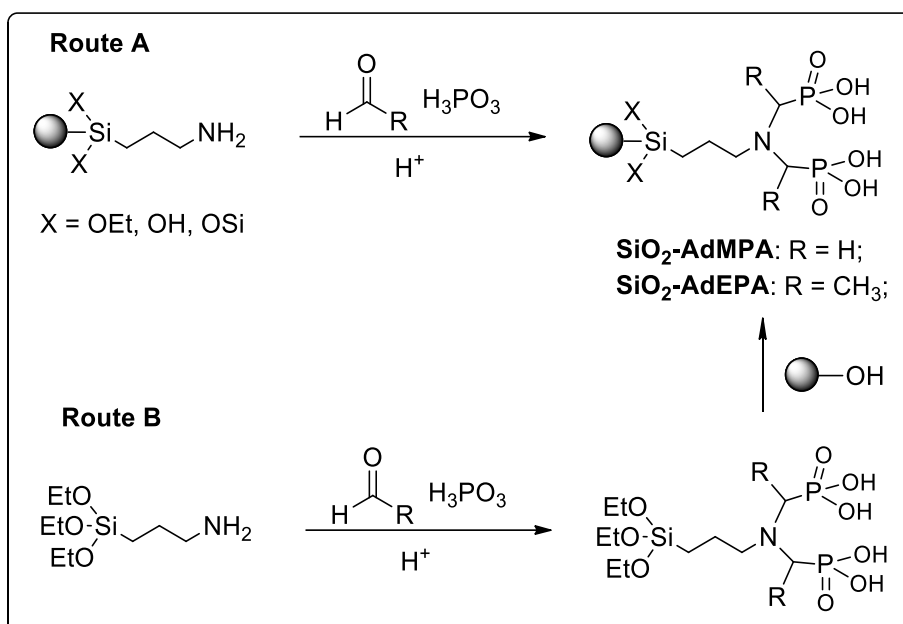


Scheme 2. Surface functionalization of silica gel with APTES.

3.3.3. Synthesis of silica gel with immobilized aminophosphonic acids

There are two main approaches (Queffélec *et al.*, 2012) for surface modification of silica gel with phosphonic acids (Scheme 3): the direct introduction of these groups (Route A) or coupling reactions using suitably functionalized phosphonate reagents (Route B). We have tested both approaches for the synthesis of silica gels with amino-di(methylene phosphonic) acid group ($\text{SiO}_2\text{-AdMPA}$) and amino-di(ethylene phosphonic) acid group ($\text{SiO}_2\text{-AdEPA}$).

Adsorbents $\text{SiO}_2\text{-AdMPA}^{1-3}$ and $\text{SiO}_2\text{-AdEPA}^{1-4}$ have been synthesized by introduction of phosphonic acid groups on organic substrates. The reactions of surface modification of silica gels $\text{SiO}_2\text{-AdMPA}^{1-3}$ and $\text{SiO}_2\text{-AdEPA}^{1-4}$ are shown in Scheme 3 (Route A). For $\text{SiO}_2\text{-AdMPA}^{4-6}$ and $\text{SiO}_2\text{-AdEPA}^{5-6}$ initially modification agent was synthesized and further, it was grafted to the surface. The reactions of surface modification of silica gels $\text{SiO}_2\text{-AdMPA}^{4-6}$ and $\text{SiO}_2\text{-AdEPA}^{5-6}$ are shown in Scheme 3 (Route B).



Scheme 3. Surface functionalization of silica gel with aminophosphonic acids.

SiO₂-AdMPA¹. In a round bottom flask, equipped with mechanical stirrer and reflux condenser, were dispersed a 7.0 g ($C_L \sim 7$ mmol) of 3-aminopropyl-silica gel obtained according to paragraph 3.3.2 in 30 mL of 1M hydrochloric acid. The reaction was kept under stirring for 45 min for protonation of amino groups. Then aqueous solution of 1.2 g of phosphonic acid (14 mmol) and 7 ml of 7% aqueous formaldehyde solution (14 mmol) were slowly mixed under heating (110 °C) and rapid stirring. The reaction mixture was refluxed for 6 h. The progress of the reaction was monitored by analysis of the residual amino groups with a 1% solution of ninhydrin in ethanol. After cooling to room temperature, the solid phase was separated by filtration, washed in a Soxhlet apparatus with ethanol during 24h and dried at 120 °C for 8h under vacuum.

SiO₂-AdMPA². In similar synthesis to the SiO₂-AdMPA¹ a 14.0 g of 3-aminopropyl-silica gel reacted with an aqueous solution of 2.4 g of phosphonic acid and 14 ml of 7% aqueous formaldehyde solution under inert dry nitrogen atmosphere.

SiO₂-AdMPA³. In similar synthesis to the SiO₂-AdMPA¹ a 5.0 g of 3-aminopropyl-silica gel reacted with 0.8 g of phosphonic acid in dipropylene glycol and 5 ml of 7% solution of formaldehyde in dipropylene glycol. For protonation of amino groups 1 mol L⁻¹ hydrochloric acid in dipropylene glycol was used. For washing in a Soxhlet apparatus was used dipropylene glycol.

SiO₂-AdMPA⁴. In a round bottom flask, equipped with mechanical stirrer, were mixed 5 mL of 7% solution of formaldehyde in diglyme, 5 mL of diglyme

acidified with hydrogen chloride and 5 ml of solution of 0.8 g phosphonic acid in diglyme. Then, 1.2 mL of 3-aminopropyltriethoxysilane was added. After 15 min a 5 g of silica gel, activated according to paragraph 3.3.1, was added. The reaction was kept under stirring and heating (90 °C) for 4h. The progress of the reaction was monitored by analysis of the residual amino groups with a 1% solution of ninhydrin in ethanol. After cooling to room temperature, the solid phase was separated by filtration, washed in a Soxhlet apparatus with ethanol during 24h and dried at 120 °C for 8h under vacuum.

SiO₂-AdMPA⁵. In this synthesis initially were mixed 5 mL of 7% solution of formaldehyde in diglyme, 5 mL of 1 mol L⁻¹ hydrochloric acid in diglyme and 5 mL solution of 0.8 g phosphonic acid in diglyme. Further procedures were performed as in synthesis SiO₂-AdMPA⁴.

SiO₂-AdMPA⁶. In this synthesis initially were mixed solution of 1.2 mL of 3-aminopropyltriethoxysilane in diglyme, 5 mL of 1 mol L⁻¹ hydrochloric acid in diglyme and 5 mL of solution of 0.8 g phosphonic acid in diglyme. Then to the mixture was slowly added solution of 1.1 mL of 37% formaldehyde in diglyme. Further procedures were performed as in synthesis SiO₂-AdMPA⁴.

SiO₂-AdEPA¹. In this synthesis initially 1.0 g of 3-aminopropyl-silica gel was suspended in diglyme. Then 0.6 ml of acetaldehyde was added. After that to the mixture 5 mL of solution of 0.8 g phosphonic acid were added in diglyme and 2 mL of 1 mol L⁻¹ hydrochloric acid in diglyme. The reaction was kept under stirring and heating (90 °C) for 4h. The progress of the reaction was monitored by analysis of the residual amino groups with a 1% solution of ninhydrin in ethanol. After cooling to room temperature, the solid phase was separated by filtration, washed in a Soxhlet apparatus with ethanol during 24h and dried at 120 °C for 8h under vacuum.

SiO₂-AdEPA². In similar synthesis to the SiO₂-AdEPA¹ a 5.0 g of 3-aminopropyl-silica gel was protonated with 1M hydrochloric acid in diglyme and then reacted with 0.8 g of phosphonic acid and 0.6 ml of acetaldehyde.

SiO₂-AdEPA³. In similar synthesis to the SiO₂-AdEPA¹ a 5.0 g of 3-aminopropyl-silica gel was protonated with 1M hydrochloric acid in diglyme and then reacted with 5 mL of solution of 1.6 g phosphonic acid and 1.2 ml of acetaldehyde.

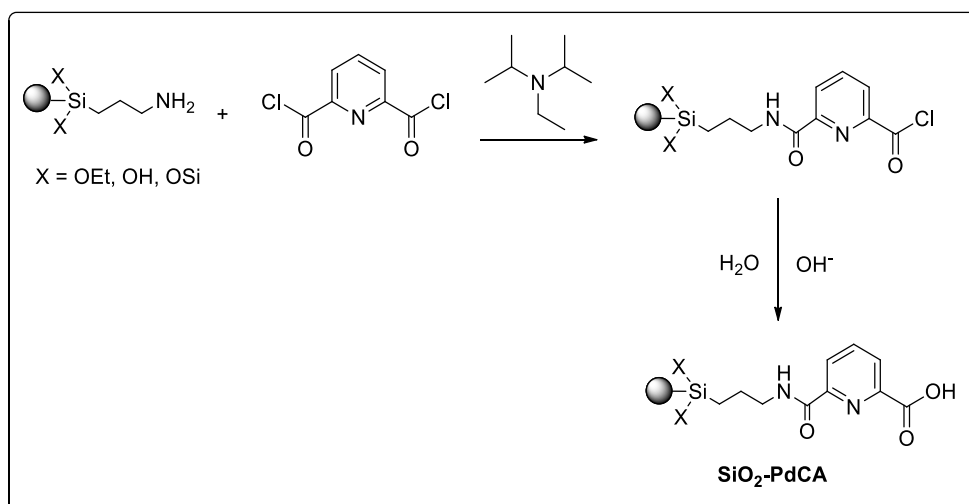
SiO₂-AdEPA⁴. In similar synthesis to the SiO₂-AdEPA¹ a 5.0 g of 3-aminopropyl-silica gel was protonated with 1.6 mL of hydrochloric acid in methanol and then reacted with 4.1 g of phosphonic acid and 2.9 ml of acetaldehyde. For

washing in a Soxhlet apparatus was used methanol during 24h and then DMF for further 24h.

SiO₂-AdEPA⁵. In a round bottom flask, equipped with mechanical stirrer, 10 mL of each solution were mixed: 1.2 mL of acetaldehyde in diglyme, 1M hydrochloric acid in diglyme and 1.6 g phosphonic acid in diglyme. Then the 1.2 mL of 3-aminopropyltriethoxysilane was added. After 15 min, 5 g of silica gel, activated according to paragraph 3.3.1, was added. Further procedures were performed as in SiO₂-AdEPA¹ synthesis.

SiO₂-AdEPA⁶. In this synthesis similar to the SiO₂-AdEPA⁵ initially were mixed solutions of 1.2 mL of 3-aminopropyltriethoxysilane in diglyme, 1M hydrochloric acid in diglyme and 0.8 g phosphonic acid in diglyme. Then to the mixture solution of 1.2 mL of acetaldehyde in diglyme was slowly added.

3.3.4. Synthesis of silica gel with immobilized 2,6-pyridinecarboxylic acid



Scheme 4. Surface functionalization of silica gel with 2,6-pyridinedicarbonyl dichloride.

The reaction of preparation of silica gel with immobilized 2,6-pyridinecarboxylic acid (SiO₂-PdCA) is shown in Scheme 4.

SiO₂-PdCA¹. In a round bottom flask, equipped with mechanical stirrer, and cooled to 0 °C in an ice bath, was placed mixture of 2.9 g (14 mmol) 2,6-pyridinedicarbonyl dichloride in 100 mL of N,N-dimethylformamide. Then slowly added under rapid stirring, the suspension of 7.0 g (C_L ~ 7 mmol) of 3-aminopropyl-silica gel obtained according to paragraph 3.3.2 and 3.4 mL of N,N-diisopropylethylamine in 50 mL of N,N-dimethylformamide. The reaction was kept under stirring for 12 h at room temperature. After this time, the temperature was increased to 50 °C for a further 4 h. The progress of the reaction was monitored by

analysis of the residual amino groups with a 1% solution of ninhydrin in ethanol. Then, the solid phase was separated by filtration, washed with N,N-dimethylformamide, transferred to a Becker and sodium acetate buffer was added for next 24 h (pH = 6.2) for hydrolysis of anhydride. Then adsorbent was separated by filtration, washed in a Soxhlet apparatus with acetonitrile for 24 hours and ethanol for 12 hours and dried at 120 °C for 8h under vacuum.

SiO₂-PdCA². In a round bottom flask, equipped with mechanical stirrer, a mixture of 2.1 g 2,6-pyridinedicarbonyl dichloride in 100 mL of acetonitrile was placed. Then slowly added under rapid stirring, the suspension of 5.0 g (C_L ~ 5 mmol) of 3-aminopropyl-silica gel and 8.7 mL of N,N-diisopropylethylamine in 50 mL of acetonitrile. The reaction was kept under stirring for 1h at room temperature. The progress of the reaction was monitored by analysis of the residual amino groups with a 1% solution of ninhydrin in ethanol. Further procedures of filtration and treatment with sodium acetate buffer were performed as in synthesis SiO₂-PdCA¹.

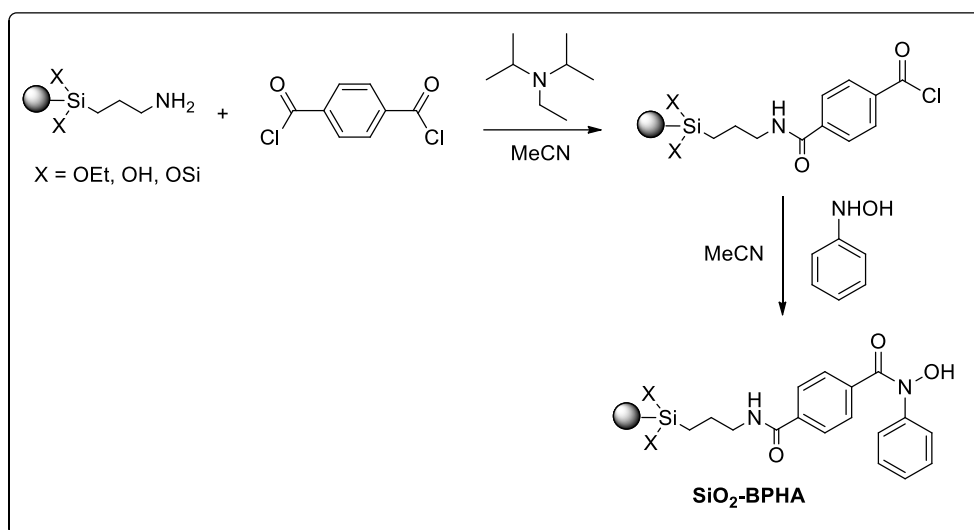
SiO₂-PdCA³. In a round bottom flask, equipped with mechanical stirrer, 0.42 g of 2,6-pyridinedicarbonyl dichloride was mixed with 1.2 mL of N,N-diisopropylethylamine in 100 mL of acetonitrile. Then 1 g of 3-aminopropyl-silica gel was added under rapid stirring. The reaction was kept under stirring for 4h at room temperature. The progress of the reaction was monitored by analysis of the residual amino groups with a 1% solution of ninhydrin in ethanol. Further procedures of filtration and treatment with sodium acetate buffer were performed as in synthesis SiO₂-PdCA¹.

SiO₂-PdCA⁴. In similar synthesis to the SiO₂-PdCA¹ 2.1 g of 2,6-pyridinedicarbonyl dichloride was mixed with 5.5 mL of pyridine in 100 mL of acetonitrile. Then 5 g of 3-aminopropyl-silica gel was added under rapid stirring. Further procedures were performed as in synthesis SiO₂-PdCA¹.

SiO₂-PdCA⁵. In similar synthesis to the SiO₂-PdCA¹ 2.1 g of 2,6-pyridinedicarbonyl dichloride was mixed with 8.4 mL of N,N-diisopropylethylamine in 100 mL of dichloromethane. Then 5 g of 3-aminopropyl-silica gel was added under rapid stirring. Further procedures were performed as in synthesis SiO₂-PdCA¹.

SiO₂-PdCA⁶. In similar synthesis to the SiO₂-PdCA¹ 2.1 g of 2,6-pyridinedicarbonyl dichloride was mixed with 5.5 mL of pyridine in 100 mL of dichloromethane. Then 5 g of 3-aminopropyl-silica gel was added under rapid stirring. Further procedures were performed as in synthesis SiO₂-PdCA¹.

3.3.5. Synthesis of silica gel with immobilized hydroxamic acid



Scheme 5. Surface functionalization of silica gel with N-Benzoyl-N-phenyl-hydroxylamine.

The reaction of surface modification of silica gels with N-Benzoyl-N-phenyl-hydroxylamine with resulting SiO₂-BPHA adsorbent is shown in Scheme 5.

SiO₂-BPHA¹. Silica gel with covalently immobilized N-Benzoyl-N-phenylhydroxylamine (SiO₂-BPHA) has been obtained in two-step surface assembling reaction:

1st step: in a round bottom flask, equipped with mechanical stirrer, 5 g of 3-aminopropyl-silica gel was suspended in 50 mL of dry acetonitrile. Then solution of terephthaloyl chloride (0.6 g) with N,N-diisopropylethylamine (0.1 mL) in the same solvent was added. The mixture was stirred for 1h at 0 °C. The progress of the reaction was monitored by analysis of the residual amino groups with a 1% solution of ninhydrin in ethanol. Then, the solid phase was separated by decantation and washed several times with dry acetonitrile.

2nd step: fresh portion of acetonitrile (50 mL) was added to the silica together with N,N-diisopropylethylamine (0.1 mL) and N-phenylhydroxylamine (0.3 g) obtained according to 3.2.1. Then the mixture was stirred at 60 °C for 4 h. Resulting product was washed in a Soxhlet apparatus with acetonitrile for 24 h and dried at 120 °C for 8h under vacuum to remove residual solvent.

SiO₂-BPHA². In similar synthesis to the SiO₂-BPHA¹ the reaction mixture on 1st step reaction was stirred for 2 h at 0 °C. And the reaction mixture on 2nd step reaction was stirred for 8h at 60 °C.

3.4. Determination of the concentration of functional groups

The concentration of immobilized functional groups was determined from several independent measurements, including direct and indirect titration, conductometric titration and elemental analysis (CHN), P-content analysis (Kingdom *et al.*, 1999).

Elemental analysis. The concentration of the groups in surface for the 1st immobilization stage (SiO₂-NH₂) was calculated according to the equation 1:

$$C_L, mmol g^{-1} = \frac{10 \times P_e}{m_a \times n} \quad (1)$$

where P_e – percentage content of the element, %; m_a – atomic mass of the element, u; n – number of atoms of the element in the immobilized molecule.

The concentration of the groups in surface for the 2st immobilization stage (SiO₂-AdMPA, SiO₂-AdEPA, SiO₂-PdCA, SiO₂-BPHA) was calculated according to the equation 2:

$$C_L, mmol g^{-1} = \frac{10 \times \Delta P}{m_a \times n} \quad (2)$$

where ΔP_e - increase in the content of element after the second stage, %; m_a – atomic mass of the element, u; n – number of atoms of the element in the 2st stage immobilized molecule.

Direct titration. To a sample of 0.1 g of amino silica gel, obtained according to paragraph 3.3.2, 10 mL of 0.1 mol L⁻¹ potassium chloride was added and the suspension was stirred for 2 h. Titration was performed with 0.01 mol L⁻¹ hydrochloric acid. Equivalence point was determined by potentiometry. The Gran method was used for processing the results. The concentration of the groups attached to the surface was calculated according to the equation 3:

$$C_L, mmol g^{-1} = \frac{C_{HCl} \times V_{HCl}}{m} \quad (3)$$

where C_{HCl} – hydrochloric acid concentration, mol L⁻¹; V_{HCl} – volume of hydrochloric acid at the equivalence point, mL; m – weight of sample, g.

Indirect titration. To a sample of 0.15 g of amino silica gel, obtained according to paragraph 3.3.2, were added 20 mL of 0.01 mol L⁻¹ hydrochloric acid (2x molar excess), kept under stirring for 24 hours. Aliquot of 10 mL was placed in a glass beaker and titrated with 0.01 mol L⁻¹ sodium hydroxide. Equivalence point was determined by potentiometry. The concentration of the groups attached to the surface was calculated according to the equation 4,5:

$$C_L, \text{mmol g}^{-1} = \frac{C}{m}; \quad (4)$$

$$C, \text{mmol} = \frac{\eta_{HCl} - (\eta_{NaOH} - \eta_{NaOH \text{ blank}})}{V_{al}}, \quad (5)$$

where η_{HCl} – the number of moles of hydrochloric acid, mmol; η_{NaOH} – the number of moles of sodium hydroxide, mmol; $\eta_{NaOH \text{ blank}}$ – the number of moles of sodium hydroxide used for titration of blank, mmol; V_{al} – aliquot volume, mL; m – weight of sample, g.

Conductometric titration. In a sample of 0.1 g of amino silica gel, obtained according to paragraph 3.3.2, were added 20 mL of deionized water. The suspension was titrated with a 0.01 mol L⁻¹ hydrochloric acid. The electrical conductivity was measured after equilibration. The time required to reach equilibrium changed from 10 min (near the equivalence point) to several seconds (after equivalence point). The concentration of the groups in the surface was calculated according to the equation 6:

$$C_L, \text{mmol g}^{-1} = \frac{C_{HCl} \times V_{HCl}}{m}, \quad (6)$$

where C_{HCl} – hydrochloric acid concentration, mol L⁻¹; V_{HCl} – volume of hydrochloric acid in the equivalence point, mL; m – weight of sample, g.

Thermogravimetric analysis. The concentration of functional grafted groups on the surface was calculated from thermogravimetric data according to the equations 7,8:

$$C_L^{NH_2}, \text{mmol g}^{-1} = \frac{\Delta m}{m \cdot M}; \quad (7)$$

$$C_L^g, \text{mmol g}^{-1} = \frac{\Delta m_2 - \Delta m_1}{m(M_2 - M_1)}, \quad (8)$$

where $C_L^{NH_2}$ – concentration of grafted amino-groups on SiO₂-NH₂, C_L^g – concentration of functional groups for two-step modified samples; $\Delta m/m$ (mg g⁻¹) - mass loss of modified silica in the temperature range corresponding to thermal

decomposition of organic fragments per 1 g of sample mass; $\Delta m_2 - \Delta m_1$ - difference of the mass loss between two-step and one-step modified samples; M - molar mass of the grafted group ($g\ mol^{-1}$).

Determination of the phosphorus content. In a sample of 0.1 g of SiO₂-AdMPA or SiO₂-AdEPA placed in the 50 mL volumetric flasks were added 0.6 mL of glacial acetic acid and 0.2 mL of bromine. The flasks were heated on a sand bath 2-5h, and then 5 mL of 25% H₂SO₄ was added and heated until complete solution discoloration. After cooling 5 mL of 25% H₂SO₄, 10 mL of 0.25% potassium vanadate solution and 10 mL of 5% ammonium vanadate solution were added and diluted with water to 50 mL. After 30 min, the absorption was measured at $\lambda=430$ nm, $l=1$ cm. The calibration plot was obtained with potassium dihydrophosphate solution. Amino-silica gel was used as the control blank. Linear regression produced the following algebraic expression relating the concentration of bonded groups (C_L , mmol/g) to the optical density of the solution, A_{430} : $C_L = 1.4554 \cdot A_{430} + 0.0038$ ($R^2 = 0.9975$).

3.5. Preparation of hybrid luminescent materials

Hybrid luminescent materials based on modified silica gels containing Eu³⁺ and Tb³⁺ ions were obtained by shaking a fixed mass of several samples of adsorbent (each sample about 0.1 g) with 10 mL of europium(III) or terbium(III) solution (concentration $2 \cdot 10^{-5}$ mol L⁻¹) with pH = 3.0. The samples were shaken about 2 h, after that washed 3 times with ultrapure water and dried at 120 °C under vacuum.

3.6. Adsorption of metal ions by functionalized adsorbents

Adsorption of metal ions on obtained adsorbents has been studied in dispersive mode. Typically, 10 mL of water solution with desired pH and metal concentration was added to the 10-50 mg of the adsorbent in centrifuge tubes. The suspension acidity was adjusted for each sample to desired pH with 0.1-1 mol L⁻¹ HNO₃ and NaOH. The tubes were agitated 1-120 min in a horizontal shaker and then the adsorbent was separated by decantation or by centrifugation. The final pH value of solutions was controlled after stirring and 5 mL of solution was collected for analysis. The samples were filtered through a 0.45 μ m membrane filter and analyzed with an inductively coupled plasma mass spectrometry (ICP-MS) or optical emission spectrometry (ICP OES).

3.6.1. Effects of pH

The studies of the effect of pH on metal adsorption were performed by typical procedure described above. The effect of pH on adsorption properties of SiO₂-PdCA, SiO₂-AdMPA, and SiO₂, SiO₂-NH₂ towards REEs was performed for multi-element solution, containing ions: Sc³⁺, Y³⁺, La³⁺, Ce³⁺, Pr³⁺, Nd³⁺, Sm³⁺, Eu³⁺, Gd³⁺, Tb³⁺, Dy³⁺, Ho³⁺, Er³⁺, Tm³⁺, Yb³⁺, Lu³⁺ and Ba²⁺. The experiment was investigated in the pH 1.0–6.0 with initial concentrations of REEs 20 µg L⁻¹ and 1.0 mg L⁻¹ of Ba²⁺, and adsorbent dosage of 10 mg. The effect of pH on adsorption properties of SiO₂-BPHA towards REEs was performed for multi-element solution, containing 100.0 µg L⁻¹ of each trivalent ions: Sc³⁺, Y³⁺, La³⁺, Ce³⁺, Pr³⁺, Nd³⁺, Sm³⁺, Eu³⁺, Gd³⁺, Tb³⁺, Dy³⁺, Ho³⁺, Er³⁺, Tm³⁺, Yb³⁺ and Lu³⁺. The study was investigated in a pH range 1.0–6.0 and adsorbent dosage of 10 mg. The effect of pH on adsorption properties of SiO₂-PdCA, SiO₂-AdEPA, SiO₂-BPHA, SiO₂ and SiO₂-NH₂ towards 22 different metals in mixture were studied for multi-element solution, containing 10.0 mg L⁻¹ of each next metals: Ag⁺, Al³⁺, Ba²⁺, Bi³⁺, Ca²⁺, Cd²⁺, Co²⁺, Cr³⁺, Cu²⁺, Fe³⁺, Ga³⁺, In³⁺, K⁺, Li⁺, Mg²⁺, Mn²⁺, Na⁺, Ni²⁺, Pb²⁺, Sr²⁺, Tl³⁺, Zn²⁺. The degree of metal adsorption (*R*, %) was calculated according to the equation 9:

$$R, \% = \frac{(C_i - C_{eq}) \times 100}{C_i}, \quad (9)$$

where *C_i* and *C_{eq}* – initial and equilibrium concentration of metal ion in the aqueous phase, mg L⁻¹.

3.6.2. Effect of contact time

The rate of adsorption extraction was studied under static conditions. The suspension of sorbent samples (10-50 mg) in water solution of metal with pH=3.0 (for SiO₂-PdCA, SiO₂-AdMPA and SiO₂-AdEPA) or pH=5.0 (for SiO₂-BPHA) and concentration 10.0 mg L⁻¹ were stirring for 0.5-250 min. After that, samples were filtered through a 0.45 µm membrane filter and analyzed with inductively coupled plasma optical emission spectroscopy (ICP OES). The sorption capacity *q_t* at time *t*, expressed in mg g⁻¹, was calculated according to the equation 10:

$$q_t = \frac{(C_i - C_{eq}) \times V}{m}, \quad (10)$$

where *C_i* and *C_{eq}* – initial and equilibrium concentration of metal ion in the aqueous phase, mg L⁻¹, *V* – volume of solution, L; *m* – sorbent mass, g.

The adsorption kinetics was analyzed with two common kinetic models – pseudo-first-order (Eq. 11) and pseudo-second-order (Eq. 12):

$$q_t = q_e(1 - e^{-k_1 t}), \quad (11)$$

$$q_t = \frac{k_2 q_e^2 t}{1 + k_2 q_e t}, \quad (12)$$

where t – time, min; q_t – adsorption capacity at time t , mg g⁻¹; k_1 - the rate constant for the pseudo-1st-order model (min⁻¹); k_2 - the rate constant of the pseudo-second-order model, g mg⁻¹ min⁻¹.

3.6.3. Adsorption capacity of functionalized materials

In order to test the metal removal ability of the synthesized materials SiO₂-AdMPA¹⁻⁶, SiO₂-AdEPA¹⁻⁵, SiO₂-PdCA¹⁻⁴, and SiO₂-BPHA¹⁻² and evaluate the efficiency of the methods of synthesis, the absorbing capacity of the adsorbents was studied in optimal pH and in excess of metal towards Fe³⁺ and Cu²⁺ ions. Sorbent sample (50 mg) of each silica gels was in a contact with 10 mL of working solution of appropriate metal (initial metal concentration 40 mg L⁻¹, pH = 3.0) during 2h under regular stirring. The following metals were chosen: Fe³⁺ for SiO₂-AdMPA¹⁻⁶, SiO₂-AdEPA¹⁻⁵ and SiO₂-BPHA¹⁻² and Cu²⁺ for SiO₂-PdCA¹⁻⁴ adsorbents (see Figure 44). After stirring, samples were filtered through a 0.45 μm membrane filter and analyzed with an inductively coupled plasma atomic emission spectrometry (ICP OES). The adsorption capacity (q_e) was calculated according to the equation 13:

$$q_e = \frac{(C_i - C_{eq}) \times V}{m \cdot m_a}, \quad (13)$$

where q_e is the adsorption capacity in μmol g⁻¹; C_o and C_{eq} – initial and equilibrium concentration of metal ion solution in the aqueous phase, mg L⁻¹; V - volume of the adsorbate solution, mL; m - mass of the adsorbent, g; m_a - atomic mass of the metal, g mol⁻¹.

3.6.4. Adsorption isotherms

Adsorption isotherms were obtained by shaking a fixed mass of several samples of adsorbent (10 mg) with 10 mL of metal solution at pH=3.0 (for SiO₂-PdCA, SiO₂-AdMPA and SiO₂-AdEPA) or pH=5.0 (for SiO₂-BPHA). The initial concentration of metal in solution varied from 0.1 to 25 mg L⁻¹. The samples were

shacked for about 2 h, and then filtered through a 0.45 μm membrane filter and solution was analyzed on metal content by an inductively coupled plasma atomic emission spectrometry (ICP OES). The adsorption capacity of sorbent (α), expressed in mg g^{-1} , calculated according to the equation 14:

$$\alpha = \frac{(C_i - C_{eq}) \times V}{m}, \quad (14)$$

where C_i and C_{eq} – initial and equilibrium concentration of copper ion solution in the aqueous phase, mg L^{-1} ; V – volume of solution, L; m – sorbent mass, g.

The adsorption data were fitted with Langmuir (Eq. 15) and Freundlich (Eq. 16) isotherm models:

$$\frac{1}{q_e} = \frac{1}{q_{max}} + \frac{1}{C_e} \frac{1}{q_{max} K_L}, \quad (15)$$

$$\ln q_e = \ln K_F + \frac{\ln C_e}{n}, \quad (16)$$

where q_e is the adsorption capacity (mg g^{-1}), C_e is the equilibrium ion concentration in the solution (mg L^{-1}), q_{max} is overall adsorption capacity (mg g^{-1}) and K_L is the Langmuir adsorption constant (L mg^{-1}), n is Freundlich constant and K_F is the binding energy constant reflecting the affinity of the adsorbents to metal ions (mg g^{-1}).

3.6.5. Evaluation of extraction capacity and selectivity

The competitive adsorption of REEs on SiO_2 -BPHA was performed in a multi-component system. A set of solutions with increasing concentration of REEs (from 0.1 to 5.0 mg L^{-1}) has been equilibrated with 10 mg of SiO_2 -BPHA at $\text{pH}=5.0$ for 30 min. The initial and equilibrium concentrations of the REEs in solutions were determined and used to calculate the distribution coefficient (K_d , mL g^{-1}) according to the equation 17:

$$K_d = \frac{(C_i - C_{eq})}{C_{eq}} \times \frac{V}{m}, \quad (17)$$

where C_i and C_{eq} – initial and equilibrium concentration of metal ion solution in the aqueous phase, $\mu\text{g L}^{-1}$; V – volume of solution, mL; m – sorbent mass, g.

Separation factor (SF) of two elements was calculated from the ratio $SF \frac{1}{2} = K_{d1}/K_{d2}$.

3.6.6. Metal desorption optimization and reusability test

Initially, the sample of adsorbents (10-50 mg) was equilibrated with 10 mL of solution containing 100.0 $\mu\text{g L}^{-1}$ of each REE, at pH = 5.0 or 10.0 mg L^{-1} of Fe^{3+} or Cu^{2+} with pH=3.0. After 30 min of agitation, the adsorbents were washed 3 times with Mili-Q water, separated by centrifugation and the supernatant was analyzed for metal content.

For desorption, 10 mL of eluting solution was added to the adsorbent. After 30 min of agitation, the adsorbent was separated by centrifugation, washed 3 times with ultrapure water and reused in the next adsorption/desorption experiments. As eluting agents were investigated:

- 1) 0.01 – 2.0 mol L^{-1} HNO_3 and HCl,
- 2) 0.01 mol L^{-1} solution of: EDTA, SSA, CiA, AmSA, HBA, OxA and AsA.

The eluate was filtered through a 0.45 μm membrane filter and the solution was analyzed for metal content by inductively coupled plasma mass spectrometry (ICP-MS) or optical emission spectrometry (ICP OES). Elution efficiency (E , %) was calculated according to the equation 18:

$$E, \% = \frac{C_{eq} \times 100}{C_i}, \quad (18)$$

where C_i and C_{eq} – initial and equilibrium concentration of metal ion solution in the aqueous phase, mg L^{-1} .

Statistical processing of the recovery data was carried out by means of a descriptive analysis summarizing mean values, standard deviation and standard error of mean (SEM) supported with the normality test of dispersion for a general (overall) recovery values, using data visualization and statistical analysis software Plotus 1.0. To specify the normality test, the D'Agostino-Pearson omnibus approach was preferred, and the recovery values distributions were plotted as violin graphs in respect to each metal ion. The $P_{D'A-P}$ -value served as a criterion of normality at 2 degrees of freedom with a parallel assessment of skewness and kurtosis for the calculated curves.

3.6.7. Interference effect of competing ions on adsorption of REEs

In a sample of silica gel (10 mg) were added 10 mL of working solutions containing REEs and interference ions at pH=2.5 (for adsorption on SiO_2 -PdCA), pH=2.0 (for SiO_2 -AdMPA) and pH=5.0 (for SiO_2 -BPHA). The following interfering ions were studied:

- 1) Na⁺, K⁺, Ca²⁺, Mg²⁺;
- 2) Fe³⁺, Cu²⁺;
- 3) Ag⁺, Al³⁺, Ba²⁺, Bi³⁺, Ca²⁺, Cd²⁺, Co²⁺, Cr³⁺, Cu²⁺, Fe³⁺, Ga³⁺, In³⁺, K⁺, Li⁺, Mg²⁺, Mn²⁺, Na⁺, Ni²⁺, Pb²⁺, Sr²⁺, Ti³⁺, Zn²⁺.

The concentration of REEs was constant (20.0 µg L⁻¹) and the concentration of interfering ions were varied from 1 to 100 mg L⁻¹. Desorption was carried out with 0.1 mol L⁻¹ HNO₃ (for SiO₂-BPHA) and 2.0 mol L⁻¹ HNO₃ (for SiO₂-PdCA and SiO₂-AdMPA). Interference effect of 22 metal ions was studied with and without constant ionic strength. 0.5 mol L⁻¹ NaCl was used to maintain constant ionic strength in the process of adsorption. The metal recovery (*R*, %) was calculated from the equation in paragraph 3.6.1.

3.6.8. Recovery of REEs from waste fluorescent lamps

For the preparation of concentrate leaching solution (**#2**), 0.5 g of waste phosphor powder was dissolved in 2.5 mL of aqua regia in a Falcon 15 mL conical centrifuge tubes. The tube was kept at 90 °C under stirring for 2 h. After that, the solution was diluted to 10 mL and filtered through a 0.45 µm membrane filter. For the preparation of diluted leaching solution (**#1**) 5 mL of concentrate leaching solution (**#2**) had been diluted 5 times. The pH of solutions was adjusted to 2.0-2.5 with 1 mol L⁻¹ NaOH. The solutions **#1** and **#2** were used for dispersive solid-phase extraction (DSPE) experiments using 50 mg of adsorbent. Desorption was carried out with 2 mol L⁻¹ HNO₃. Degree of metal adsorption and desorption were calculated from the equations in paragraph 3.6.1 and 3.6.6. Overall recovery (*R_{ov}*, %) was calculated according to the equation 19:

$$R_{ov}, \% = \frac{A \times E}{100}, \quad (19)$$

where *A* and *E* – degree of metal adsorption and desorption, %.

4 Results and discussion

Adsorption properties of silicas with immobilized functional groups depend on chemical composition of the surface layer and concentration of bonded groups (Vladimir N. Zaitsev, 1997). It is particularly important for the adsorbents, received by multistep process of ligand assembling (see chapter 1.6 of this report). All adsorbents used for REE recovery in this research have been obtained by assembling of the target ligands on silica surface. Therefore, major attention has been given in the control of the adsorbents' composition and chemical nature of immobilized functional groups. The adsorbents were characterized by various complementary methods such as elemental analysis, FTIR, XPS, MAS NMR, and TGA. Additionally, the adsorbent's capacity towards metal ion has been studied in order to quantify the concentration of the target centers of adsorption. The OSAd preparation procedures were optimized, by monitoring the adsorbent capacity.

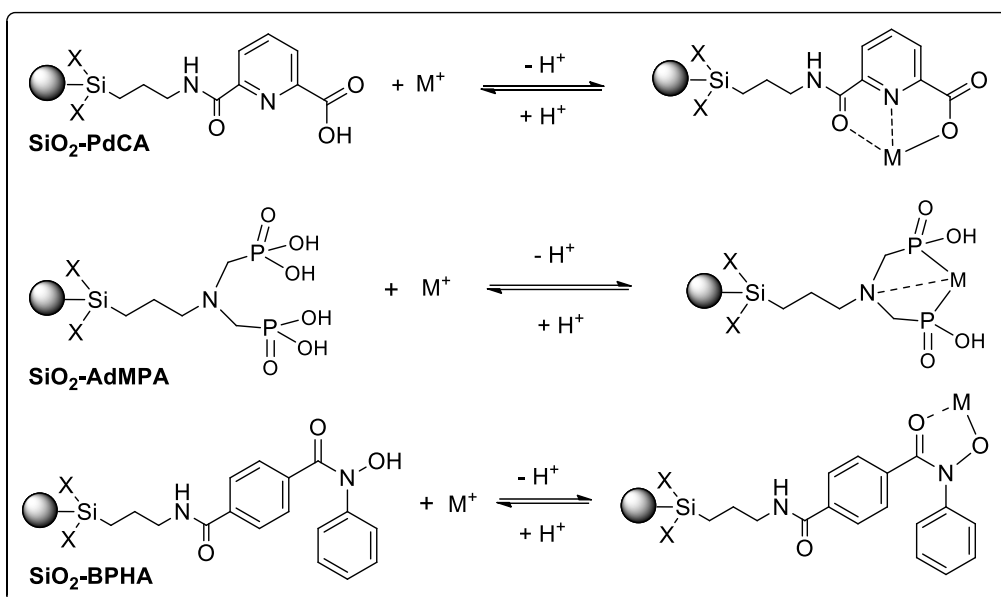
In order to prove that adsorption of REEs from solution is observed due to complexation with target functional groups, the compositions of immobilized complexes were studied by UV-vis diffuse reflectance spectroscopy and luminescent spectroscopy.

The adsorbents, which demonstrated the highest affinity towards REE ions, were utilized for preconcentration of metals prior to their analytical determination. Among the OSAd studied in this work, silica with immobilized aminophosphonic acids and 2,6-pyridinecarboxylic acid demonstrated very high affinity towards REEs that allows the adsorbent utilization for removing metal ions from acidic solutions. Contrary immobilized hydroxamic acid demonstrated advanced properties in REEs separation.

4.1. Quantitative characterization of the adsorbents

4.1.1. Adsorption capacity of functionalized materials

The adsorbents presented in this research belong to the class of complexing organo-silicas that bear chelating ligands immobilized on silica gel surface. Therefore, adsorption on such OSAd is observed due to binding of metals by immobilized ligands, as it is schematically demonstrated in Scheme 6.



Scheme 6. Metal adsorption process on adsorbents.

Therefore total metal capacity of such adsorbents towards metal ions can be an instrument for evaluation of concentration of the immobilized target ligands (Kholin e Zaitsev, 2008). Such approach has been used in the current research as an express characteristic of the yield in OSA_d synthesis. Since immobilized ligands form stable complexes with Cu²⁺ and Fe³⁺ ions in acidic media, total capacity of the adsorbents towards these ions has been used to evaluate the optimum conditions for OSA_d preparation. The results of the investigation for different samples of SiO₂-AdMPA (samples 1-6), SiO₂-AdEPA (samples 1-6), SiO₂-BPHA (samples 1-2) and SiO₂-PdCA (samples 1-6) are presented in Figure 2. The metal adsorptions have been studied in the conditions that prevent non-selective adsorption of Fe³⁺ and Cu²⁺ by silica matrix.

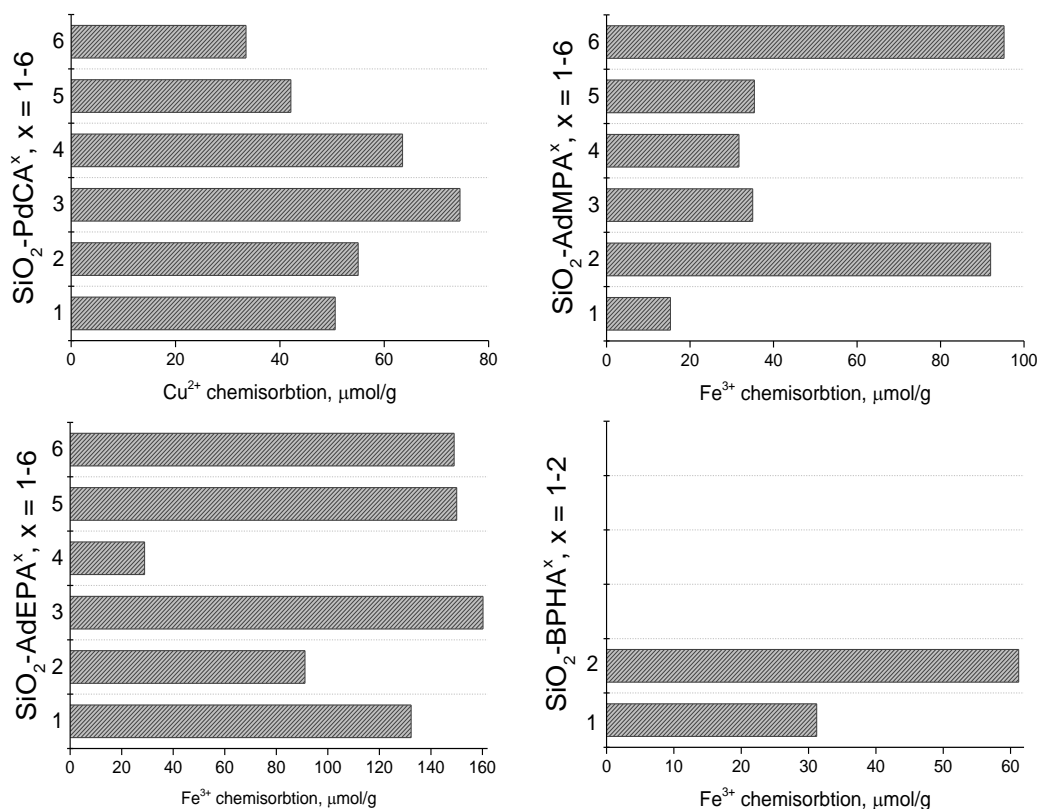


Figure 2. Adsorption capacity of functionalized materials.
 $m_{ads} = 50$ mg, $C_i(M^{*+}) = 40$ mg L⁻¹, pH = 3.0, V = 10 mL, t = 2h.

As it can be seen from Figure 2, the maximum adsorption of Cu²⁺ (75 μmol g⁻¹) capacity for SiO₂-PdCA¹⁻⁶ adsorbents is achieved for synthesis conditions used for preparation of SiO₂-PdCA³. This synthesis was performed by reaction of 2,6-pyridinedicarbonyl dichloride with 3-aminopropyl-silica gel in acetonitrile in the presence of N,N-diisopropylethylamine.

The maximum adsorption capacity of Fe³⁺ for synthesizes SiO₂-AdMMPA¹⁻⁶ is achieved for synthesis SiO₂-AdMMPA² (92 μmol g⁻¹) and SiO₂-AdMMPA⁶ (95 μmol g⁻¹). Adsorbent SiO₂-AdMMPA² was synthesized by surface assembling method and SiO₂-AdMMPA⁶ by one-step immobilization of P-containing organo-silane. The latter one has been selected for further investigation.

For SiO₂-AdEPA¹⁻⁶ the maximum adsorption capacity of Fe³⁺ is achieved for several OSAd: 1) SiO₂-AdEPA¹ (132 μmol g⁻¹), 2) SiO₂-AdEPA³ (160 μmol g⁻¹), 3) SiO₂-AdEPA⁵ (150 μmol g⁻¹) and 4) SiO₂-AdEPA⁶ (149 μmol g⁻¹). The SiO₂-AdMMPA³ was selected for further investigations.

The maximum adsorption capacity (61 μmol g⁻¹) for synthesizes SiO₂-BPHA¹⁻² is achieved for synthesis SiO₂-BPHA², therefore for the subsequent synthesis of SiO₂-BPHA, this method was selected.

As it can be seen from Figure 2, synthetic conditions are very important for the correct preparation of OSA_d, since concentration of target chelating groups on the adsorbent can be varied five times and so metal capacity.

The following abbreviations without superscript will be further used in the manuscript for the selected adsorbents:

- SiO₂-PdCA for silica gel with covalently immobilized 2,6-pyridine-dicarboxylic acid synthesized by method SiO₂-PdCA³;
- SiO₂-AdMPA for silica gel with covalently immobilized amino-di(methylene phosphonic) acid synthesized by method SiO₂-AdMPA⁶;
- SiO₂-AdEPA for silica gel with covalently immobilized amino-di(ethylene phosphonic) acid synthesized by method SiO₂-AdEPA³;
- SiO₂-BPHA for silica gel with covalently immobilized N-Benzoyl-N-phenylhydroxylamine synthesized by method SiO₂-BPHA².

4.1.2. Elemental analysis

The elemental analysis of silica samples on carbon and nitrogen contents gives us an idea about loading of organic functional groups. The results of elemental analysis of organo-silica samples and calculated concentration of functional groups determined from different loadings are shown in Table 5.

The percentage content of H usually has auxiliary character due to the content of variable adsorbed water on silica. Also, as it can be seen from Table 5, concentration of bonded amino groups, determined from carbon loading is higher than those ones from nitrogen. It is commonly observed for functionalized silicas due to solvent adsorption or incomplete hydrolysis of anchoring ethoxy-groups. Similar to other researchers, carbon loading was used for reference purposes only.

Table 5. Results of elemental analysis of organo-silica samples.

Adsorbent	Mass fraction of the element, %			Concentration of bonded groups (C_L^i)*, mmol/g		
	H	C	N	C_L^H	C_L^C	C_L^N
SiO₂-NH₂	1.4	5.2	1.2	1.44	1.39	0.86
SiO₂-PdCA	1.6	7.0	1.7	0.40	0.21	0.36
SiO₂-AdMPA	1.9	8.1	1.6	0.99	1.21	0.29
SiO₂-AdEPA	1.6	7.6	1.5	0.20	0.50	0.21
SiO₂-BPHA	1.8	9.3	1.6	0.32	0.23	0.29

* C_L^i – concentration of functional groups L calculated from mass fraction of element i determined from CHN analysis.

4.1.3. Thermogravimetric analysis

Thermal decomposition of organic fragments and thermal stability of selected silica-based materials was analyzed in the temperature range 25-900 °C and concentrations of bonded groups were calculated. Thermogravimetric analysis (TGA) revealed that all samples lost about 2-3 wt.% between 25 and 100 °C that can be attributed to desorption of water due to partial dehydration of silica gel. This process is common for all chemically modified silica gels. The TGA thermograms show the intensive weight loss step <700 °C, which corresponds to decomposition of organic modified groups.

TGA thermograms of functionalized silica gels are presented in Figure 3.

For SiO₂-NH₂ weight loss is 6.5% (200-800 °C) can be attributed to thermal desorption of immobilized groups and thus their concentration determined as it is described above. The decomposition of organic component (200-800 °C) of SiO₂-PdCA, SiO₂-AdMPA, SiO₂-AdEPA, and SiO₂-BPHA resulted in a weight loss of 11.7, 10.4, 10.2 and 13.8% respectively. The calculated results of concentration of grafted functional groups are presented in Table 6.

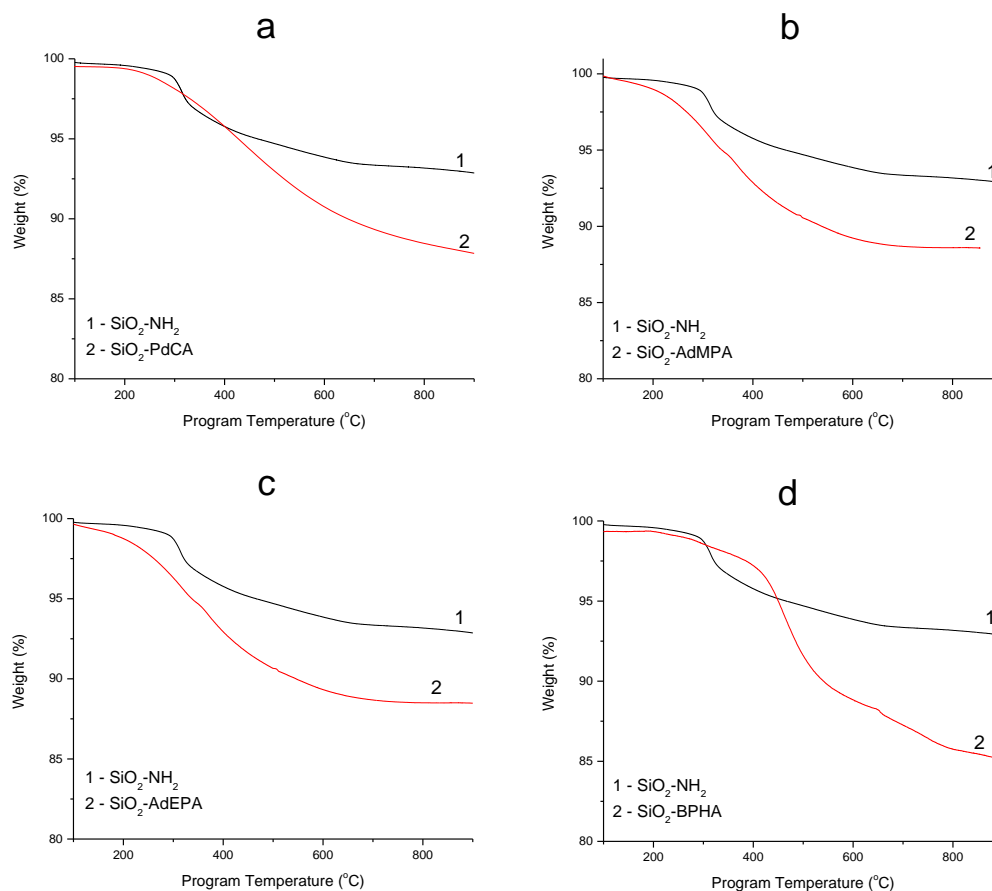


Figure 3. TGA thermograms of functionalized silica gels.

Table 6. The estimated concentration of grafted functional groups.

T range, °C	Type of functionality	M, g/mol	$\Delta m/m$, mg/g	C_L , mmol/g
	SiO₂-NH₂			
200-800	-(CH ₂) ₃ NH ₂	58.0	65.0	1.1
	SiO₂-PdCA			
200-800	-(CH ₂) ₃ NH-C(O)C ₅ H ₃ N(COOH)	207.0	117.0	0.35
	SiO₂-AdMPA			
200-800	-(CH ₂) ₃ N(PO ₃ H ₂) ₂	187.0	104.0	0.30
	SiO₂-AdEPA			
200-800	-(CH ₂) ₃ N(CH ₃) ₂ (PO ₃ H ₂) ₂	217.0	102.0	0.23
	SiO₂-BPHA			
200-800	-(CH ₂) ₃ NHC(O)C ₆ H ₄ C(O)N(OH)C ₆ H ₅	297.0	138.0	0.30

4.1.4. Concentration of immobilized groups

The concentration of immobilized groups determined from several independent measurements has been summarized in Table 7. As can be seen, the values obtained by elemental analysis are higher than those measured by other methods. It can be observed because of incomplete combustion during elemental analysis or the accessibility of functional groups. For example, the excess of amino groups calculated from elemental analysis can be inaccessible for further coupling reactions. According to titration data, it may be concluded that more than 90% of immobilized amino groups are accessible.

Table 7. Concentration of immobilized groups.

Adsorbent	<i>Number of functional groups, mmol/g</i>					
	CHN, C_L^N	TGA	Direct titration	Indirect titration	Conduct. titration	P content
SiO₂-NH₂	0.86	1.1	0.77±0.02	0.80±0.06	0.72±0.02	-
SiO₂-PdCA	0.36	0.35	-	-	-	-
SiO₂-AdMPA	0.29	0.30	-	-	-	0.35
SiO₂-AdEPA	0.21	0.23	-	-	-	0.24
SiO₂-BPHA	0.29	0.30	-	-	-	-

4.2. Spectroscopic characterization of the adsorbents

4.2.1. FT-IR characterization

FTIR spectroscopy is a powerful tool to confirm the grafting of the organic ligands to the surface, since FTIR provides information about the chemical bonds in the surface. To confirm the presence of functional groups in the material, FT-IR spectra were recorded for SiO₂ (pure), SiO₂-NH₂, SiO₂-PdCA, SiO₂-AdMPA,

SiO₂-AdEPA and SiO₂-BPHA. Unfortunately, only narrow parts of IR spectra can be successfully used for silica sorbents characterization due to the strong matrix effect.

Compared to bulk silica, SiO₂-NH₂ spectrum exhibits new peaks, Figure 4. The peaks at 2900 cm⁻¹ and 2865 cm⁻¹ are observed for CH asym/sym stretching and confirmed presence of methylene group. The band at 1550 cm⁻¹ is assigned to presence of NH bend of primary amine. Expected peak of NH stretching vibration between 3400-3380 cm⁻¹ cannot be identified due to significant interference in the region.

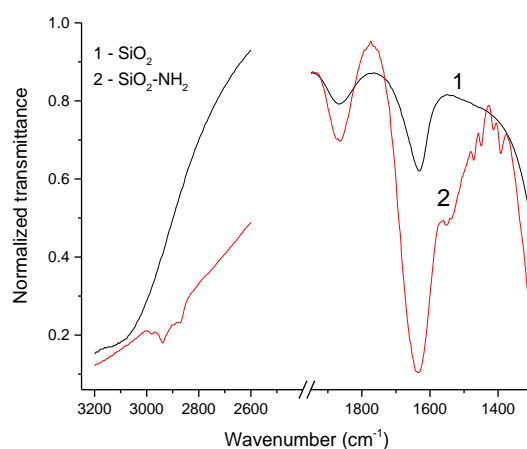


Figure 4. FT-IR spectra of SiO₂ (pure) and SiO₂-NH₂.

There are some spectral changes in the IR spectrum of SiO₂-PdCA compared to SiO₂-NH₂ (Figure 5a). The IR spectrum of SiO₂-PdCA has absorbance bands at 1646, 1546, 1450, 1420 and 1384 cm⁻¹. The observed band (Amide-I) at 1646 cm⁻¹ is associated with the C=O stretching vibration. The band at 1546 cm⁻¹ (Amide-II) results from the N-H bending vibration and C-N stretching vibration. The peak at 1384 cm⁻¹ is due to ν_{C-N} and δ_{N-H} . The peaks at 1420 cm⁻¹ and 1450 cm⁻¹ are attributed to the stretching vibration of C=C and C=N of pyridine ring, respectively. It indicates the anchoring of the organic molecule onto the silica surface.

The IR spectrum of SiO₂-BPHA has absorbance bands at 1660, 1545, 1500 cm⁻¹ (Figure 5b). The most intensive ones are at 1660 and 1550 cm⁻¹. Regarding their intensity and position, they can be attributed to Amide-I and Amide-II absorbance respectively and it proves the hydroxamic acid formation on the silica surface.

There is no significant difference between spectrums of SiO₂-AdMPA and SiO₂-AdEPA (Figure 5c,d). Successful phosphorylation of surface confirms

appearance of the band of P-O stretching in a region near 2500 cm^{-1} . An intensive absorption of the Si—O bond stretching vibration in the $950\text{--}1200\text{ cm}^{-1}$ range gives significant interference to observe the vibration bands $V_{\text{as}}(\text{PO})$ of phosphonic groups in the $918\text{--}1190\text{ cm}^{-1}$ range. Although in this region, there are some differences between SiO_2 spectrum and its phosphorylated products that can be proof of successful modification of the surface.

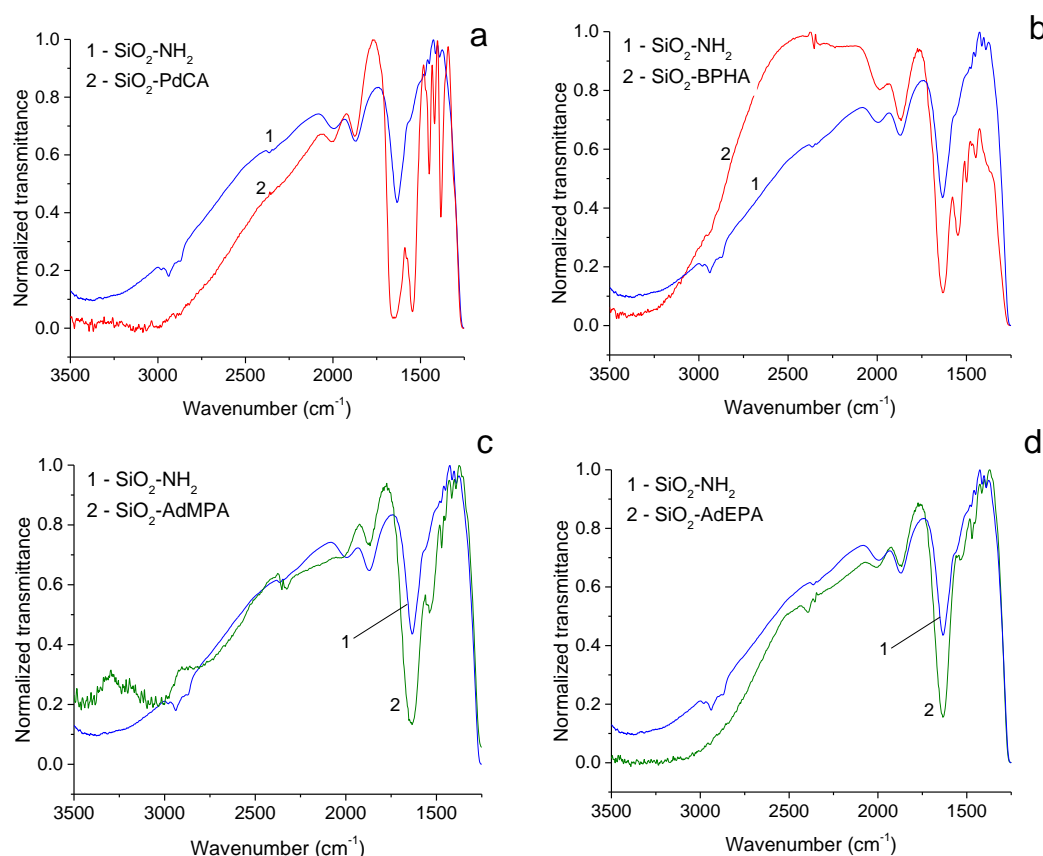


Figure 5. FT-IR spectra of functionalized silica gels.

4.2.2. X-ray photoelectron spectroscopy

Adsorbents $\text{SiO}_2\text{-PdCA}$, $\text{SiO}_2\text{-AdMPA}$ and $\text{SiO}_2\text{-BPHA}$ were characterized by X-ray photoelectron spectroscopy (XPS). Immobilization of organic compounds has practically no effect on the shape and intensity of the spectral lines of the silica matrix elements: Si2p (103.2 eV), Si2s (154.3 eV) e O1s (532.5 eV). At the same time, in the spectra of immobilized silica gels were identified lines absent in the spectra of SiO_2 : C1s (284.8 eV), N1s (400.5 eV) for all adsorbents, and P2p for silicas with immobilized phosphonic acids (Figure 6). The P2p line in the spectra is represented by one undivided doublet in 134.0 eV (Figure 6b) that corresponds according to the literature data for phosphonic acids (Viornerly *et al.*, 2002). The

absence of other peaks indicates the equivalence of all phosphorus atoms (absence of phosphoric acid, for example) in the grafted layer.

N1s high-resolution XPS of SiO₂-AdMPA. The N1s line in the XPS spectrum of SiO₂-NH₂ consists of two components: NH₂, at 399.7 eV and NH₃⁺ at 401.6 eV, Figure 7d. While N1s line of SiO₂-AdMPA has peaks at 399.7 and 402.3 eV, Figure 7a. The line shift of protonated amines (402.3 eV) in comparison with SiO₂-NH₂ is due to the presence of highly acidic centers in structure. Also, the proportions of the integrated intensities of these peaks for SiO₂-AdMPA and SiO₂-NH₂ are significantly different: in the SiO₂-NH₂ sample, the free amino group predominates, while in the SiO₂-AdMPA - protonated. The presence of a certain number of protonated groups for SiO₂-NH₂ is in accordance with the model of the clustering structure of organosilic-grafted layer, and the presence of a small number of free amino groups in the XPS SiO₂-AdMPA spectrum is in accordance with incomplete conversion of amino groups to aminophosphonic.

N1s high-resolution XPS of SiO₂-PdCA. Unfortunately, interpretation of the N1s high-resolution spectra for SiO₂-PdCA does not permit to differentiate the nitrogen species (amine, amide) grafted on the surface because they do not have a significant difference in their chemical shifts, Figure 7c.

N1s and C1s high-resolution XPS of SiO₂-BPHA. Besides two kinds of groups at 399.7 eV and at 401.6 eV that correspond to non-protonated and protonated amines, respectively, the spectrum of SiO₂-BPHA additionally displays the characteristic band for -NH-C(O)- fragments at 400.6 eV (Figure 7b). In C1s line of SiO₂-BPHA, can be observed fragments from SiO₂-NH₂: C-C/C-H (285.0 eV), C-N (286.3 eV) and C-O (287.7 eV) and also an intensive band attributed to >C=O fragments from immobilized benzoyl-N-phenylhydroxylamine fragments at 288.8 (Figure 8), that confirm successive coupling of BPHA on amino silica.

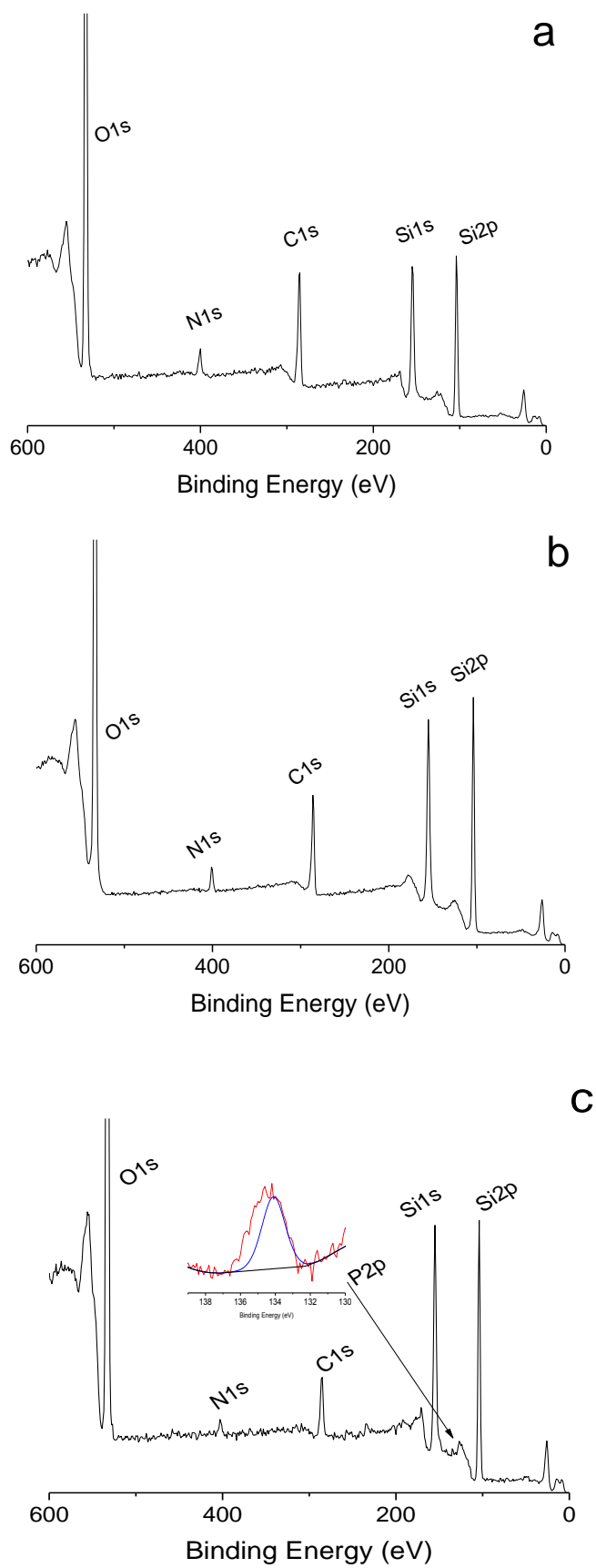


Figure 6. XPS low-resolution spectra of SiO₂-PdCA (a), SiO₂-BPHA (b), SiO₂-AdMPA (c).

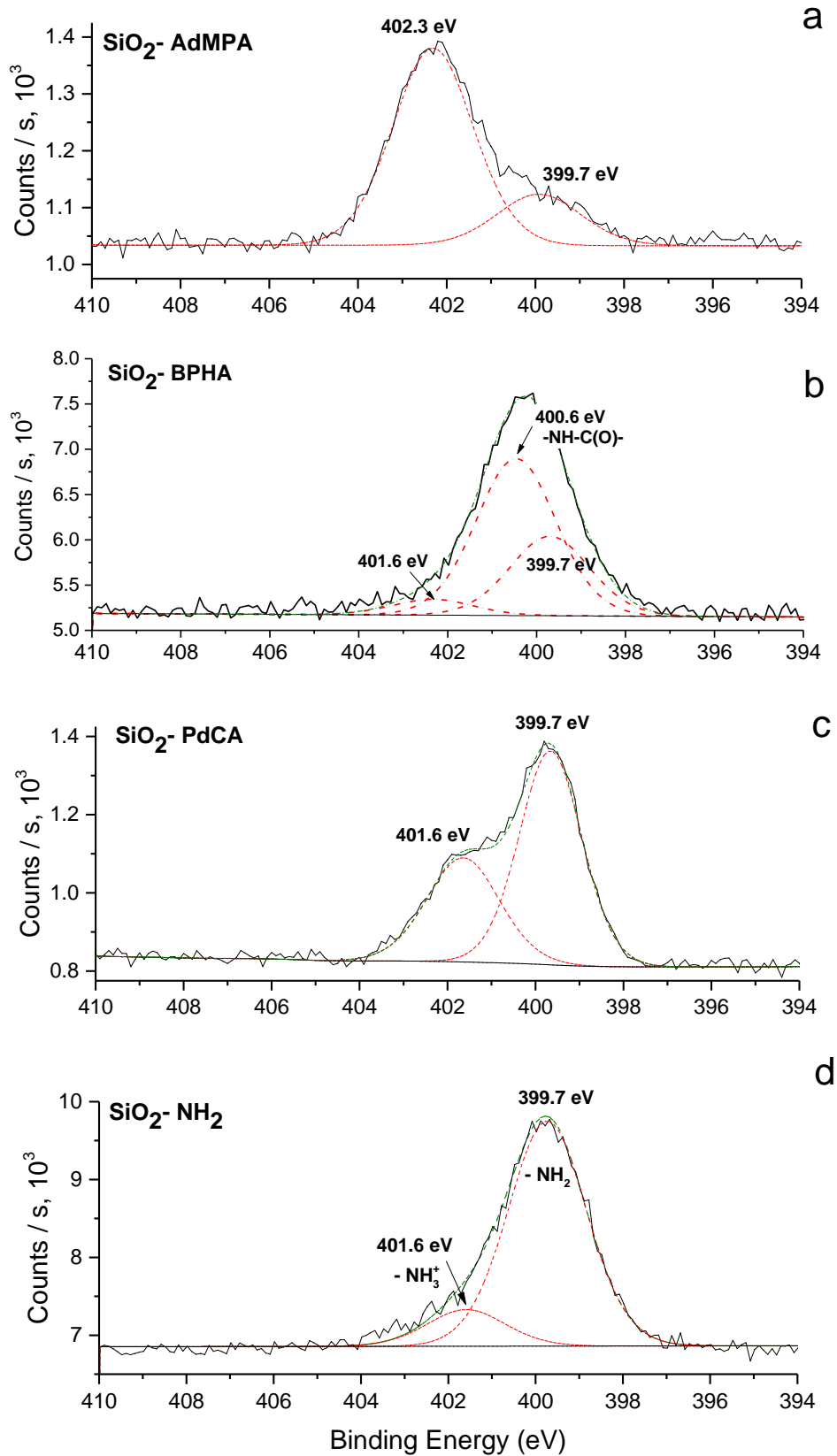


Figure 7. XPS high-resolution N1s spectra of functionalized silica gels. Partially reproduced from (Artiushenko *et al.*, 2019).

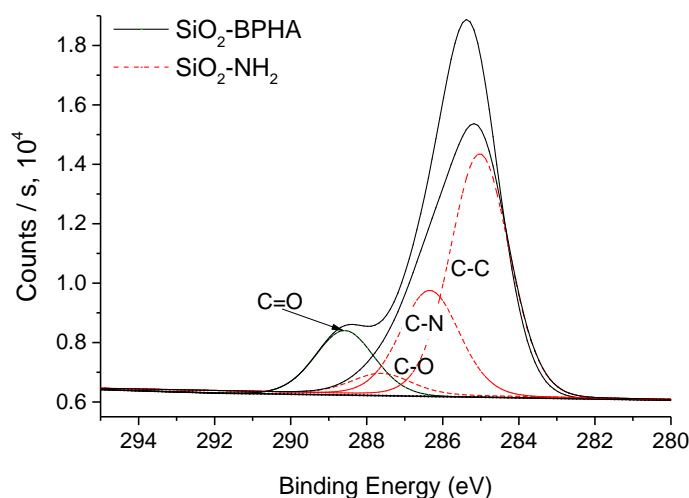


Figure 8. XPS high-resolution C1s spectra of SiO₂-BPHA and SiO₂-NH₂. Partially reproduced from (Artiushenko *et al.*, 2019)..

4.2.3. NMR characterization

The successful functionalization of silica gel with aminophosphonic acids SiO₂-AdMPA and SiO₂-AdEPA was confirmed by solid-state ²⁹Si, ¹³C, and ³¹P MAS-NMR spectroscopy. The ²⁹Si MAS-NMR spectra of the adsorbents are shown in Figure 9.

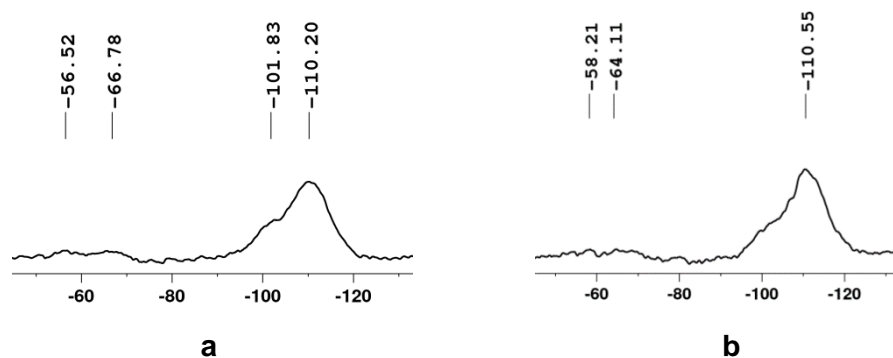


Figure 9. Solid state ²⁹Si MAS-NMR spectra of SiO₂-AdMPA (a) and SiO₂-AdEPA (b).

Quantitative peak intensities in ²⁹Si MAS-NMR spectra requires using long enough repetition time (~600 s delays) (Sutra *et al.*, 1999) to allow complete relaxation of all silicon nucleus types. In this work in order to reduce very long delay, a repetition time of 10 s was used. As it can be assumed from the ²⁹Si NMR spectra, the studied materials present several peaks which can be assigned to Q_n and T_n local environments, Figure 10. The peak around -110 ppm is assigned to the Q₄ atoms. The silicon atoms with a chemical shift around -102 ppm are

attributed to the Q_3 silanol or siloxy species. There is no peak near -90 ppm, which indicates the absence of geminal species Q_2 . For the functionalized silicas, peaks near -66-64 and 58-56 ppm can be also observed, which are assigned to T_3 and T_2 sites respectively. Appearance of the peaks of T_3 and T_2 sites in the spectra is one of the proofs of successful modification of silica surface.

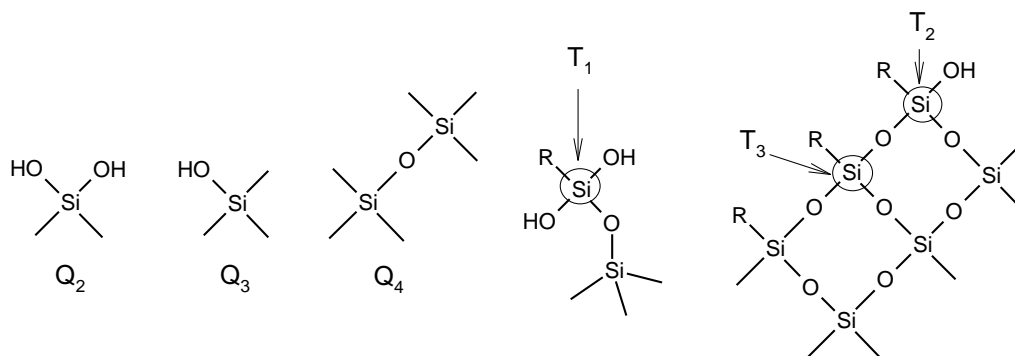


Figure 10. Q_n type ($n=2,3,4$) and T_n type ($n=1,2,3$) Si local environments. Adapted from (Topel *et al.*, 2014).

Figure 11 shows the ^{13}C MAS-NMR spectra of functionalized materials grafted with phosphonate derivatives.

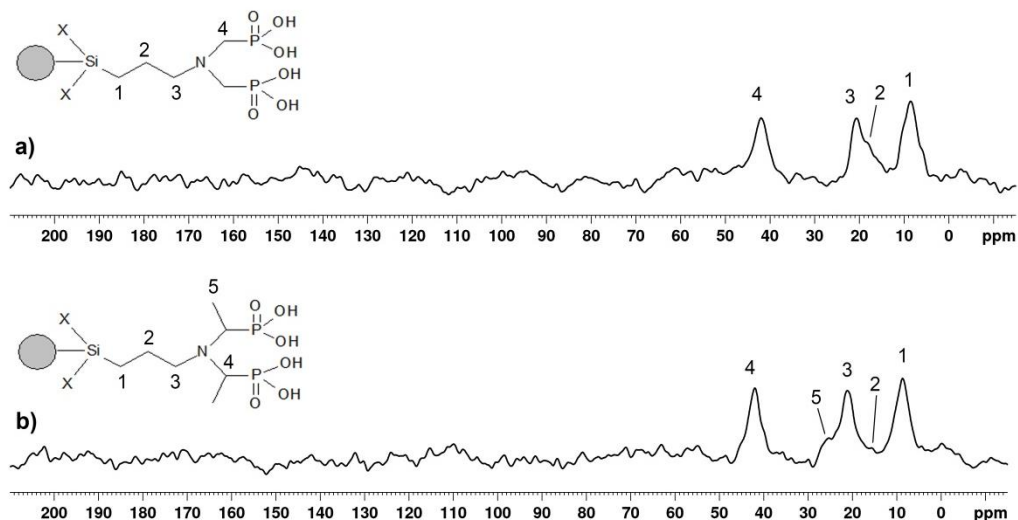


Figure 11. Solid state ^{13}C MAS-NMR spectra of SiO_2 -AdMPA (a) and SiO_2 -AdEPA (b).

All the resonance signals in the ^{13}C MAS-NMR spectra can be assigned to appropriate C atoms, as represented. The significant signal broadening in the NMR spectra of the modified silica leads us to believe that there are strong hydrogen bonding interactions between grafted species and the silica matrix (Zaitsev e Vassilik, 1999). This strong interaction prevents free rotation of grafted groups on the surface and causes their differentiation.

The ^{31}P MAS-NMR spectra of the adsorbent $\text{SiO}_2\text{-AdMPA}$ is shown in Figure 12. As it can be observed, there is one broad characteristic signal attributed to P-containing groups, which resonates at 6.92 ppm for methylenephosphonic groups ($\text{SiO}_2\text{-AdMPA}$) and 6.97 for ethylenephosphonic groups ($\text{SiO}_2\text{-AdEPA}$).

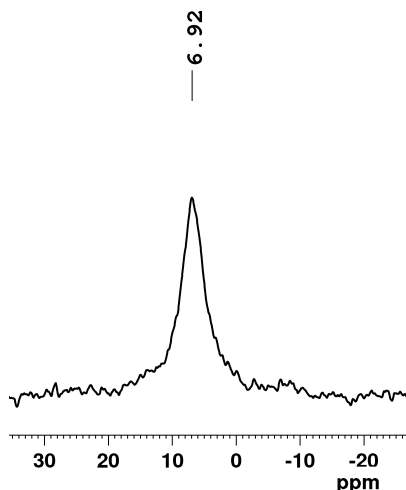


Figure 12. Solid state ^{31}P MAS-NMR spectra of $\text{SiO}_2\text{-AdMPA}$.

4.3. Morphological characteristics of the adsorbents

4.3.1. The pore size and morphology of synthesized materials

Nitrogen adsorption/desorption analysis was used to characterize the porous structure of modified silica gels. The isotherms for next silica samples: SiO_2 (pure), $\text{SiO}_2\text{-NH}_2$, $\text{SiO}_2\text{-PdCA}$, $\text{SiO}_2\text{-AdMPA}$, $\text{SiO}_2\text{-AdEPA}$ and $\text{SiO}_2\text{-BPHA}$ at 77 K are shown in Figure 13. All isotherms are associated with type H1. The condensation processes happen in the relative pressure range of 0.5–0.9, indicating the porous silica materials possess mesopores. The hysteresis loop and the quite steep adsorption and desorption branches are indicative of the narrow pore size distributions. This is also confirmed by pore size distributions calculated from nitrogen desorption branch by Barrett–Joyner–Halenda (BJH) method, Figure 14.

The obtained parameters – pore diameter (d), Brunauer-Emmett-Teller (BET) surface area (S_{BET}) and pore volume (V_p) for all samples are presented in Table 8.

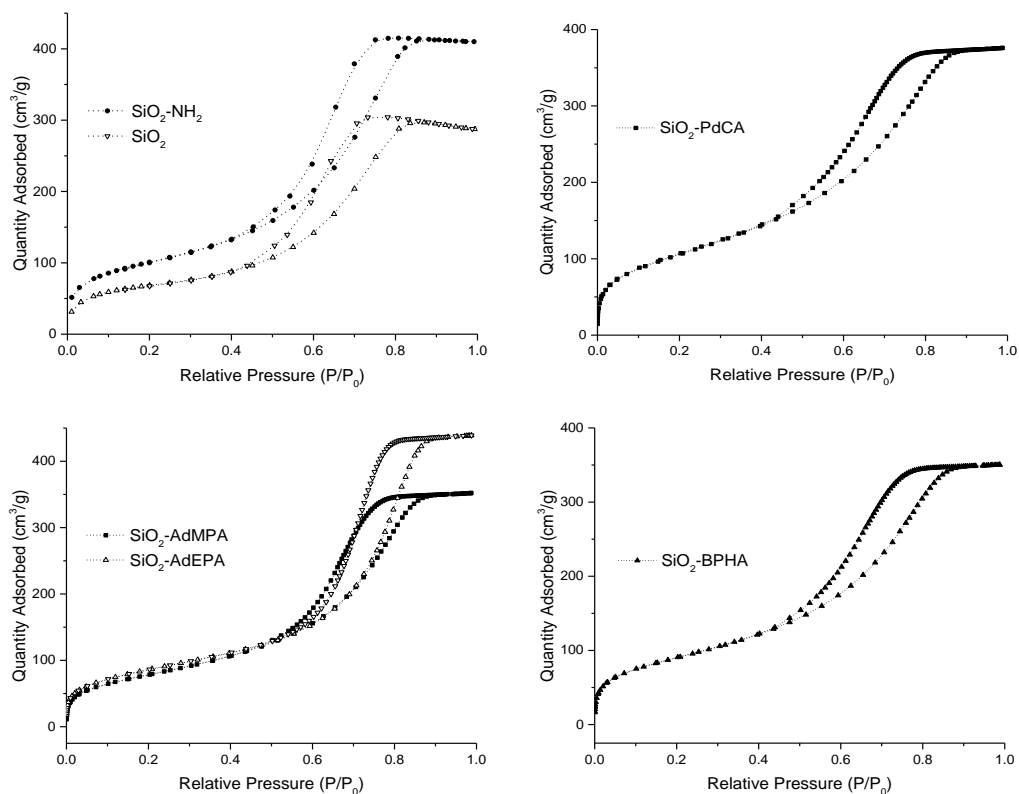


Figure 13. N₂ adsorption–desorption isotherms of silica materials.

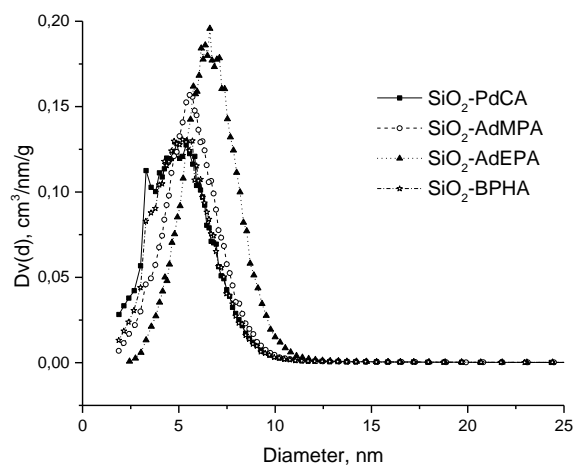


Figure 14. Pore size distribution obtained by BJH method.

Table 8. The morphological characteristics of obtained materials.

Material	d, nm	S _{BET} , m ² g ⁻¹	V _p , cm ³ g ⁻¹
SiO₂	7.90	360.3	0.75
SiO₂-NH₂	8.21	236.8	0.48
SiO₂-PdCA	4.76	389.1	0.58
SiO₂-AdMPA	7.73	287.9	0.54
SiO₂-AdEPA	6.41	308.3	0.67
SiO₂-BPHA	5.20	329.2	0.52

4.3.2. Scanning electron microscopy

The scanning electron microscopy (SEM) images of pure unmodified (SiO_2) and functionalized silica gels are presented in Figure 15. As can be seen, there is no change in the morphology of silica gel matrix after manipulations attributed to the chemical bonding for all modified silica gels. At the second stage of the surface modification silica gel particles incurred insignificant defragmentation that has no influence on porosity and surface area of modified silicas.

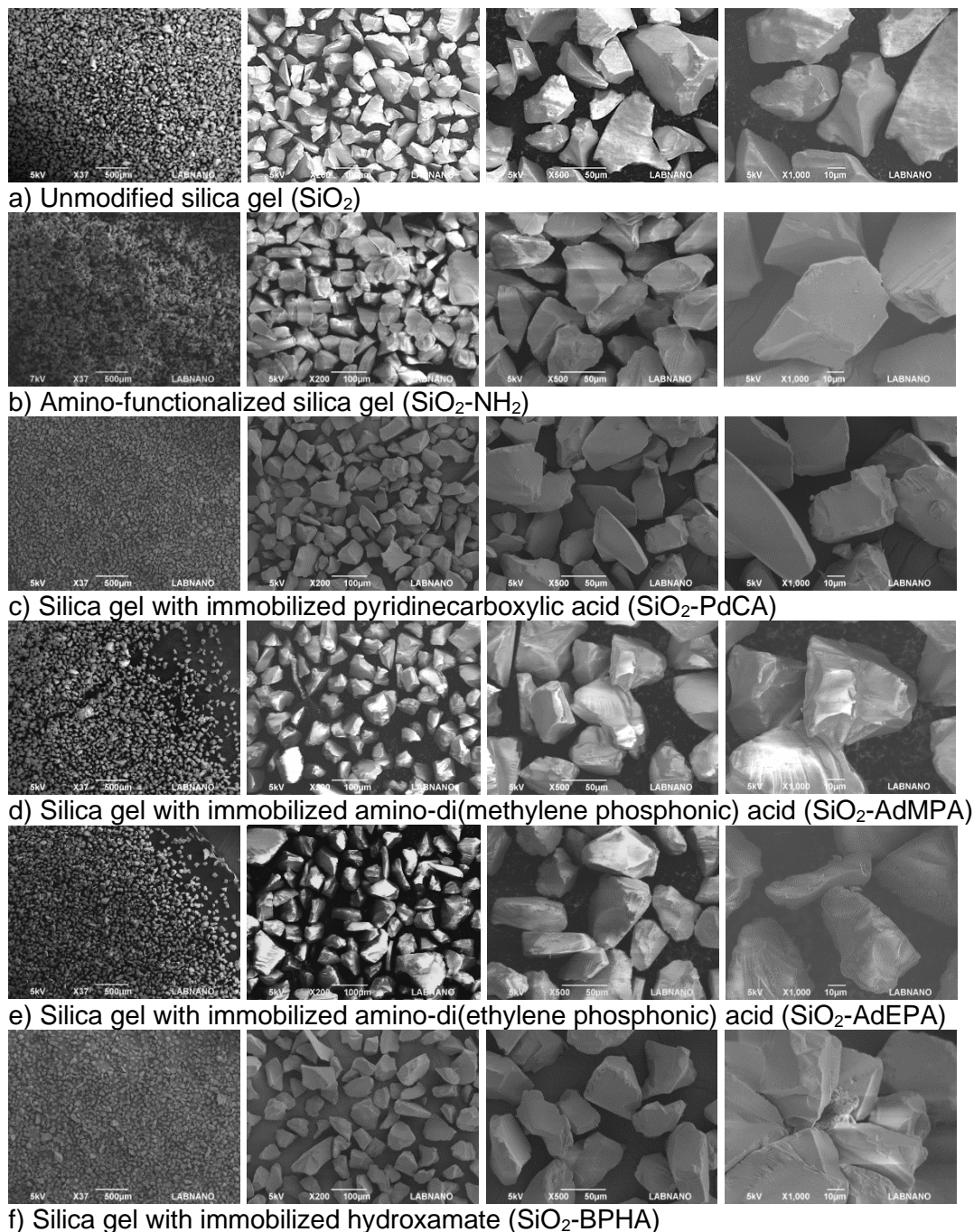


Figure 15. SEM images of unmodified and functionalized silica gels. Partially reproduced from (Artiushenko *et al.*, 2019).

4.4. Spectroscopic characterization of the immobilized complexes

4.4.1. Luminescent properties of REE complexes with immobilized ligands

Silica gels with covalently immobilized with 2,6-pyridinedicarboxylic acid SiO₂-PdCA and amino-di(methylene phosphonic) acid SiO₂-AdMPA were used as ligands to coordinate some of REE ($M^{n+} = Tb^{3+}$ and Eu^{3+}) for producing luminescent organic-inorganic hybrid materials.

As can be seen from photos provided, after adsorption of Eu^{3+} and Tb^{3+} ions (Figure 16), SiO₂-PdCA demonstrates strong red and green luminescent and can be used as luminescent probes for monitoring of Eu^{3+} and Tb^{3+} ions in water samples.

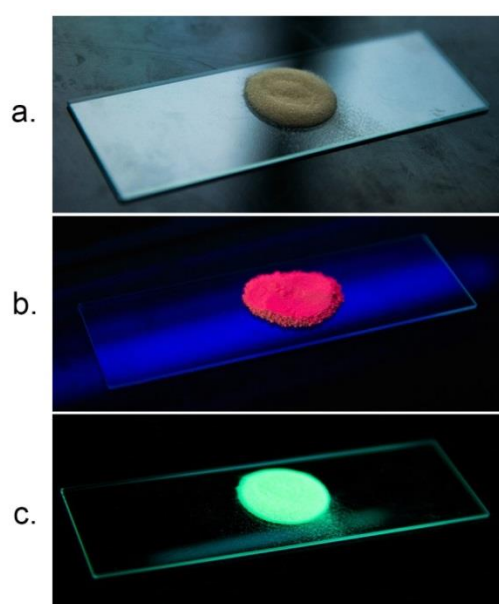


Figure 16. Luminescent hybrid materials a) SiO₂-PdCA pure; b) SiO₂-PdCA-Eu, $\lambda = 365$ nm; c) SiO₂-PdCA-Tb, $\lambda = 254$ nm.

The emission 3D spectrum excited in energy range 4-6 eV for each complex is shown in Figure 17.

After adsorption of Eu^{3+} and Tb^{3+} ions, each complex demonstrates strong luminescent emissions between 480 and 650 nm, designated to $4f \rightarrow 4f$ transitions of the 5D_0 excited state to the low-lying 7F_J ($J = 0, 1, 2, 3, 4$) levels of Eu^{3+} ions and $^5D_4 \rightarrow ^7F_n$ ($n = 3, 4, 5, 6$) electron transitions of the Tb^{3+} ions. No emission peaks from the ligands were observed under this excitation.

The 2D emission spectra excited in 6.00 eV for complexes of 2,6-pyridinedicarboxylic acid immobilized in surface with Eu^{3+} and Tb^{3+} ions are shown in Figure 18. From the emission spectrum of SiO₂-PdCA- Eu^{3+} , the transitions of $^5D_0 \rightarrow ^7F_0$ are forbidden for europium chelate complexes by the selection rules and

$^5D_0 \rightarrow ^7F_3$ (magnetic and electric dipole transitions) are very weak, while those of $^5D_0 \rightarrow ^7F_1$ (magnetic dipole transition), $^5D_0 \rightarrow ^7F_2$ and $^5D_0 \rightarrow ^7F_4$ (electric dipole transition) are strong. It is known that the nature of the magnetic dipole transition $^5D_0 \rightarrow ^7F_1$ is independent of the coordination environment surrounding the metal ion. A prominent feature noted in hypersensitive transition $^5D_0 \rightarrow ^7F_2$ as its intensity strongly depends on the local symmetry of the Eu^{3+} ions and chemical environment around the Eu^{3+} center. When the interactions of the Ln^{3+} complex with its local environment were stronger, the complex became more unsymmetrical and the intensity of the electric dipole transitions became more intense. A similar picture is observed for the sample $\text{SiO}_2\text{-AdMPA-Eu}^{3+}$.

Emission spectra of $\text{SiO}_2\text{-PdCA-Tb}^{3+}$ and $\text{SiO}_2\text{-AdMPA-Tb}^{3+}$ exhibits insensitive peaks at 490, 546, 585 and 620 nm that corresponds $^5D_4 \rightarrow ^7F_6$, $^5D_4 \rightarrow ^7F_5$, $^5D_4 \rightarrow ^7F_4$, $^5D_4 \rightarrow ^7F_3$ transitions of Tb^{3+} , respectively. The most intense prominent band is $^5D_4 \rightarrow ^7F_5$, due to which the complex gives green luminescence at 546 nm.

The presence of $^5D_0 \rightarrow ^7F_2$ transitions of Eu^{3+} and $^5D_4 \rightarrow ^7F_5$ of Tb^{3+} provides that metal adsorption on $\text{SiO}_2\text{-PdCA}$ and $\text{SiO}_2\text{-AdMPA}$ take place due to formation of the metal complexes with immobilized derivatives of 2,6-pyridinedicarboxylic acid and amino-di(methylene phosphonic) acid on the surface.

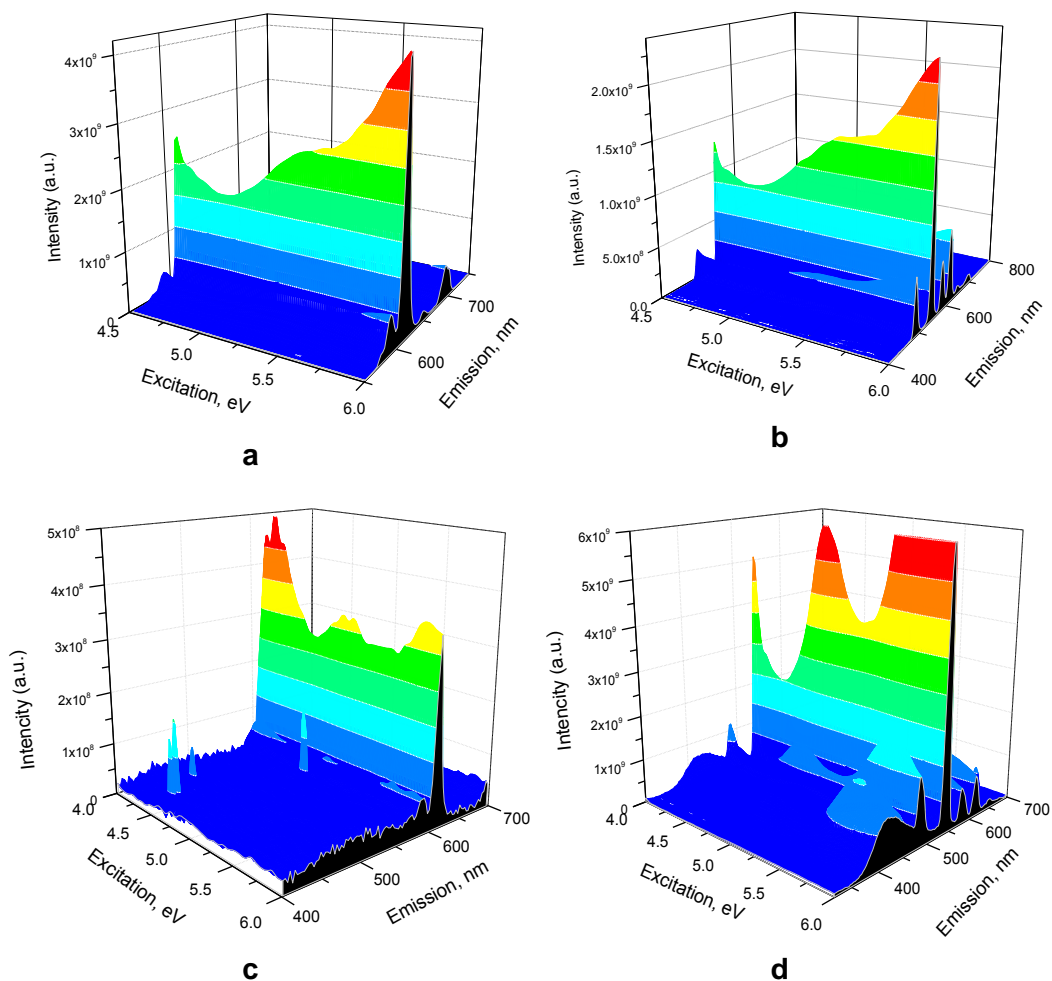


Figure 17. 3D mapping around the optical band gap of luminescent hybrid materials – $\text{SiO}_2\text{-PdCA-Eu}^{3+}$ (a), $\text{SiO}_2\text{-PdCA-Tb}^{3+}$ (b), $\text{SiO}_2\text{-AdMPA-Eu}^{3+}$ (c), $\text{SiO}_2\text{-AdMPA-Tb}^{3+}$ (d).

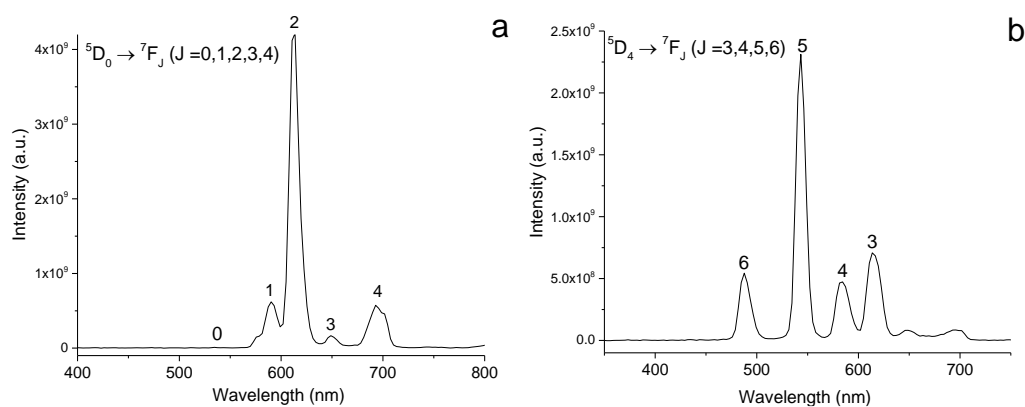


Figure 18. Luminescence emission spectra of $\text{SiO}_2\text{-PdCA-Eu}^{3+}$ (a) and $\text{SiO}_2\text{-PdCA-Tb}^{3+}$ (b).

4.4.2. Diffuse reflectance spectroscopy of Fe(III) complexes with SiO₂-BPHA

Diffuse reflectance spectroscopy (DRS) was used to study the nature of the surface interaction and complex formation between silica gel with immobilized fragments of hydroxamic acid (SiO₂-BPHA) and metal ions. For this purpose, it was used the ability of SiO₂-BPHA to form intense-red color complexes with Fe³⁺ ions (Zaitsev *et al.*, 1999). After adsorption of Fe³⁺ ions, in DRS spectra of SiO₂-BPHA in visible region, one intensive band with maximum at 500 nm is observed, Figure 19. The position of the absorbance maximum doesn't change with increasing metal loading indicates chemisorption of Fe³⁺ on SiO₂-BPHA.

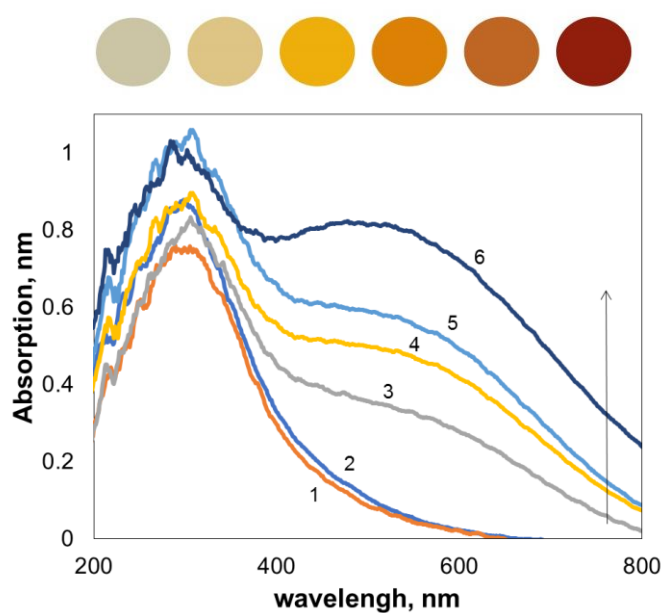


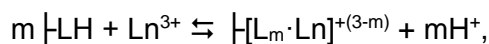
Figure 19: UV-Vis diffuse reflectance spectra of SiO₂-BPHA with different metal loading. $C_{\text{Fe}^{3+}}$, mg g⁻¹ = 1) $5.0 \cdot 10^{-3}$, 2) $5.0 \cdot 10^{-2}$, 3) 0.1, 4) 0.25, 5) 0.5, 6) 1.0.

4.5. Adsorption and separation of REEs

The idea of the present investigation is to explore the synergism in a combination of selectivity of immobilized ligands and technological advances of SPE in preconcentration of REEs from large volumes of diluted solutions.

The adsorbents can be applied for impurities removal in dynamic (solid-phase extraction, SPE) or static (dispersive solid-phase extraction, DSPE) conditions (Ribeiro *et al.*, 2014; Yang *et al.*, 2011). In the case of DSPE, adsorption equilibrium is reached and thus the results of separation are more predictable and recovery degree of analytes could be higher than for dynamic SPE. Therefore, DSPE demonstrates better results for removing traces of target compounds. In this research, DSPE has been used in all adsorption/desorption studies.

Selectivity and affinity of metal to adsorbent are the key factors determining the effectiveness of the adsorption. The selectivity of the adsorbents for the metal ions is provided by nature of immobilized chelating groups on the surface. Degree of metal ions extraction from solution (recovery) depends on stability of metal complexes between REE and immobilized ligands:



where $\text{---} \text{L}$ – immobilized ligand, $\text{---} [\text{L}_m \cdot \text{Ln}]^{+(3-m)}$ – immobilized complex.

This chapter describes the study of parameters and selection of conditions for application of silica-based adsorbents with immobilized ligands - derivatives of aminophosphonic, pyridine-carboxylic and hydroxamic acids (SiO_2 -AdMPA, SiO_2 -PdCA, and SiO_2 -BPHA) in dispersive solid-phase extraction and preconcentration of rare earth elements traces in the presence of competitive ions.

4.5.1. The adsorption kinetics and adsorption isotherms

Conditions of metal adsorption on OSAd (kinetics, recovery degree, range of solution pH) depend on the composition of immobilized layer and chemical nature of immobilized ligands the adsorbent affinity to the ions and the solution pH. For example, phosphonic acid cation exchangers change their selectivity with increase of pH because of the presence of ionizable OH groups in ion-exchange site (Zaitsev, Kostenko e Kobylinskaya, 2006). From the schematic representation of metal adsorption process on SiO_2 -PdCA, SiO_2 -AdMPA and SiO_2 -BPHA (Scheme 6), the adsorption ability of the adsorbents is strongly depend on pH. Moreover, due to the multifunctional nature of the surface complexation ability of the

adsorbent, it is also depends on additional interaction of metal ions with residual groups (aminopropyl and silanol) due to incomplete conversion during synthesis. Therefore, adsorption properties of the adsorbents varied from sample to sample and must be studied for every sample.

Effect of contact time

In order to optimize the contact time required for achieving the equilibrium, adsorption experiments of Eu^{3+} and Tb^{3+} (initial concentration 10 mg L^{-1}) from aqueous solutions were performed for 0.5-30 min by using 10 mg of adsorbents at $\text{pH}=3.0$ ($\text{SiO}_2\text{-PdCA}$, $\text{SiO}_2\text{-AdMPA}$) and $\text{pH}=5.0$ ($\text{SiO}_2\text{-BPHA}$). The results for adsorption are shown in Figure 20. As can be seen from the curves, adsorption of metal ions on all adsorbents is very fast and adsorption equilibrium reached less than 20 min for all adsorbents.

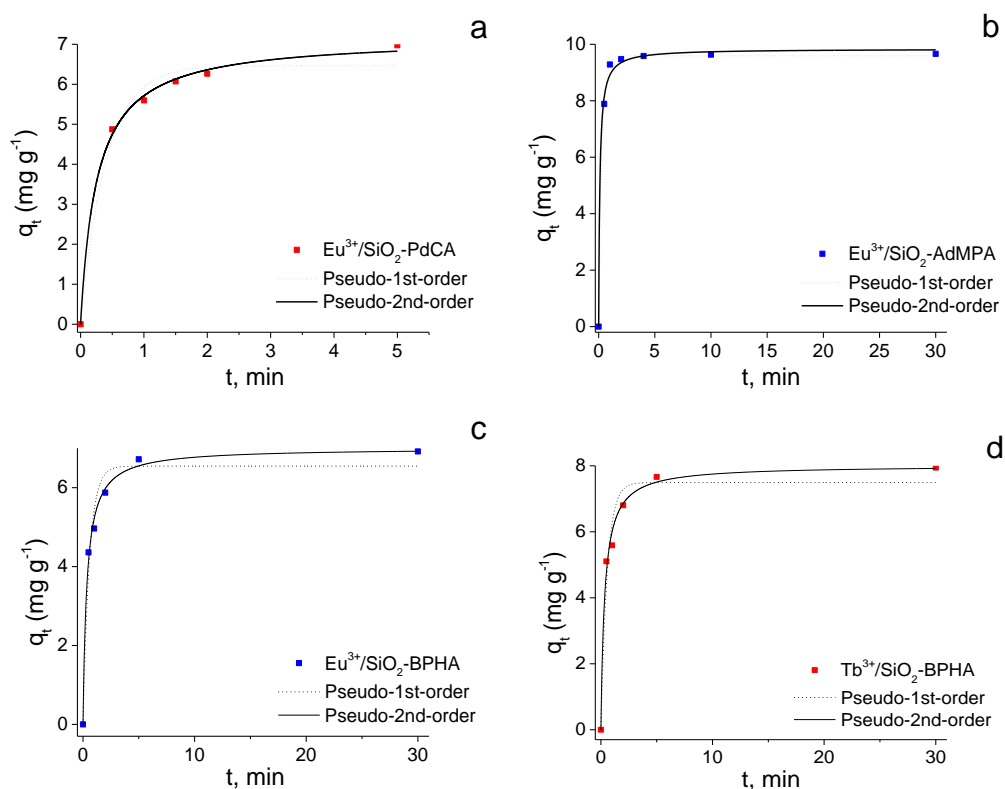


Figure 20. Effect of contact time on the removal of metal ions.
 $m_{\text{ad}} = 10 \text{ mg}$, $C_0(\text{M}^{3+}) = 10 \text{ mg L}^{-1}$, $V = 10 \text{ mL}$, $t = 0.5\text{-}30 \text{ min}$.

The related kinetic parameters are presented in Table 9. According to correlation coefficient (R^2), the pseudo-second-order model, which is frequently associated with chemical sorption mechanism, gives a better fit for the adsorption data of all adsorbents. The adsorption curve and kinetic model fitting suggest that

the uptake of metal ions is carried out due to chemical sorption of ions contributed by functional groups on the surface.

Table 9. Kinetic parameters for metal adsorption.

Adsorbent	Metal	Pseudo-1 st -order			Pseudo-2 nd -order		
		q_e , calc., mg g^{-1}	k_1 L min^{-1}	R^2	q_e , calc., mg g^{-1}	k_2 L min^{-1}	R^2
SiO₂-PdCA	Eu ³⁺	6.47	2.49	0.9796	7.18	0.543	0.9975
SiO₂-AdMPA	Eu ³⁺	9.59	3.41	0.9999	9.84	0.978	0.9961
SiO₂-BPHA	Eu ³⁺	6.54	1.77	0.9660	7.00	0.415	0.9945
	Tb ³⁺	7.49	1.79	0.9608	8.01	0.372	0.9915

Adsorption isotherms

For understanding the removal mechanism of metal ions by proposed adsorbents, the study of adsorption mechanisms becomes important. Equilibrium studies give the adsorption capacity of the adsorbent; provide information of affinity between adsorbates and adsorbents. The equilibrium relationships between adsorbent and adsorbate are described by adsorption isotherms that usually relate the metal uptake per unit mass of adsorbent (q_e) to the adsorbate concentration at equilibrium (C_e) in the bulk phase. Distribution of metal ions between the liquid phase and the solid phase is generally explained by adsorption isotherms, such as Freundlich, Langmuir and Temkin isotherms. In the case of Langmuir isotherm model, it is assumed sorption on homogeneous surface by monolayer adsorption, without any interaction between adsorbed species.

Affinity and capacity of the adsorbents SiO₂-PdCA, SiO₂-AdMPA, and SiO₂-BPHA towards REEs were evaluated from the adsorption isotherms of Eu³⁺ and Tb³⁺ ions. Adsorption isotherms were performed at pH=3.0 for SiO₂-PdCA and SiO₂-AdMPA and pH=5.0 for SiO₂-BPHA. The concentration of metal in solutions varied from 0.1 to 25 mg L⁻¹. The adsorption data were fitted with Langmuir and Freundlich isotherm models.

The adsorption data with fitted curves of linear Langmuir model (in inserts) are shown in Figure 21 and Figure 22. All adsorption isotherms are of H- and L-type. The angle of inclination indicates the affinity of the sorbent to the metal ions and the formation of stable complexes with the functional groups of the sorbent.

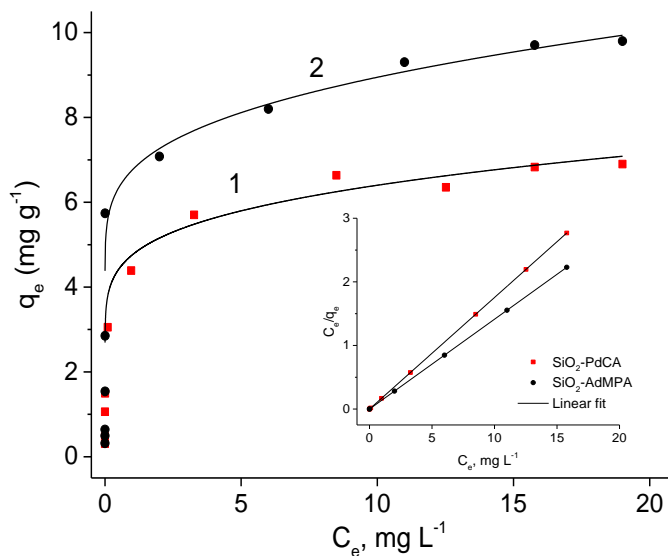


Figure 21. Adsorption isotherm of Eu^{3+} by $\text{SiO}_2\text{-PdCA}$ (1) and $\text{SiO}_2\text{-AdMPA}$ (2). $m_{\text{ad}} = 10 \text{ mg}$, $C_0(\text{Eu}^{3+}) = 0.1\text{-}25 \text{ mg L}^{-1}$, $V = 10 \text{ mL}$, $\text{pH} = 3.0$, $t = 2 \text{ h}$.

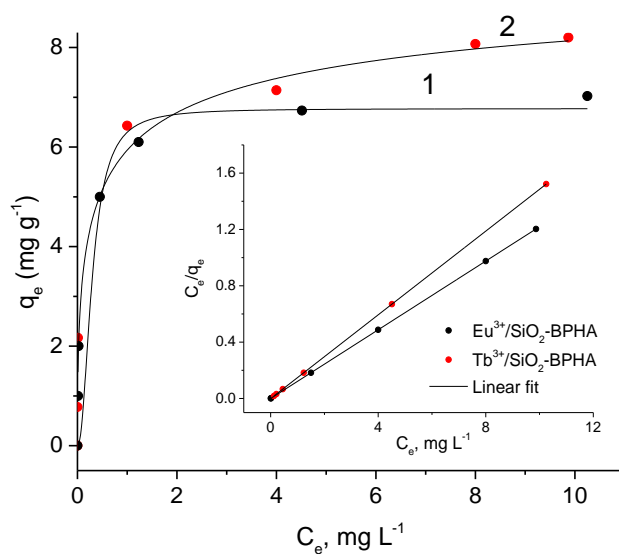


Figure 22. Adsorption isotherm of Eu^{3+} (1) and Tb^{3+} (2) by $\text{SiO}_2\text{-BPHA}$. Reproduced from (Artiushenko *et al.*, 2019). $m_{\text{ad}} = 10 \text{ mg}$, $C_0(\text{M}^{3+}) = 0.1\text{-}25 \text{ mg L}^{-1}$, $V = 10 \text{ mL}$, $\text{pH} = 5.0$, $t = 2 \text{ h}$.

The fitted calculated parameters of the adsorption isotherm are shown in Table 10. The adsorption behavior of Eu^{3+} and Tb^{3+} on all adsorbents has been better fitted by Langmuir model with the coefficients (R^2) 0.9999-1.00. This indicates the formation of a monolayer of adsorbate. The R^2 value of Freundlich model indicated that the model has not been able to adequately describe the adsorption behavior in our experiment.

Table 10. Adsorption isotherm parameters.

Adsorbent	Metal	Langmuir isotherm model			Freundlich isotherm model		
		q_{\max} , mg g^{-1}	K_L , L mg^{-1}	R^2	K_F , mg g^{-1}	$1/n$	R^2
SiO₂-PdCA	Eu ³⁺	5.7	0.361	0.9999	3.9	0.270	0.9111
SiO₂-AdMPA	Eu ³⁺	7.1	0.448	0.9999	5.5	0.277	0.7458
SiO₂-BPHA	Eu ³⁺	6.7	0.657	1.00	3.9	0.394	0.7339
	Tb ³⁺	8.2	0.830	1.00	4.1	0.386	0.5594

Effects of pH on adsorption

The adsorption properties of SiO₂-PdCA, SiO₂-AdMPA, and SiO₂, SiO₂-NH₂ (have been taken for comparison) were investigated in the pH 1.0–6.0 range for lanthanide and barium ions in mixture. Initial concentrations of REEs 20 $\mu\text{g L}^{-1}$ and adsorbent dosage of 10 mg. Barium was taken in 50-fold excess with respect to lanthanide ions. The adsorption study of REEs on SiO₂-BPHA was investigated in a pH range 2.0–6.0 under the initial concentrations of REEs 100 $\mu\text{g L}^{-1}$ and adsorbent dosage of 10 mg.

Effects of pH on adsorption of REEs by SiO₂ and SiO₂-NH₂ are shown in Figure 23.

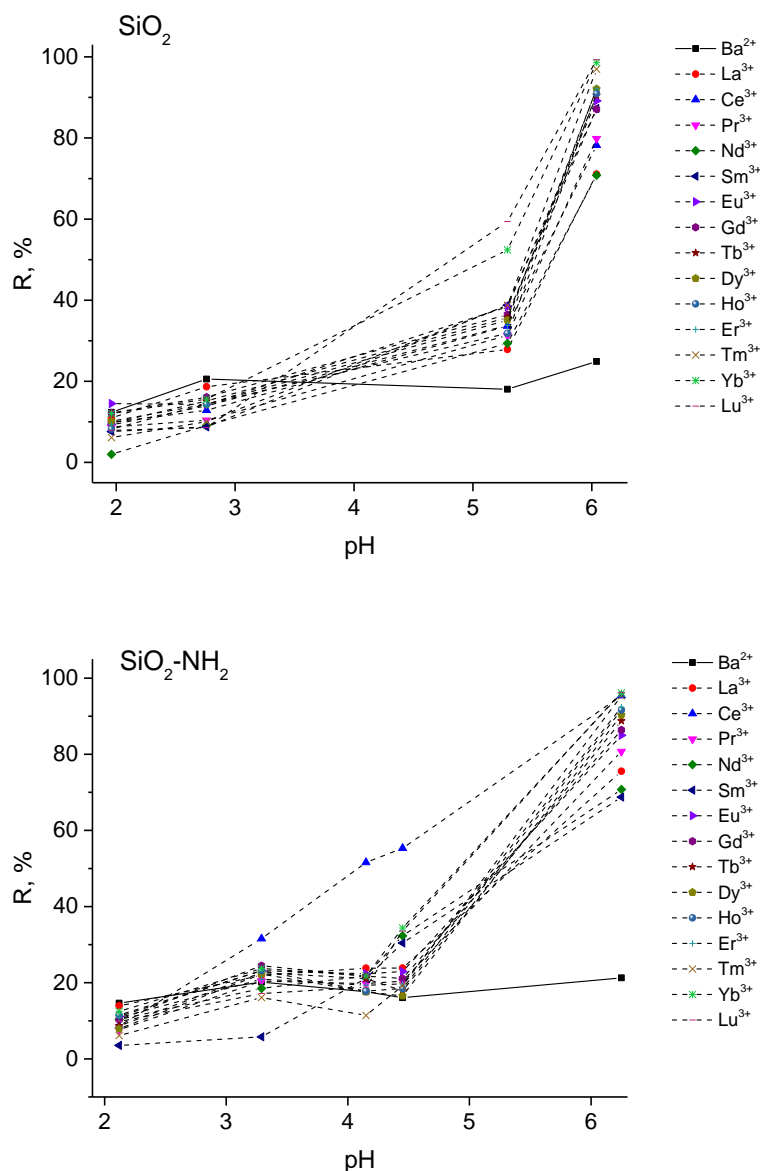


Figure 23. Effects of pH on adsorption of REEs by SiO_2 and $\text{SiO}_2\text{-NH}_2$.
 $m_{\text{ads}} = 10 \text{ mg}$, $C_0(\text{M}^{3+}) = 20.0 \text{ } \mu\text{g L}^{-1}$, $C_0(\text{Ba}^{2+}) = 1000.0 \text{ } \mu\text{g L}^{-1}$, $V = 10 \text{ mL}$, $t = 2 \text{ h}$.

At pH above 6.0 experiments were not performed on purpose to study only the adsorption of trivalent ion form of REE ions. As it is shown (İçhedef, Şişmanoğlu e Teksöz, 2018), at pH 7.0 several forms of REE coexist in solution, including Ln^{3+} and $\text{Ln}(\text{OH})^+$. And at pH higher than 8.0 occurs formation of the corresponding insoluble hydroxides $\text{Ln}(\text{OH})_3$. Coexistence of several ion forms complicates the study of adsorption equilibrium at $6.0 < \text{pH} < 8.0$ and at $\text{pH} > 8.0$, the hydroxides simply precipitate on the surface of the silica matrix.

As it is seen from Figure 23 bulk silica and amino-silica gel are weak adsorbents for all rare earth metals even in low concentration. For example, all REEs cannot be fully extracted from solution with $\text{pH} < 5.5$. At $\text{pH} > 5.5$ these metal

ions are fully removed from solution. It is common for all silica-based adsorbents and is observed due to hydrolysis of the ions and its precipitation on silica surface.

The adsorption curves look completely different for SiO₂-PdCA and SiO₂-AdMPA, Figure 24.

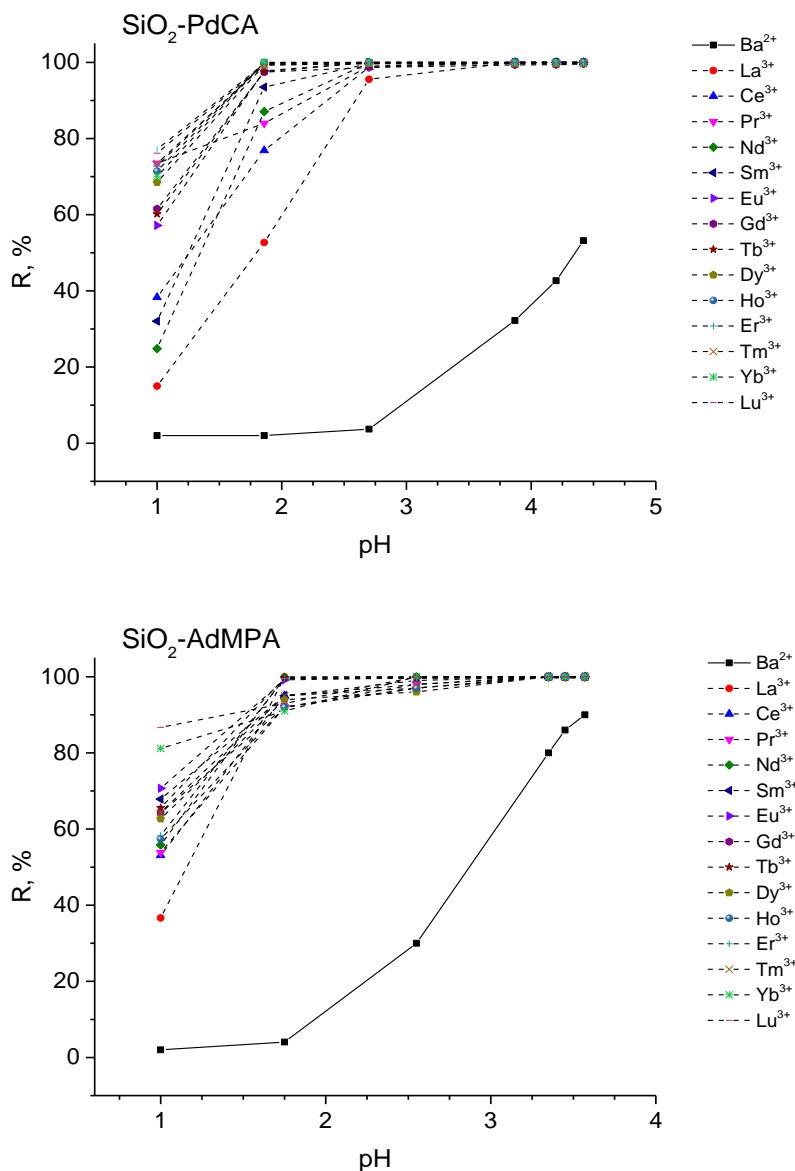


Figure 24. Effects of pH on adsorption of REEs by adsorbents.
 $m_{ads} = 10 \text{ mg}$, $C_o(M^{3+}) = 20.0 \mu\text{g L}^{-1}$, $C_o(Ba^{2+}) = 1000.0 \mu\text{g L}^{-1}$, $V = 10 \text{ mL}$, $t = 2 \text{ h}$.

Contrary to bulk and amino silica, SiO₂-PdCA uptakes REE at pH>2.5 for more than 95%, while Ba²⁺ ions start to remove from solution at pH>3.5-4. SiO₂-AdMPA fully uptakes REEs in all studied range, Ba²⁺ ions start to remove from solution at pH>2.5 and reached 90% at pH>3.5. Since immobilized complexes of REEs are stable in pH range of 2 to 6 and Ba²⁺ ions have no influence on REE adsorption until pH>3.0-3.5. Adsorbents SiO₂-PdCA and SiO₂-AdMPA can be used

as adsorbents for pre-concentration of these metals and their separation from Ba^{2+} ions, that are commonly presented in most samples, mainly geological ones, as macro component. Since ICP-MS determination of Nd^{3+} , Gd^{3+} , Sm^{3+} , and Eu^{3+} ions is limited on single quadrupole ICP-MS because of serious polyatomic interferences from barium matrix (such as BaO^+ and BaOH^+). For this reason, investigations of the adsorbent application for REEs removal were performed for the suspensions with $\text{pH} = 2.5$ for $\text{SiO}_2\text{-PdCA}$ and 2.0 for $\text{SiO}_2\text{-AdMPA}$.

The results of the REEs adsorption on $\text{SiO}_2\text{-BPHA}$ are shown in Figure 25. No essential adsorption is observed with $\text{pH} < 3.0$, while $\text{SiO}_2\text{-BPHA}$ uptakes REE at $\text{pH} > 4.5$ for more than 80% and achieve >95% at $\text{pH} = 5.0$. Therefore, investigations of the adsorbent application for REEs removal were performed for the suspensions with $\text{pH} = 5.0$.

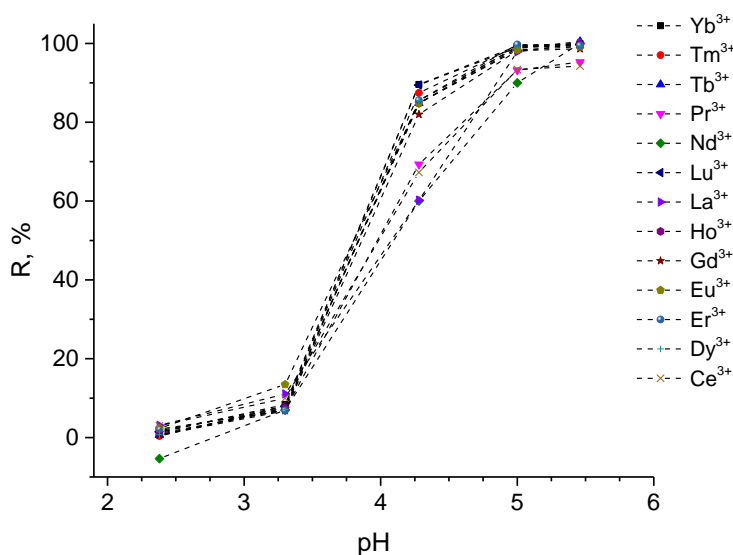


Figure 25. Effects of pH on adsorption of REEs by $\text{SiO}_2\text{-BPHA}$.

Adapted from (Artiushenko *et al.*, 2019).

$m_{\text{ads}} = 10 \text{ mg}$, $C_0(\text{M}^{3+}) = 100.0 \mu\text{g L}^{-1}$, $V = 10 \text{ mL}$, $t = 2 \text{ h}$.

4.5.2. REEs adsorption from multi-component solution

Affinity of $\text{SiO}_2\text{-PdCA}$, $\text{SiO}_2\text{-AdMPA}$, $\text{SiO}_2\text{-BPHA}$ towards REEs was quantitatively characterized by metal distribution coefficient (K_d), determined for REEs adsorption from multi-component solution with initial concentration of each REE ion 1.0 mg L^{-1} . K_d value obtained for adsorbents was compared with K_d value for $\text{SiO}_2\text{-NH}_2$ and bulk silica.

The results as a function of K_d versus atomic number of REE are presented in Figure 26. The results shown that K_d values for lanthanides adsorbed by modified adsorbents are significantly higher in comparison with pure silica and

silica gel with aminopropyl groups. This indicates a higher affinity and higher extraction capacity of functionalized adsorbents towards REEs and proves their chemisorption resulting in formation of metal complexes with immobilized ligands.

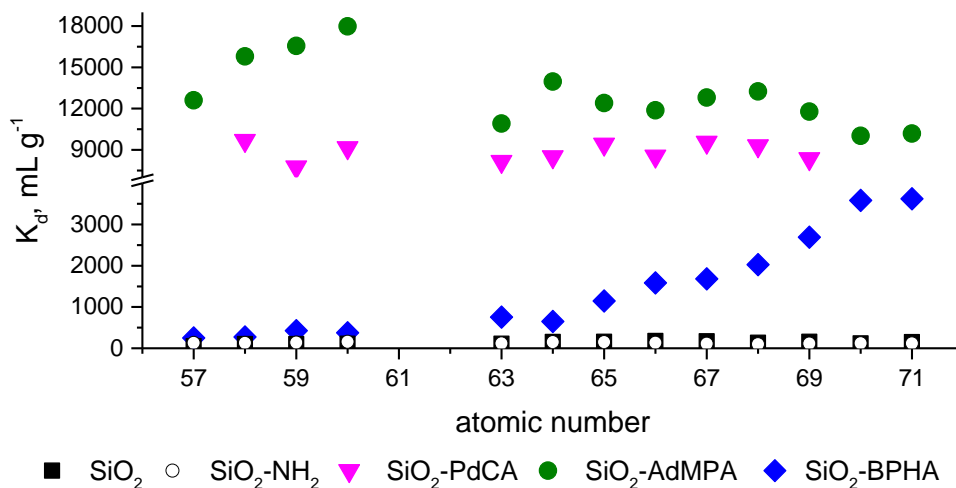
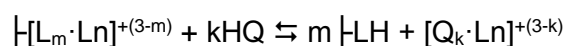


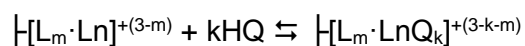
Figure 26. Distribution coefficients (K_d) values for REEs adsorption. Partially reproduced from (Artiushenko *et al.*, 2019). $m_{ad} = 10$ mg, $C_0(M^{3+}) = 1.0$ mg L⁻¹, $V = 10$ mL, $t = 2$ h.

4.5.3. Desorption study

For REE recuperation, efficiencies of the ions adsorption and desorption are equally important, because they have the same impact on the recovery of target compounds. After the process of adsorption, the adsorbent should be easily regenerated with an effective, cheap, non-polluting and non-damaging desorbing agent. Similar to REE removal from solution, elution degree of REE depends on stability of the REE complexes with ligands used in eluent mixture. As a result, adsorbent with high efficiency of REE adsorption commonly demonstrates low overall recovery of REEs and poor reusability since incomplete metal desorption (Ashour *et al.*, 2017; Hu *et al.*, 2017; Ramasamy, Repo, *et al.*, 2017). Typically, metal ions are better removed in a strongly acidic medium. However, high concentration of acid is not acceptable for most organo-mineral adsorbents, due to their instability in such conditions, therefore utilization of chelating agents is more appropriate for REE elution. In this case, a competing ligand solution (HQ) is added to the adsorbent and the desorption process described by scheme:



In accordance with this scheme, the nature and concentration of the ligand HQ primarily affect the desorption of metal ions. This allows to reduce the acidity of the eluting solution to acceptable values. The method of competitive complexation has a significant limitation: because of REEs high coordination numbers, there is the possibility of the formation of immobilized mixed ligand complexes, for example, according to scheme:



As a result, the addition of a competing ligand may not lead to the desorption of lanthanide ions into the solution.

Desorption from SiO₂-PdCA and SiO₂-AdMPA

For the purpose to remove adsorbed metals from SiO₂-PdCA and SiO₂-AdMPA adsorbents with maximized overall recovery, we studied several promising desorbing agents, which effects are based on proton exchange: strong mineral acids (HCl or HNO₃) in concentration 0.1-2 mol L⁻¹, or metal chelating abilities: ethylenediaminetetraacetic acid disodium salt (EDTA), 5-sulfosalicylic acid (SSA), citric acid (CiA), aminosulfonic acid (AmSA), α-hydroxyisobutyric acid (HBA), oxalic acid (OxA) and L-ascorbic acid (AsA) in concentration 0.01 mol L⁻¹. The eluting agents were used in large excess (10⁻⁵ mol) to total loading of REEs (≈10⁻⁷ mol). Chemical formulas of the chelating agents used for eluting of REEs are shown in Figure 27.

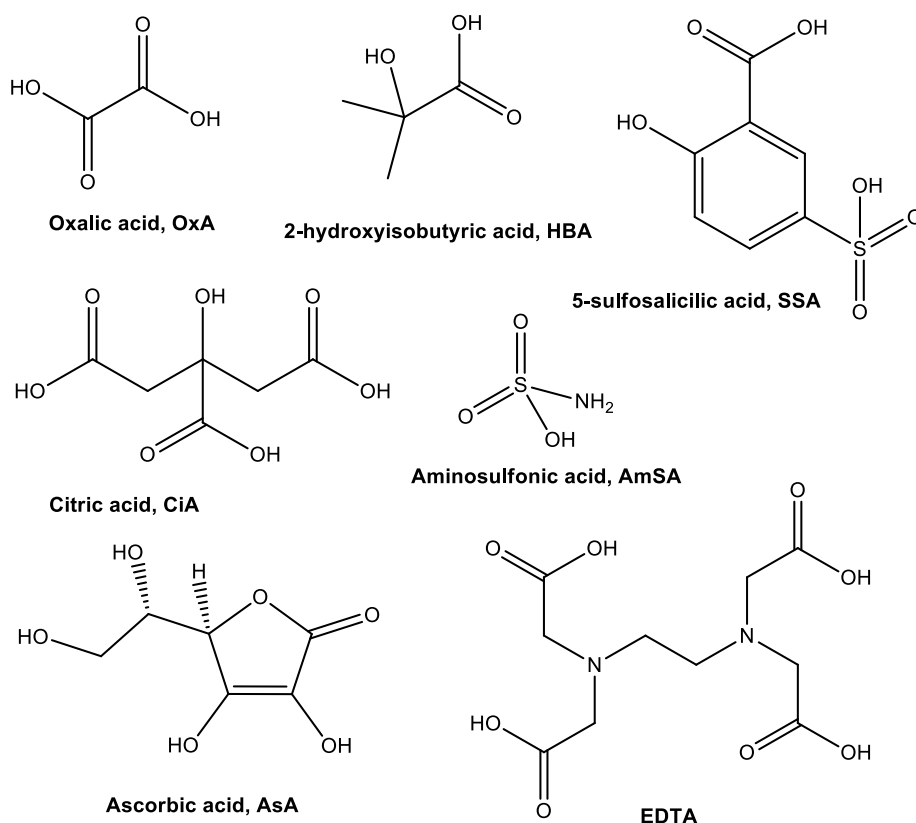


Figure 27. Chemical formulas of chelating agents.

Elution efficiency of mentioned desorbing agents for REEs desorption from $\text{SiO}_2\text{-PdCA}$ and $\text{SiO}_2\text{-AdMPA}$ are shown in Figure 28 and Figure 29.

Organic acids and mineral acid in low concentration (up to 0.1 mol L^{-1}) have no or little effect on REE desorption from both adsorbents. Only with OxA has been eluted 80% of La^{3+} ions from $\text{SiO}_2\text{-PdCA}$ and about 40% of others REE. From $\text{SiO}_2\text{-PdCA}$ 0.1 mol L^{-1} HCl or HNO_3 can elute about 60-80% of light REE (La^{3+} , Ce^{3+} , Pr^{3+} and Nd^{3+}) and not effective for desorption ($E, \% < 60$) of heavy REEs.

In case of $\text{SiO}_2\text{-PdCA}$ most promising results were obtained when EDTA was used as eluting agent. In this case elution degree of REEs was about 60 - 80%, increasing from light to heavy elements. Complete (95-100%) elution of most REEs from $\text{SiO}_2\text{-PdCA}$ was achieved only on using of 2 mol L^{-1} HNO_3 solution.

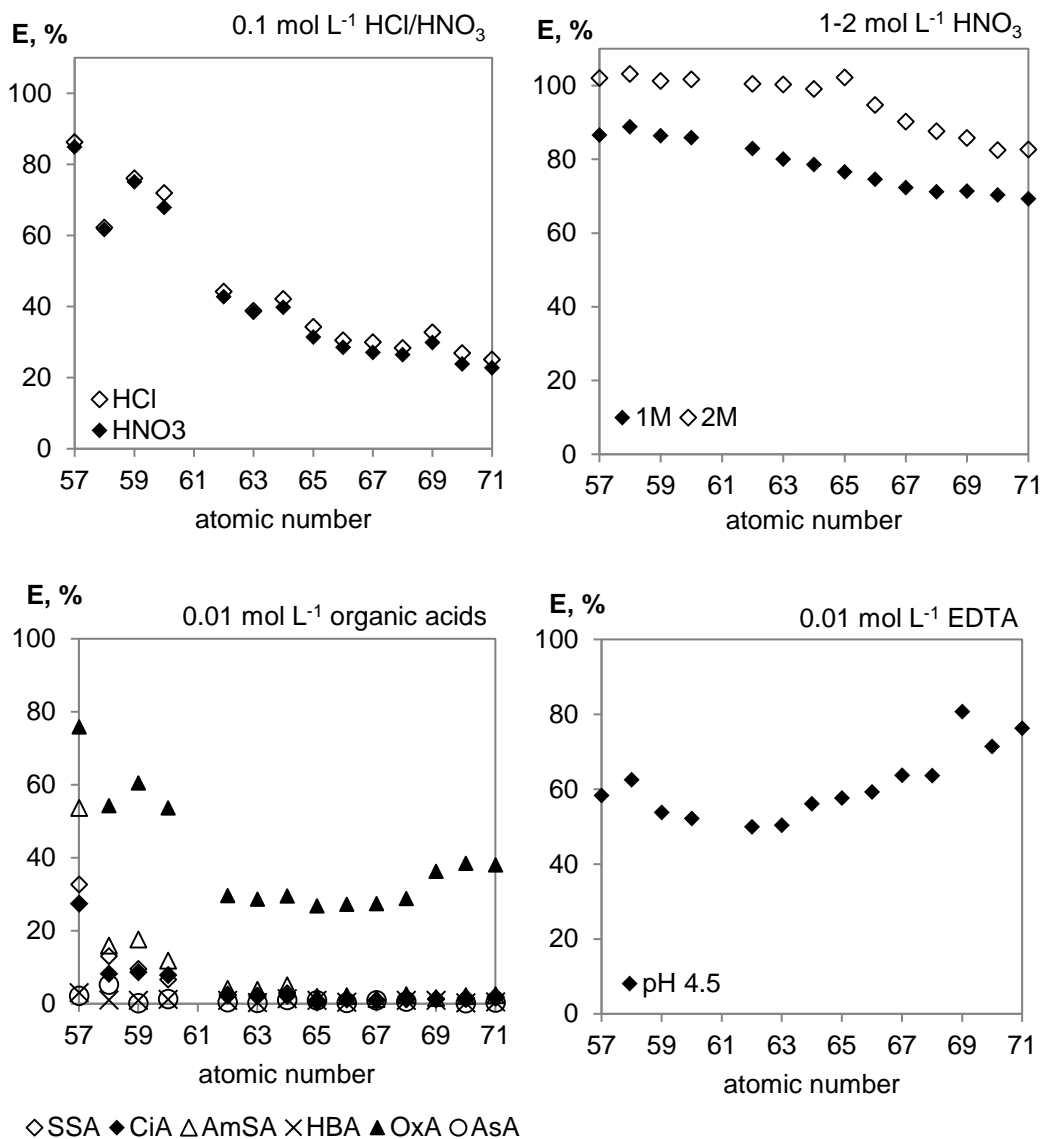


Figure 28. Desorption of REEs from SiO₂-PdCA. Adapted from (Artiushenko *et al.*, 2018).
 $m_{ads} = 10 \text{ mg}$, $C_{ads}(M^{X+}) = 100.0 \text{ } \mu\text{g L}^{-1}$, $V = 10 \text{ mL}$, $t = 2 \text{ h}$.

SiO₂-AdMPA has higher affinity towards REEs than SiO₂-PdCA, therefore the metal desorption from SiO₂-AdMPA is more problematic. For example, eluting of La³⁺ and Ce³⁺ from SiO₂-PdCA by OxA solution achieved 76% and 60%, while from SiO₂-AdMPA it does not exceed 10%.

For both adsorbents, 2 mol L⁻¹ HNO₃ and 0.01 mol L⁻¹ EDTA were identified as the most promising eluting agents of REEs. Application of 2 mol L⁻¹ HNO₃ is not desirable for several reasons including pure reusability of the adsorbents; therefore EDTA was further studied as eluting agent. Particularly, eluting properties of EDTA in desorption of Eu³⁺ were studied as a function of the solution pH. Results are shown in Figure 30.

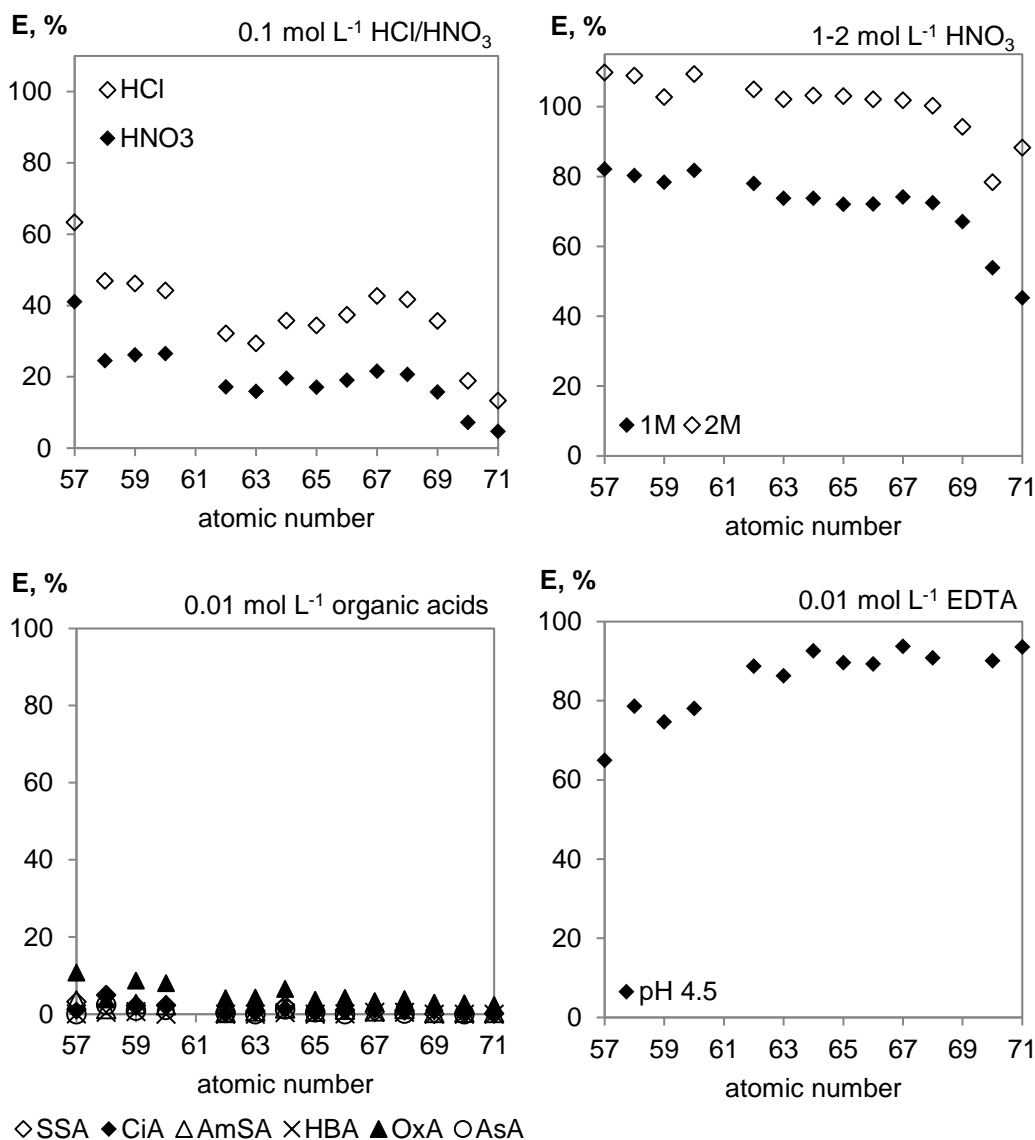


Figure 29. Desorption of REEs from SiO₂-AdMPA.
 $m_{\text{ads}} = 10 \text{ mg}$, $C_{\text{ads}}(\text{M}^{\text{x}+}) = 100.0 \text{ } \mu\text{g L}^{-1}$, $V = 10 \text{ mL}$, $t = 2 \text{ h}$.

As it can be seen, desorption ability of 0.01 mol L⁻¹ EDTA increases with increasing pH and the experiments for desorption of REEs were performed at pH=8.0. Elution efficiency of 0.01 mol L⁻¹ EDTA at pH 8.0 for REEs desorption from SiO₂-PdCA and SiO₂-AdPA is shown in Figure 31.

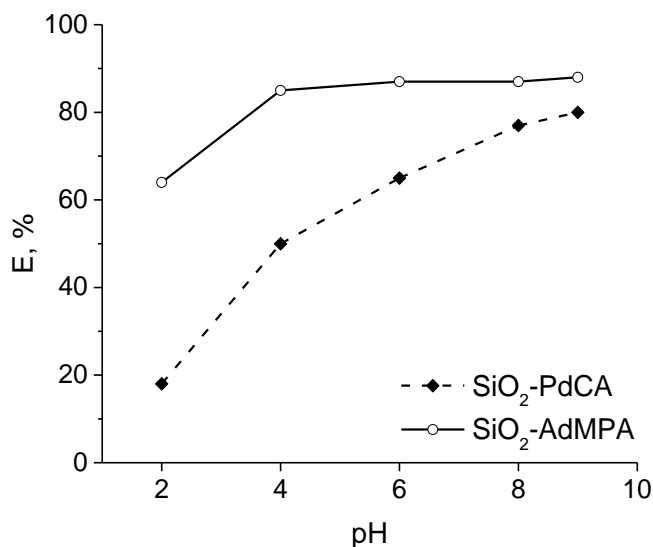


Figure 30. Desorption of Eu³⁺ from adsorbents. Adapted from (Artiushenko *et al.*, 2018).
 $m_{\text{ads}} = 10 \text{ mg}$, $C_{\text{ads}}(M^{X+}) = 100.0 \mu\text{g L}^{-1}$, $V = 10 \text{ mL}$, $t = 2 \text{ h}$.

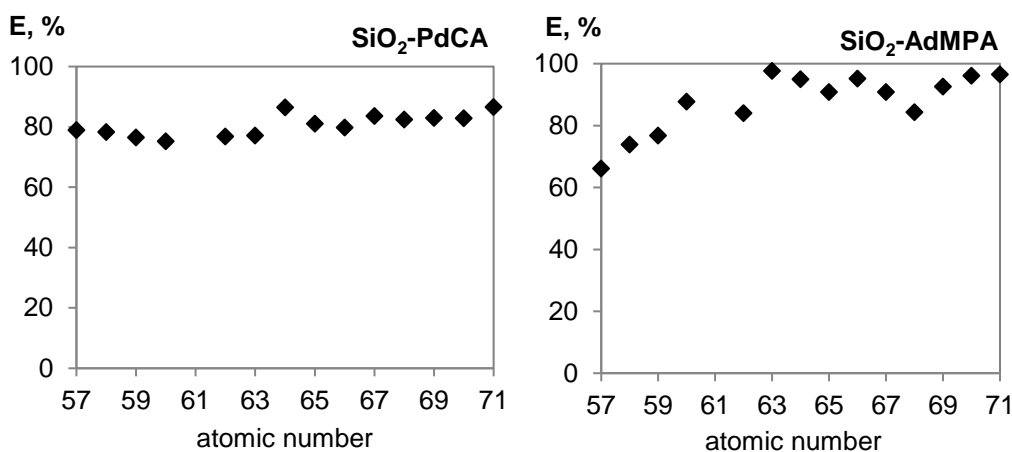


Figure 31. Desorption of REE from adsorbents using 0.01 mol L^{-1} EDTA at pH 8.
 Adapted from (Artiushenko *et al.*, 2018).
 $m_{\text{ads}} = 10 \text{ mg}$, $C_{\text{ads}}(M^{X+}) = 100.0 \mu\text{g L}^{-1}$, $V = 10 \text{ mL}$, $t = 2 \text{ h}$.

From the provided results, it can be concluded that application of 0.01 mol L^{-1} water solution of EDTA at pH=8.0 as well as 2 mol L^{-1} HNO₃, allow quantitative desorption of REEs to solution from SiO₂-PdCA and SiO₂-AdMPA adsorbents.

Desorption from SiO₂-BPHA

Since adsorption of the REEs on SiO₂-BPHA is rapidly decreased with increasing of the solution acidity, desorption from SiO₂-BPHA should occur under milder conditions than from SiO₂-PdCA and SiO₂-AdMPA, that's why desorption of

REEs from the SiO₂-BPHA was studied in acid media using 0.01-1.0 mol L⁻¹ water solution of HCl and HNO₃. Results of desorption of the REEs from SiO₂-BPHA are shown in Figure 32. As can be seen, with 0.1 mol L⁻¹ HNO₃ complete desorption of all REEs is observed. The same behavior is observed for 0.1 mol L⁻¹ HCl. Since HNO₃ commonly have fewer metal impurities, it was chosen for REEs desorption from SiO₂-BPHA.

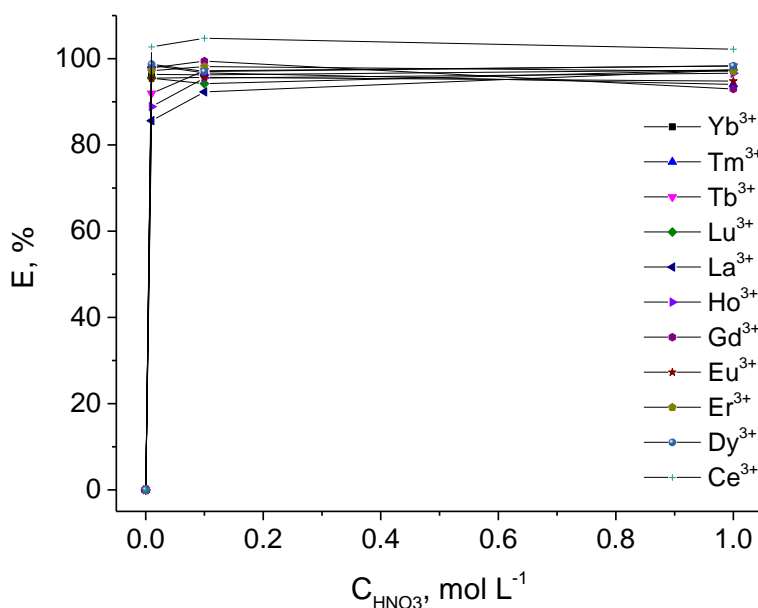


Figure 32. Desorption of REEs from SiO₂-BPHA with HNO₃.
Adapted from (Artiushenko *et al.*, 2019)
 $m_{\text{ads}} = 10 \text{ mg}$, $C_{\text{ads}}(M^{X+}) = 100.0 \mu\text{g L}^{-1}$, $V = 10 \text{ mL}$, $t = 2 \text{ h}$.

4.5.4. Reusability of adsorbents

Reusability of adsorbents was studied in five adsorption-desorption cycles. Desorption from SiO₂-PdCA and SiO₂-AdMPA was performed with water solution of 0.01 mol L⁻¹ EDTA with pH=8.0 and 2 mol L⁻¹ HNO₃. For desorption from SiO₂-BPHA was used 0.1 mol L⁻¹ HNO₃. The results are presented as an average value with upper and lower limits of the metal adsorption (A,%) and desorption (E,%) from multi-element solutions in five consecutive adsorption cycles by the same adsorbent.

Reusability studies of SiO₂-PdCA and SiO₂-AdPA are presented in Figure 33 and Figure 34. Results demonstrate that both adsorbents remain their adsorption properties in full after five adsorption/desorption cycles.

As it can be assumed from Figure 33, EDTA solution is more suitable for desorption of heavy lanthanides (Figure 33b) from SiO₂-PdCA, while HNO₃ solution is better to use for extraction of light elements (Figure 33d).

For both adsorbents, it's observed large dispersion of the elution degrees in desorption experiment. This can be explained by incomplete desorption of REEs when the metal ions remaining on the adsorbent will be desorbed together with other freshly adsorbed ions in the second desorption cycle and the total amount of the eluting metals increases. Residuals of the metals remaining on adsorbents play no essential role in their adsorption properties, because of the high metal capacity.

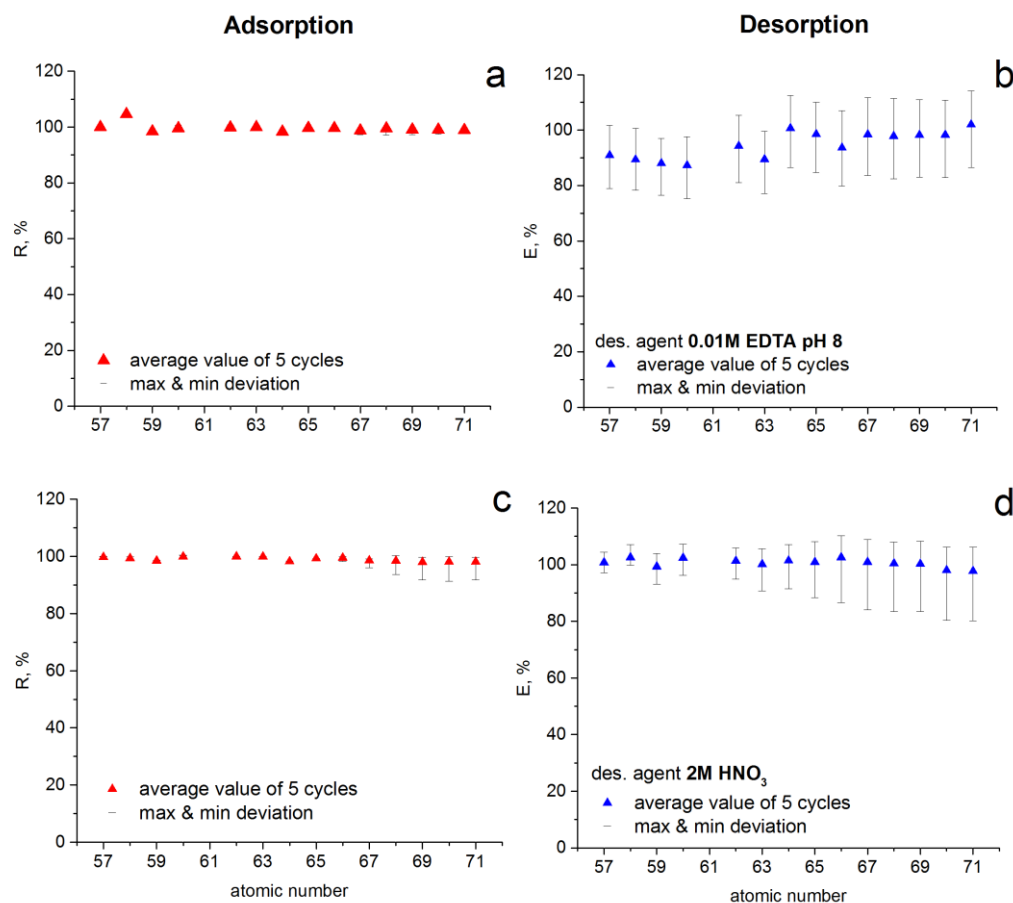


Figure 33. Adsorption recovery (R,%) and desorption efficiency (E,%) of REEs on $\text{SiO}_2\text{-PdCA}$ in five adsorption/desorption cycles. Adapted from (Artiushenko *et al.*, 2018). $m_{\text{ads}} = 10 \text{ mg}$, $C_{\text{ads}}(\text{M}^{x+}) = 100.0 \mu\text{g L}^{-1}$, $V = 10 \text{ mL}$, $t = 2 \text{ h}$.

Reusability studies of $\text{SiO}_2\text{-BPHA}$ are presented in Figure 35. As it can be seen, the adsorption properties remain unchanged for all cycles. There is no decrease in adsorption capacity of the adsorbent and no dispersion during desorption. In $0.1 \text{ mol L}^{-1} \text{ HNO}_3$, average elution degree for all REEs was more than 80%, Figure 35. This data shows that $\text{SiO}_2\text{-BPHA}$ can be easily regenerated by treatment with cheap and non-damaging the structure of the sorbent solute.

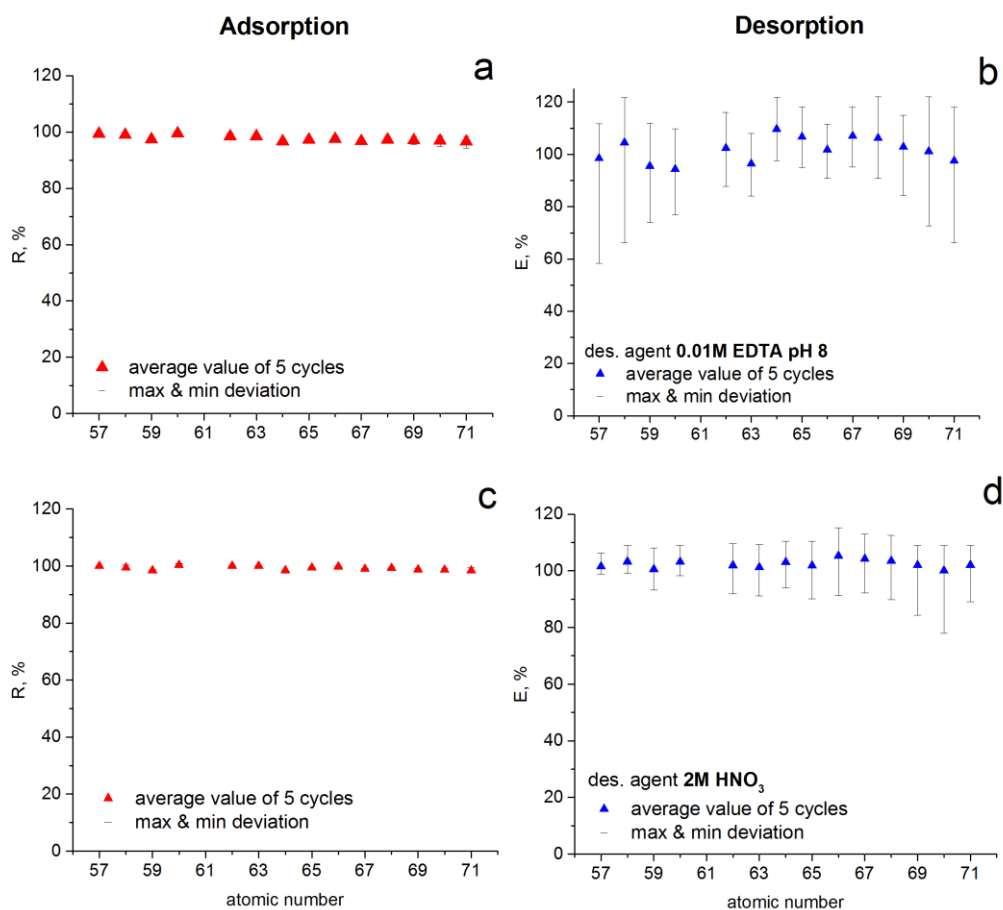


Figure 34. Adsorption recovery (R,%) and desorption efficiency (E,%) of REEs on SiO₂-AdMPA in five adsorption/desorption cycles.
 $m_{\text{ads}} = 10 \text{ mg}$, $C_{\text{ads}}(M^{X+}) = 100.0 \mu\text{g L}^{-1}$, $V = 10 \text{ mL}$, $t = 2 \text{ h}$.

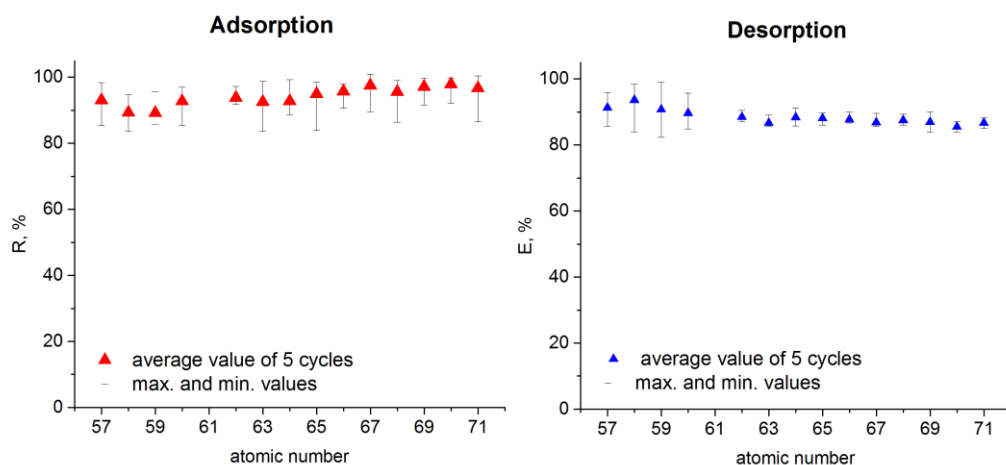


Figure 35. Adsorption recovery (R,%) and desorption efficiency (E,%) of REEs on SiO₂-BPHA in five adsorption/desorption cycles.
 $m_{\text{ads}} = 10 \text{ mg}$, $C_{\text{ads}}(M^{X+}) = 100.0 \mu\text{g L}^{-1}$, $V = 10 \text{ mL}$, $t = 2 \text{ h}$.

4.5.5. Statistical analysis of desorption data

Desorption from SiO₂-PdCA. The distribution of REEs desorption from SiO₂-PdCA depending on eluent (0.01M EDTA pH 8.0 and 2 mol L⁻¹ HNO₃) are presented in Figure 36.

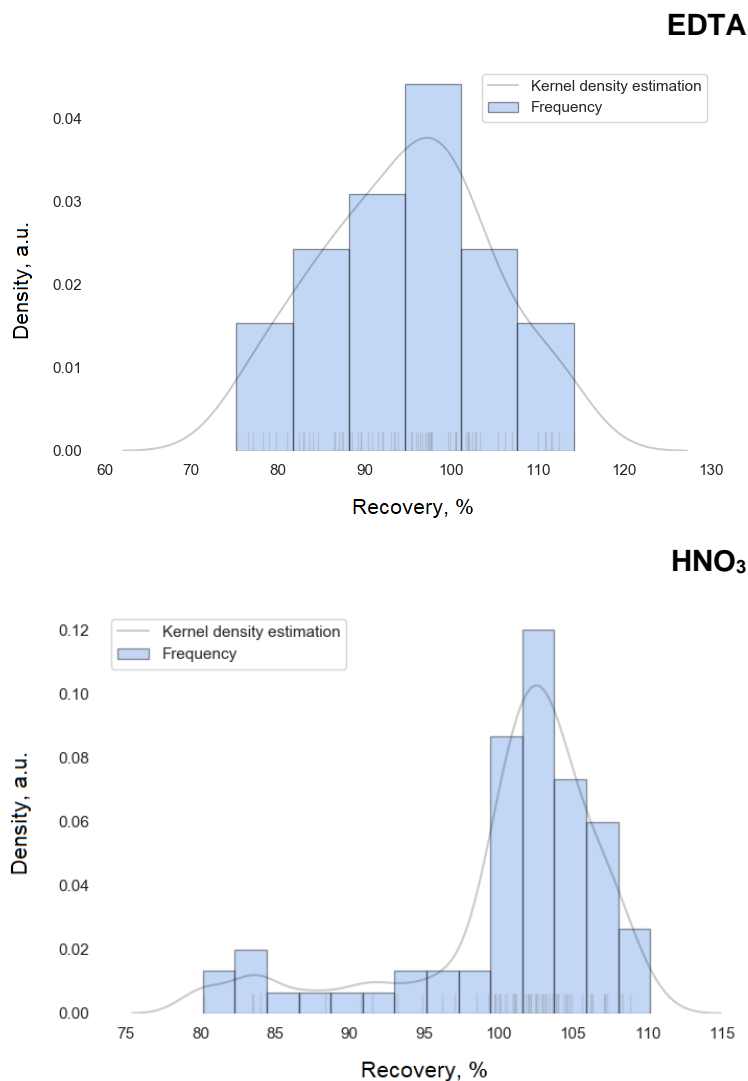


Figure 36. A general distribution of the recovery data over the entire group of lanthanides from SiO₂-PdCA.

Desorption under the action of EDTA has a normal distribution (D'Agostino-Pearson coefficient ($P_{D'A-P} > 0.05$)), in contrast to the general distribution of desorption caused by nitric acid ($P_{D'A-P} = 2.25 \cdot 10^{-6}$). Due to an obvious heteroscedasticity proven with Levene's test ($p_L = 5.69 \cdot 10^{-4} \ll 0.05$), the distributions cannot be analyzed (compared) with the help of ANOVA method. Thus, to check H_0 hypothesis, non-parametric Wilcoxon's two-tailed approach is preferable at the critical $T_{70;0.05} = 907$ (Zar, 2009). The calculations have revealed that minimal sum (for positive ranks) at 271 is less than the critical value ($271 <$

907). Evidently, this condition speaks for a significant difference between two distributions and H_0 -hypothesis cannot be considered.

The desorption values in both cases are not equally distributed depending on the metal ion. That is illustrated with violin plots, Figure 37, where there is a different scope (level of error) for both eluents, reflecting also different trends in the variation of errors and in the position of averages with an increase of atomic number. Despite noticeable differences in the degree of desorption of elements with a lower atomic number, starting at 64, desorption with EDTA is aligned with the eluting ability of nitric acid except for element 66 (dysprosium), where the effectiveness of nitric acid exceeds that of the complexing agent.

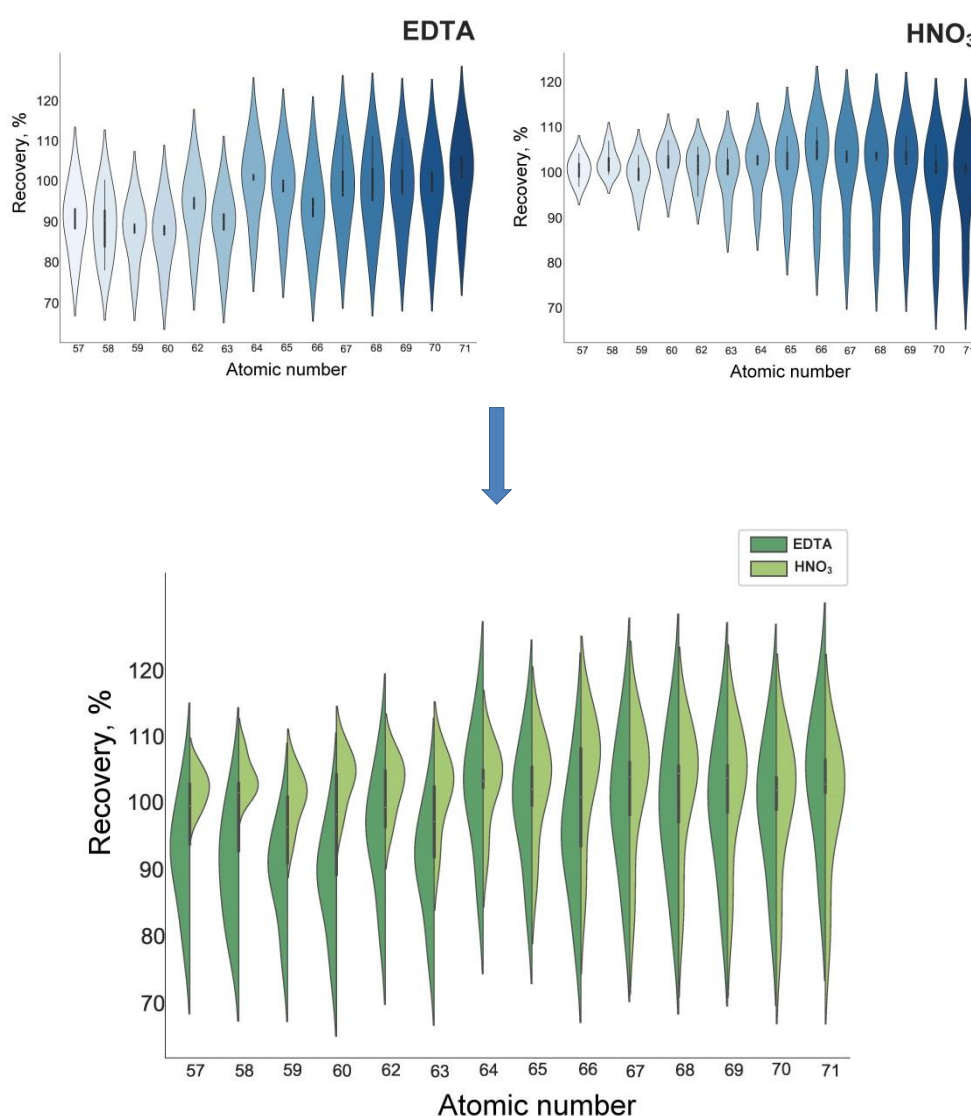


Figure 37. The violin plots on the recovery of lanthanides from SiO₂-PdCA.

Calculated total standard deviation (Table 11) in case of nitric acid is 1.4 times lower than in the experiment with EDTA, which is due to a narrower range of values (see *min* and *max* values). In general, elution with nitric acid shows a higher desorption rate for lanthanides.

Table 11. Statistical parameters of desorption from SiO₂-PdCA.

Eluent	Repetitions	Mean value, %	Minimal value, %	Maximal value, %	Standard deviation	Standard error of mean
EDTA	5	94.8	75.2	114.1	9.6	1.2
HNO ₃	5	100.7	80.2	110.2	6.8	0.8

The proportional change in the error (standard deviation or standard error of the mean) for every metal in the case of elution with nitric acid is described by a linear relationship with a small fitting area of the curve with Pearson's correlation coefficient is 0.97, Figure 38.

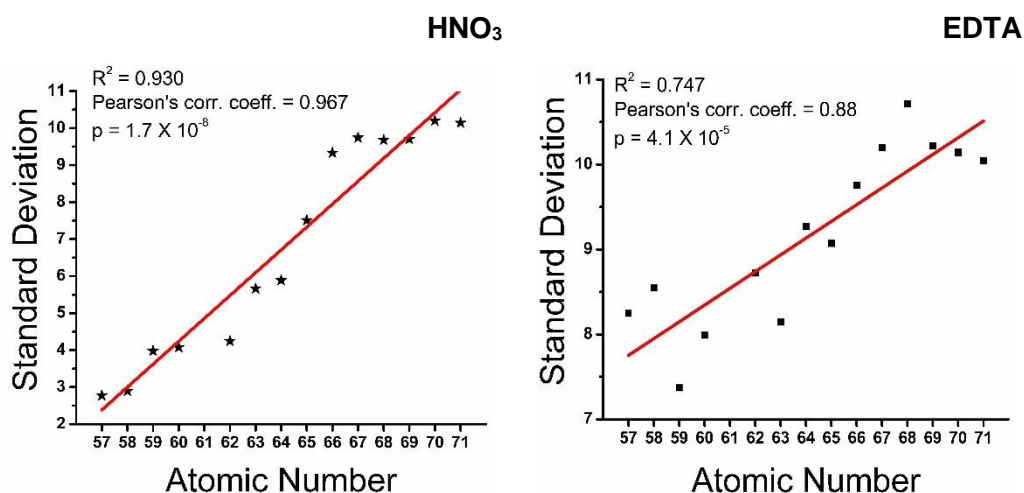


Figure 38. Linear plots of standard deviations for desorption from SiO₂-PdCA.

In the case of EDTA, a gradual increase in error is also observed, however, when desorption of ions of elements with a lower serial number (up to 64) the standard deviation fluctuates between 7.37 and 8.73, then starting from gadolinium, the error limits exceed 9.00 and reach a limit up to 10.22 (thulium). Such a difference is a condition for a larger deviation from the linear dependence - the Pearson correlation coefficient in the case of EDTA is reduced to 0.88, Figure 38.

In order to understand the contribution of each element in deviation, a stepwise extraction analysis was performed using EDTA for each element. It was

found that for elements with lower atomic numbers, the desorption linearity with each subsequent of the five stages is observed with higher Pearson coefficients (0.91 - 0.99), however, when going from 67 (holmium), the correlation coefficients are significantly reduced (0.87–0.88).

Desorption from SiO₂-AdMPA. The distribution of REEs desorption from SiO₂-AdMPA depending on eluent (0.01M EDTA pH 8.0 or 2 mol L⁻¹ HNO₃) is presented in Figure 39.

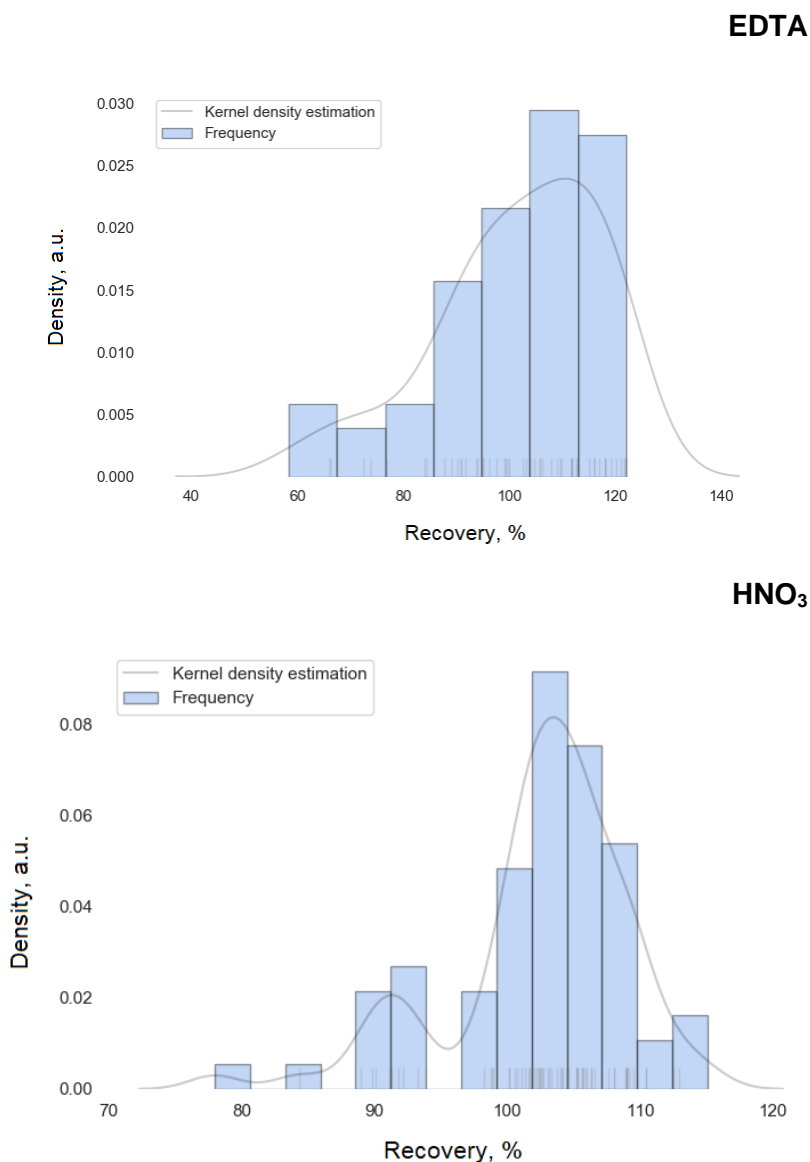


Figure 39. General distribution of the recovery data over the entire group of lanthanides from SiO₂-AdMPA.

As in the case of SiO₂-PdCA, the histograms of the distribution by eluent are different by the results of the test for normality - $P_{D'AP} = 0.036$ (EDTA), $P_{D'AP} = 8.22 \cdot 10^{-5}$ (HNO₃). Likewise, Levene's test does not meet the criteria of

homoscedasticity ($p_L = 1.09 \cdot 10^{-8} \ll 0.05$). Non-parametric Wilcoxon's analysis has revealed the validity of H_0 -hypothesis due to higher value of the rank sum in comparison to the critical tabulated value. Thus, close elution rates – as the mean, and as the median ones - together with Wilcoxon's test results and small allow one to suggest small contrast in two variances, as opposed to the case of $\text{SiO}_2\text{-PdCA}$, which is illustrated with violin plots, Figure 40.

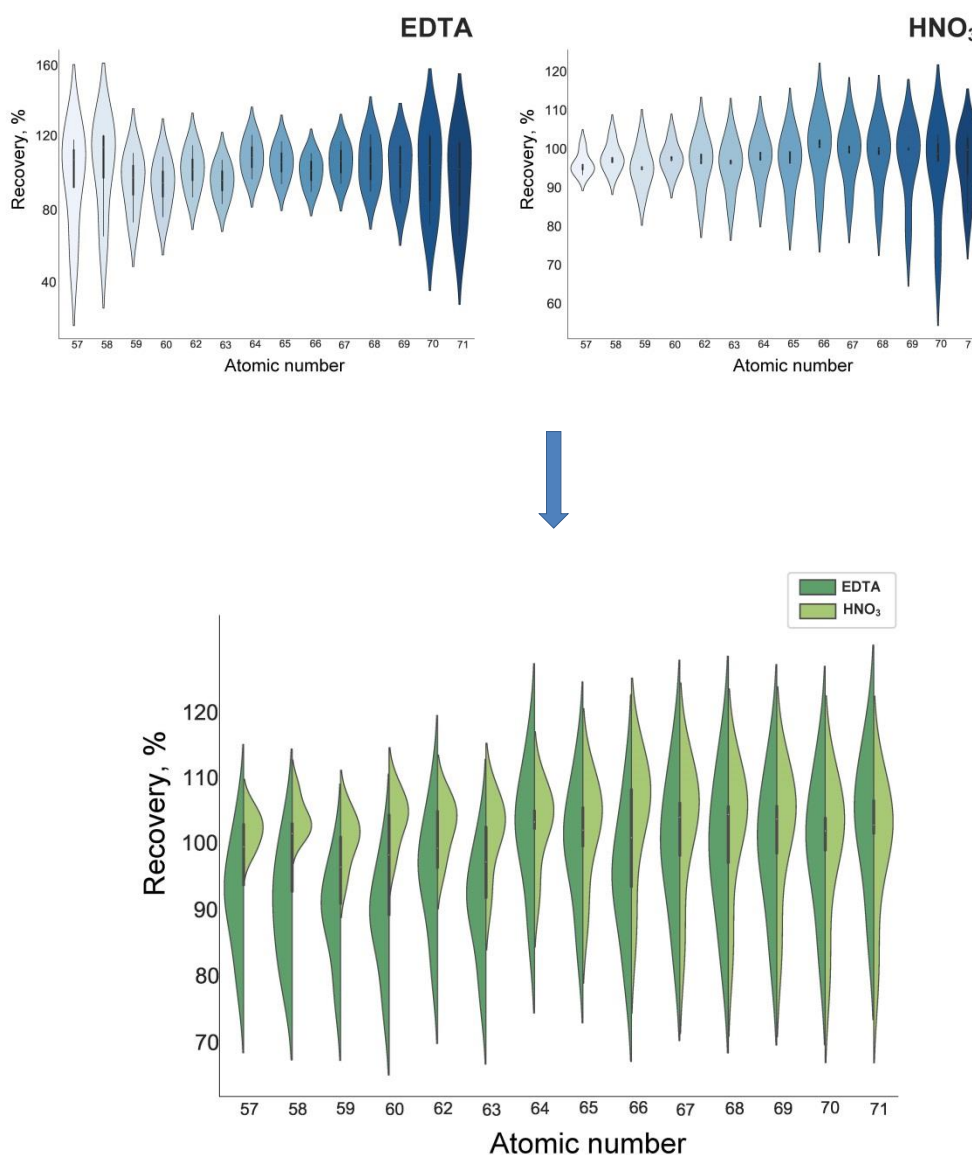


Figure 40. The violin plots on the recovery of lanthanides from $\text{SiO}_2\text{-AdMPA}$.

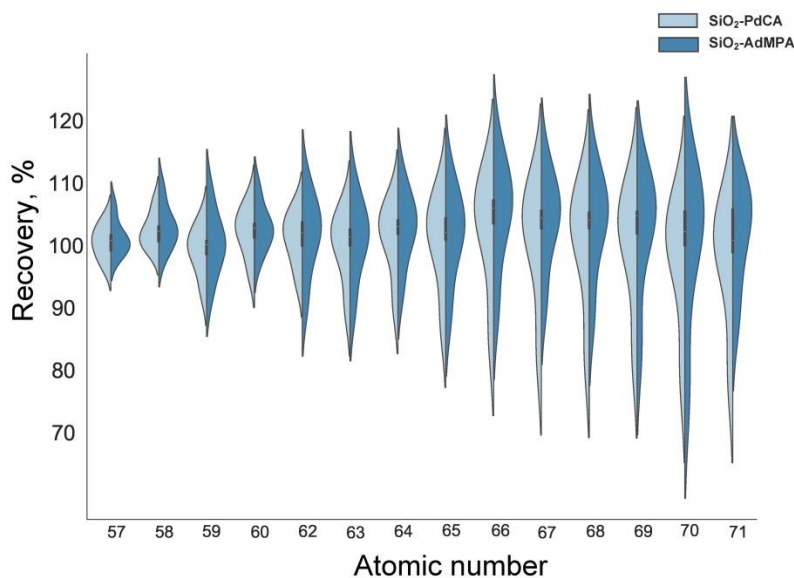
The two most important dissimilarities in the distributions are the differences in both standard deviations — the total one (more than twice) (Table 12) and for each sample — and also the change in these differences from elements 57 to 71.

Table 12: Statistical parameters of desorption from SiO₂-AdMPA.

Eluent	Repetitions	Mean value, %	Minimal value, %	Maximal value, %	Standard deviation	Standard error of mean
EDTA	5	101.8	58.3	122.0	15.7	2.1
HNO ₃	5	102.1	78.0	110.2	7.2	0.9

Thus, elution of EDTA has a higher error, which varies nonlinearly from 57 to 71 with a minimum in the middle of the lanthanide series (8.95 for 66 - dysprosium), while in the presence of nitric acid, similarly to SiO₂-PdCA adsorbent, the error increases congruently with atomic number. Moreover, since the recovery distribution by EDTA is normal (SiO₂-PdCA) or close enough to (SiO₂-AdMPA), the process at the presence of this eluent is stochastic (chanced). Thus, elution with nitric acid has a predictable change in the error, both in the form of a trend in the transition in a series of elements and in terms of the absolute values of the standard deviation.

Comparing desorption distributions for both adsorbents under the action of nitric acid, a unique correspondence (homoscedasticity, $p_L = 0.914 \gg 0.05$) was found, which is illustrated by the symmetry of the violin plots, Figure 41. Since the variances are strongly homoscedastic, one-way ANOVA is an adequate method to analyze the variances. The statistical significance is higher than 0.05 (0.131) at the Fischer coefficient of 2.306. Thus, the variances are not characterized by statistically significant difference.

Figure 41. The violin plots on the recovery of lanthanides with HNO₃.

Taking all above, generally, elution with the formation of EDTA-Ln complexes for both sorbents is lower compared with desorption with nitric acid and has a higher deviation.

Desorption from SiO₂-BPHA. Taking a closer look at the desorption (further: recovery) process for the lanthanide group from SiO₂-BPHA can conclude that no atomic number-correlated tendencies in the recovery are established (Figure 42). Particularly, they lie within the 82.23 – 91.39 % range at standard deviation and standard error of mean not higher than 7.83 and 3.5 (Er³⁺), respectively. The only cation (Yb³⁺) exhibits an outstanding value at 101.5% with a low standard deviation – 2.85 (Table 13).

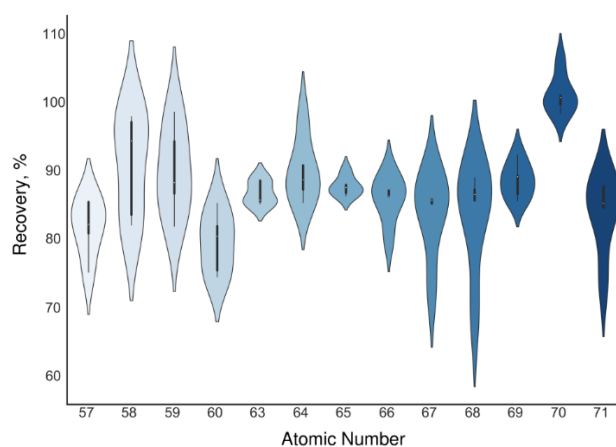


Figure 42. The violin plot on the recovery over the lanthanide ions group from SiO₂-BPHA.

Table 13. The descriptive statistics summary on the recovery of lanthanides from SiO₂-BPHA.

Ln	Repetitions	Mean Value, %	Standard Deviation	Minimal Value, %	Maximal Value, %	Standard Error of Mean
Ce	5	91.4	7.6	82.5	98.3	3.4
Dy	5	86.3	3.4	80.6	89.9	1.5
Er	5	84.0	7.8	70.2	89.4	3.5
Eu	5	87.1	1.7	85.6	89.0	0.8
Gd	5	90.3	4.7	85.7	98.0	2.1
Ho	5	84.2	6.2	73.5	89.5	2.8
La	5	82.2	4.3	75.6	86.0	1.9
Lu	5	84.2	5.7	74.4	88.2	2.5
Nd	5	79.9	4.5	74.9	85.6	2.0
Pr	5	90.3	6.6	82.3	99.0	2.9
Tb	5	88.1	1.4	86.7	90.4	0.6
Tm	5	89.0	2.6	86.0	92.7	1.2
Yb	5	101.5	2.9	98.8	106.3	1.3

Such recovery profile can speak for a normal distribution of the recovery and the calculated $P_{D'A-P}$ ($0.336 > 0.05$) confirms the assumption for normal distribution at the skewness and kurtosis indices of 0.168 and 0.811, respectively – the latter two parameters lie within the acceptable range ($-1.96/+19.6$) for passing the normality test correctly (Figure 43).

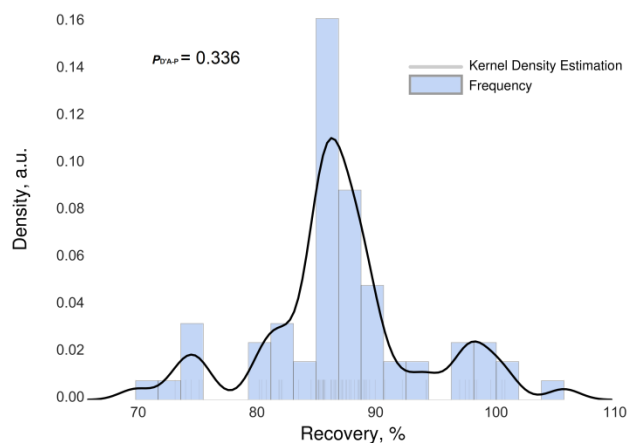


Figure 43. General distribution of the recovery data over the entire group of lanthanides from SiO₂-BPHA.

4.5.6. Application of the adsorbents for removal and separation of REE ions from complex metal-containing solution

In order to evaluate the possible interfering effect of other ions on REEs adsorption in complex metal-containing solution, the adsorption properties of functionalized adsorbents SiO₂-PdCA, SiO₂-AdMPA, SiO₂-BPHA and SiO₂ (was taken for comparison) were investigated in the pH 1.0 – 6.0 range for different metals in mixture. Similar to the study of REEs adsorption, pH higher than 6.0 was not considered because precipitation occurred in the solution, indicating the hydrolysis of the metal ion with the formation of the corresponding insoluble hydroxide.

Results shown in Figure 44 reveal that the metal ion uptake of the adsorbents varies significantly for pure and functionalized silica gels. For all adsorbents, adsorption of some other metals is observed in the pH range of REEs adsorption. For example, SiO₂-PdCA uptakes Cu²⁺ at pH>2 for more than 90%, Figure 44b. Therefore, to use the adsorbents to remove REEs from multicomponent matrixes, the study of interfering effect of different ions on REEs adsorption is essential.

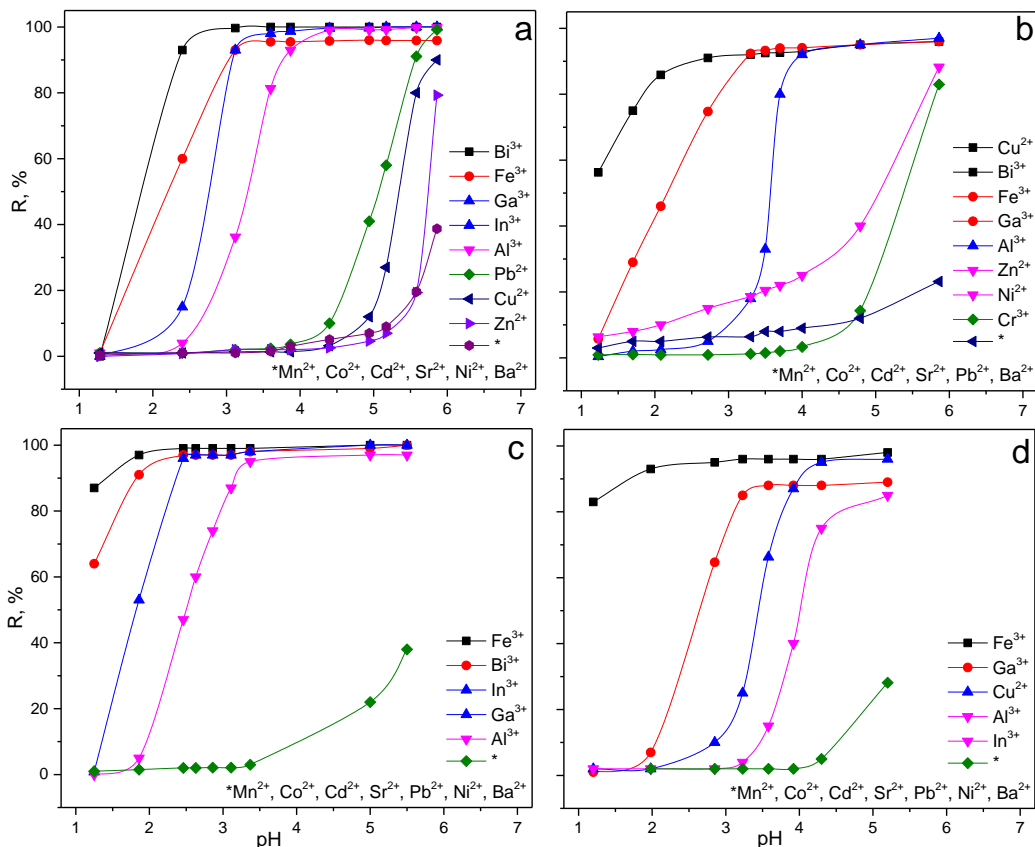


Figure 44. Effects of pH on adsorption of different metals by SiO₂ (a), SiO₂-PdCA (b), SiO₂-AdMPA (c) and SiO₂-BPHA (d). $m_{\text{ads}} = 10 \text{ mg}$, $C_0(M^{x+}) = 10 \text{ mg L}^{-1}$, $V = 10 \text{ mL}$, $t = 2 \text{ h}$.

The selectivity of SiO₂-PdCA and SiO₂-AdMPA toward REEs was demonstrated by studying the interference effect of different competition ions on recovery of REEs. The following competition ions were tested: Fe³⁺ and Cu²⁺ in their mixture and mixture of 22 metal ions (Ag⁺, Al³⁺, Ba²⁺, Bi³⁺, Ca²⁺, Cd²⁺, Co²⁺, Cr³⁺, Cu²⁺, Fe³⁺, Ga³⁺, In³⁺, K⁺, Li⁺, Mg²⁺, Mn²⁺, Na⁺, Ni²⁺, Pb²⁺, Sr²⁺, Tl³⁺, Zn²⁺). Interference effect of 22 metal ions was carried out with and without constant ionic strength. Recoveries of REEs in the presence of competitive ions are presented in Table 14 and Table 15. The presented results were processed in the form of graphs for better visibility; plots are shown in Figure 45 and Figure 46.

The results indicate that up to 200-fold excess of Fe³⁺ and Cu²⁺ ions for SiO₂-PdCA and 400-fold for SiO₂-AdMPA do not cause significant interference to adsorption of REEs. Interference effect of 22 metal ions on REEs recovery is insignificant up to 200-fold excess for both adsorbents. Maintaining a constant ionic strength in solution have practically no effect on REE recovery by SiO₂-AdMPA and slightly weakens the interference effect on adsorption of heavy REEs on SiO₂-

PdCA. The high recoveries of all REEs in the presence of interfering ions demonstrate selectivity of chosen adsorbents toward REEs.

Table 14. Interference effect of Fe³⁺ and Cu²⁺ ions on REEs recovery.

R, %														excess
La ³⁺	Ce ³⁺	Pr ³⁺	Nd ³⁺	Sm ³⁺	Eu ³⁺	Gd ³⁺	Tb ³⁺	Dy ³⁺	Ho ³⁺	Er ³⁺	Tm ³⁺	Yb ³⁺	Lu ³⁺	
SiO₂-PdCA														
99.8	99.4	98.5	100.0	100.1	99.9	98.3	99.3	99.6	98.6	98.5	98.0	98.1	98.2	0
73.5	70.5	81.7	71.8	79.6	67.5	79.7	79.0	77.5	75.8	76.7	79.2	78.0	79.6	50
66.6	66.0	76.2	67.5	79.8	63.5	75.4	73.3	73.3	71.4	71.3	69.3	73.1	74.3	100
21.8	21.2	44.0	44.1	69.7	58.0	56.0	55.9	54.9	53.3	54.4	59.3	55.8	57.4	200
1.6	17.6	12.5	18.5	27.4	26.7	29.1	31.2	31.2	30.6	30.5	36.4	33.2	34.9	400
0.6	11.7	5.2	7.8	10.3	12.5	13.7	14.7	14.5	14.7	13.6	15.8	16.1	16.1	800
SiO₂-AdMPA														
100.0	99.5	98.5	100.4	100.1	100.1	98.5	99.4	99.8	99.0	99.3	98.8	98.7	98.5	0
88.6	91.0	90.2	96.1	85.1	86.9	89.5	87.9	86.9	87.7	86.5	90.4	87.6	86.8	50
87.3	84.6	87.8	87.7	88.3	88.4	87.6	89.5	90.6	88.7	89.1	90.3	90.6	90.9	100
85.8	85.4	83.8	82.5	76.8	79.2	79.0	80.3	79.5	81.7	80.7	81.2	82	77.2	200
74.9	85.0	82.4	82.6	75.7	74.6	77.7	75.6	77.1	79.4	80.2	79.3	74.4	71.2	400
1.80	4.10	6.30	7.20	17.1	17.5	13.0	14.9	14.5	10.8	11.4	13.8	20.4	23.5	800

Table 15. Interference effect of 22 metal ions on REEs recovery.

R, %														excess
La ³⁺	Ce ³⁺	Pr ³⁺	Nd ³⁺	Sm ³⁺	Eu ³⁺	Gd ³⁺	Tb ³⁺	Dy ³⁺	Ho ³⁺	Er ³⁺	Tm ³⁺	Yb ³⁺	Lu ³⁺	
SiO₂-PdCA														
99.8	99.4	98.5	100.0	100.1	99.9	98.3	99.3	99.6	98.6	98.5	98.0	98.1	98.2	0
73.5	70.5	81.7	71.8	70.5	67.5	79.7	79.0	77.5	75.8	76.7	75.1	78.0	79.6	50
66.6	66.0	76.2	67.5	68.5	63.5	75.4	73.3	73.3	71.4	71.3	69.9	73.1	74.3	100
21.8	21.2	44.0	44.1	48.1	48.0	56.0	55.9	54.9	53.3	54.4	52.8	55.8	57.4	200
1.6	17.6	12.5	18.5	20.7	26.7	29.1	31.2	31.2	30.6	30.5	30.4	33.2	34.9	400
0.6	11.7	5.2	7.8	10.5	12.5	13.7	14.7	14.5	14.7	13.6	14.9	16.1	16.1	800
with constant ionic strength (0.5 mol L ⁻¹ NaCl)														
98.2	98.8	98.1	99.9	98.9	97.9	98.2	98.6	99.0	98.3	97.8	97.8	97.8	98.0	0
68.5	70.6	77.6	69.2	67.5	65.1	77.4	76.4	74.7	73.4	74.2	72.2	75.4	77.0	50
59.1	63.0	75.3	70.0	69.5	63.3	74.1	74.0	71.8	70.1	71.0	69.6	72.5	74.0	100
36.5	45.7	63.2	59.4	48.0	56.2	65.0	63.8	62.4	60.8	60.7	60.1	62.8	64.1	200
9.3	18.7	36.7	47.9	46.6	55.5	61.8	63.5	60.8	58.9	59.7	58.4	62.2	64.4	400
7.5	15.9	35.8	45.5	42.5	51.7	58.4	60.8	58.2	57.0	57.3	55.8	59.8	62.4	800
SiO₂-AdMPA														
100.0	99.5	98.5	100.4	100.1	100.1	98.5	99.4	99.8	99.0	99.3	98.8	98.7	98.5	0
75.9	84.9	86.4	72.9	78.4	85.8	86.6	83.3	87.8	59.6	69.8	80.9	78.9	70.2	50
75.3	84.6	86.6	76.3	73.8	86.6	85.6	81	85.9	55.5	70.9	78.9	77.1	72.0	100
56.3	65.7	68.1	60.4	65.7	67.1	65.1	78.0	63.9	46.5	56.6	58.9	57.4	57.3	200
34.1	40.6	43.8	40.1	44.2	45.1	40.3	63.4	38.9	30.8	37.6	35.8	35.0	44.5	400
40.2	44.2	46.7	41.4	46.7	46.3	43.4	58.4	42.0	29.9	40.7	40.6	40.7	43.8	800
with constant ionic strength (0.5 mol L ⁻¹ NaCl)														
99.5	98.7	97.4	95.2	98.2	97.8	97.4	98.6	99.5	98.4	99.1	97.5	94.2	97.8	0
71.6	58.1	70.1	68	69.8	68.1	81.9	83.3	82.3	82.2	82.9	77.0	75.7	74.2	50
71.6	54.1	68.3	67.8	68.8	65.9	78.5	81.0	78.5	77.9	78.1	72.2	71.4	70.5	100
52.5	52.7	68.5	68.4	64.9	64.1	76.8	78.0	74.6	74.4	74.2	68.2	67.5	66.8	200
33.4	39.5	52.3	55.8	56.5	54.5	62.3	63.4	61.5	59.3	60.0	57.4	60.8	62.0	400
30.3	32.8	48.1	50.6	54.1	49.3	56.8	58.4	54.8	53.0	53.2	52.5	55.4	56.0	800

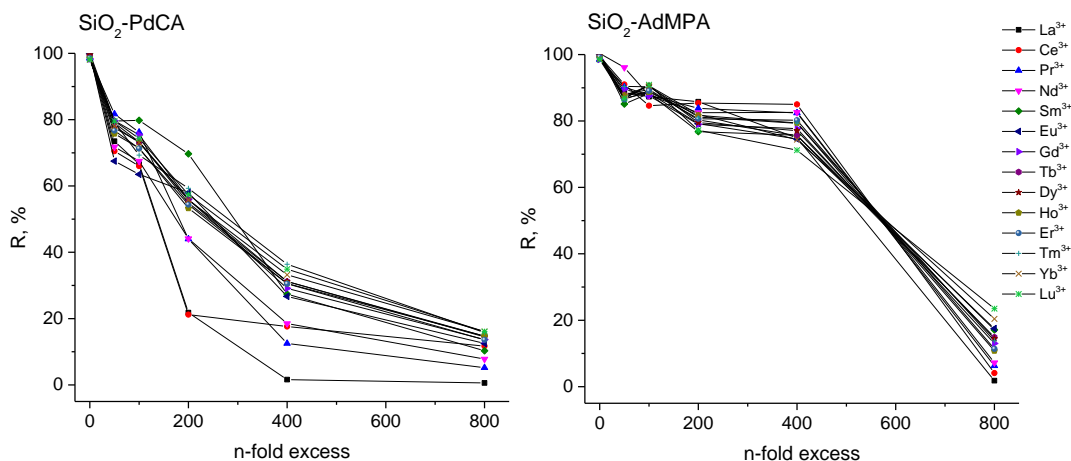


Figure 45. Interference effect Fe^{3+} and Cu^{2+} ions on REEs recovery from SiO_2 -PdCA and SiO_2 -AdMPA.

$m_{\text{ads}} = 10 \text{ mg}$, $C_{\text{ads}}(\text{M}^{x+}) = 20.0 \mu\text{g L}^{-1}$, $V = 10 \text{ mL}$, $t = 2 \text{ h}$.

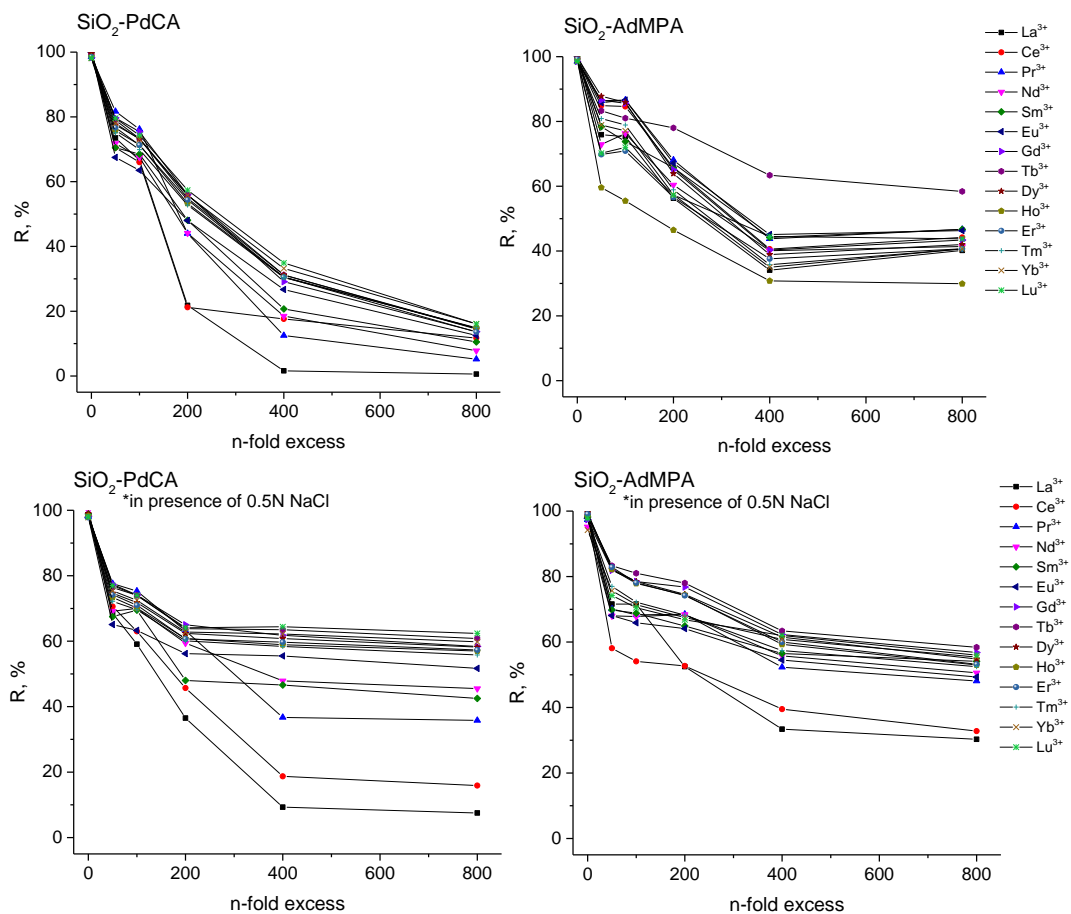


Figure 46. Interference effect of 22 metal ions on REEs recovery from SiO_2 -PdCA and SiO_2 -AdMPA.

$m_{\text{ads}} = 10 \text{ mg}$, $C_{\text{ads}}(\text{M}^{x+}) = 20.0 \mu\text{g L}^{-1}$, $V = 10 \text{ mL}$, $t = 2 \text{ h}$.

The selectivity of SiO₂-BPHA toward REEs was demonstrated by studying the interference effect of the competing ions (Na⁺, K⁺, Ca²⁺, Mg²⁺) on recovery of REEs. Results are presented in Table 16 and Figure 47.

Table 16. Interference effect of Na⁺, K⁺, Ca²⁺, Mg²⁺ ions on REEs recovery.

Metal	R, %				
	0	total n-fold excess			
	0	400	800	2000	4000
La ³⁺	95.7	72.3	51.7	4.9	2.8
Ce ³⁺	101.0	49.9	49.9	13.5	13
Pr ³⁺	101.9	62.8	59.9	13.8	8.3
Nd ³⁺	93.9	55.7	52.3	9.3	6.1
Eu ³⁺	96.3	79.4	65.8	36.7	28.4
Gd ³⁺	99.8	74.1	53.2	29	25.2
Tb ³⁺	96.5	83.1	77.1	26.1	16.3
Dy ³⁺	99.3	84.7	79.2	26.6	17.1
Ho ³⁺	98.3	83.8	78.1	25.5	15.7
Er ³⁺	96.8	84.2	79.4	29.3	19.1
Tm ³⁺	99.2	86.8	79.8	33.5	21.8
Yb ³⁺	98.7	86.7	79.1	37.8	25.1
Lu ³⁺	96.9	86.5	78.2	37.6	24.7

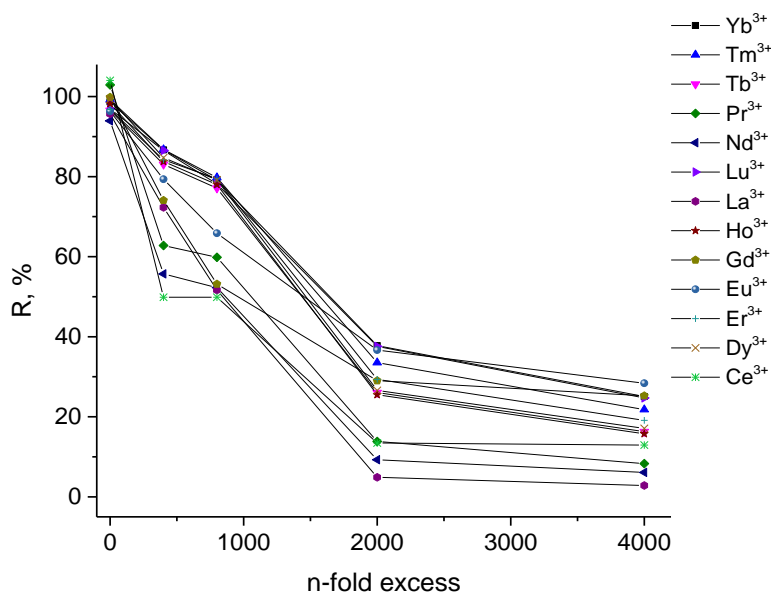


Figure 47. Interference effect of Na⁺, K⁺, Ca²⁺, Mg²⁺ ions on REEs recovery from SiO₂-BPHA. Adapted from (Artiushenko *et al.*, 2019).
 $m_{\text{ads}} = 10 \text{ mg}$, $C_{\text{ads}}(\text{Ln}^{x+}) = 100.0 \text{ } \mu\text{g L}^{-1}$, $\text{pH} = 5.0$, $V = 10 \text{ mL}$, $t = 2 \text{ h}$.

The results indicated that up to 200-fold excess of each ion Na⁺, K⁺, Ca²⁺, Mg²⁺ (total excess of interference ions 800-fold) do not cause significant interference to adsorption of REEs. The high recoveries of all REEs in the presence of interfering ions demonstrate selectivity of SiO₂-BPHA toward REEs.

4.5.7. Separation of REEs on SiO₂-BPHA

An interesting effect is observed during REEs adsorption on SiO₂-BPHA. K_d value growth more than 100 times with atomic number of REEs, Figure 26. Based on the K_d value, the affinity of SiO₂-BPHA towards REEs in multi-element solution can be presented as follows: $\text{Lu}^{3+}=\text{Yb}^{3+} > \text{Tm}^{3+} > \text{Er}^{3+} > \text{Dy}^{3+} =\text{Ho}^{3+} > \text{Tb}^{3+} > \text{Eu}^{3+} > \text{Gd}^{3+} > \text{Nd}^{3+} > \text{Ce}^{3+} > \text{La}^{3+}$. Significant difference in K_d indicates that SiO₂-BPHA can be used for separation of the REE ions. To prove this, metal adsorption on SiO₂-BPHA was studied for a set of multi-element solutions with increasing concentration of REEs.

The results presented in Figure 48 suggest that, in multi-element solution, the capacity of SiO₂-BPHA essentially depends on atomic number of REE. For example, one gram of SiO₂-BPHA can absorb about 4 $\mu\text{mol g}^{-1}$ of La^{3+} and about 6 $\mu\text{mol g}^{-1}$ of Ce^{3+} , which have lower atomic number and up to 15 μmol of Lu^{3+} and Yb^{3+} - elements with higher atomic number. Such difference in selectivity of adsorption is explained by competition among the REE ions for adsorption sites available on the surface of complexing adsorbent (Callura *et al.*, 2018; Ramasamy, Khan, *et al.*, 2017). Metal ions that form stronger complexes with immobilized ligands substitute less strongly bind metals. Commonly heavy REEs give more stable complexes with O-ligand, therefore, they better adsorb on SiO₂-BPHA.

In order to evaluate ability of SiO₂-BPHA for selective adsorption of REEs from multi-element solution, separation factors for pairs Ln/La were calculated: lanthanides (Ln^{3+}) – La^{3+} in solution with different concentrations of REEs (1.0, 2.0, 5.0 mg L^{-1}). In Figure 49 separation factors are presented as a function of atomic number of REE. SF depends on metal concentration in solution, but it is growing with increasing of atomic number of REE and in optimal conditions, SF can be about 80 for Lu/La and Yb/La, and about 60 for Tm/La.

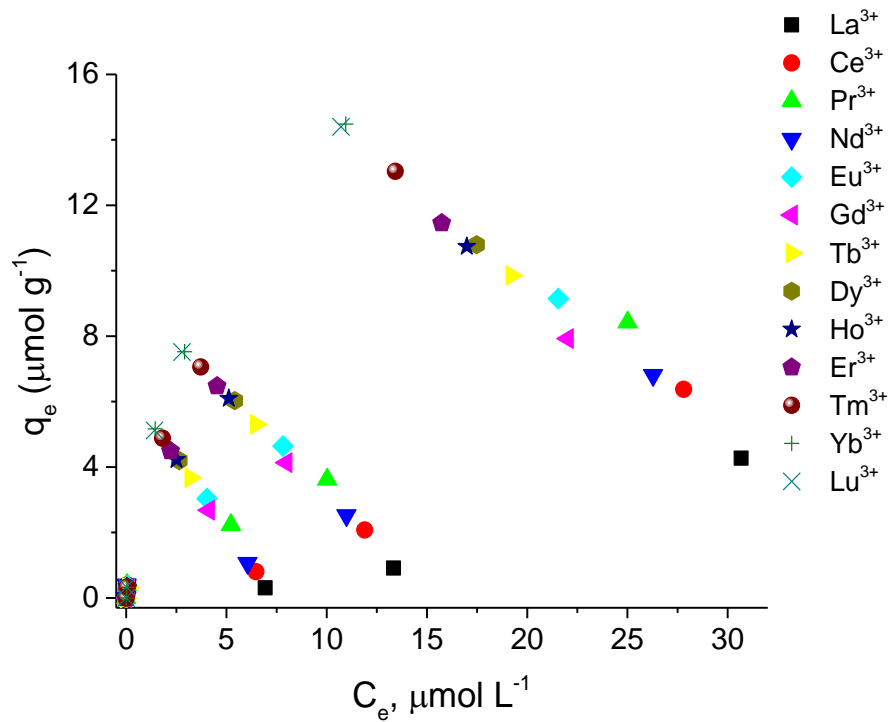


Figure 48. Adsorption of REEs on SiO₂-BPHA from multi-element solutions. Reproduced from (Artiushenko *et al.*, 2019).
 $m_{\text{ads}} = 10 \text{ mg}$, $C_{\text{ads}}(\text{Ln}^{x+}) = 0.1 - 5 \text{ mg L}^{-1}$, $\text{pH} = 5.0$, $V = 10 \text{ mL}$, $t = 30 \text{ min}$.

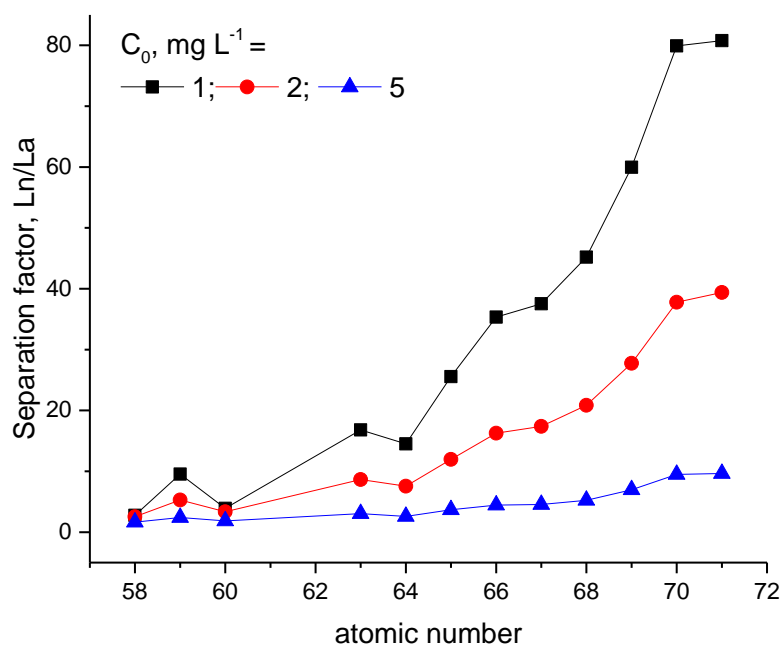


Figure 49. Separation factor for pairs Ln/La. Reproduced from (Artiushenko *et al.*, 2019).
 $m_{\text{ads}} = 10 \text{ mg}$, $C_{\text{ads}}(\text{Ln}^{x+}) = 1.0, 2.0, 5.0 \text{ mg L}^{-1}$, $\text{pH}_{\text{ads}} = 5.0$, $V = 10 \text{ mL}$, $t = 2 \text{ h}$.

4.5.8. Recovery of REEs on SiO₂-PdCA and SiO₂-AdMPA from waste fluorescent lamps

The content of REEs in phosphors lamps can reach 27.9% and such waste can be good alternative source of REEs in the future. Today only 10% of REE is being recovered from phosphors (Tan, Deng e Li, 2017), and so these end-of-life products have promising potential as a secondary source of REEs. Red phosphors (Y₂O₃:Eu³⁺), blue phosphors (BaMgAl₁₀O₁₇:Eu²⁺) and green phosphors (LaPO₄:Ce³⁺,Tb³⁺; (Gd,Mg)B₅O₁₂:Ce³⁺,Tb³⁺; (Ce,Tb)MgAl₁₁O₁₉) are the three main phosphorus compounds of the fluorescent lamps (Song, Chang e Pecht, 2013). Commonly a combination of pyrometallurgy and hydrometallurgy is used for the recycling of recyclable components (Tan, Li e Zeng, 2015). Only recently some alternative technologies were proposed such as supported liquid membranes (Pavón *et al.*, 2019) and ionic liquid extraction (Pavón *et al.*, 2018).

In this research, strong chelating adsorbents having immobilized fragments of 2,6-pyridinedicarboxylic acid (SiO₂-PdCA) and aminodiphosphonic acid (SiO₂-AdMPA) have been studied for REEs recycling.

These two OSA have different nature of immobilized functional groups. Because of immobilized 2,6-pyridinedicarboxylic acid, SiO₂-PdCA adsorb most of d- and f-elements from solution with pH > 4.0 (see Figure 44). This feature of the adsorbent can be used to recycle most of the components of phosphor from loose fluorescent lamps. Contrary, SiO₂-AdMPA has harp selectivity to highly charged ions, such as REEs, Figure 44. Therefore, the SiO₂-AdMPA can be used for recycling of rare earth ions only from complex matrix. The latter is important in case of low content of REE in leaching solution with high concentration of color metal ions, when total capacity of the adsorbent is not high enough to recover all essential elements.

The adsorbents (SiO₂-PdCA and SiO₂-AdMPA) were applied for DSPE of metal ions from leaching solution obtained from phosphor powders of linear tube fluorescent lamps produced in Brazil. The phosphor's composition can vary for different venders, therefore two leaching solutions (#1 and #2) were prepared from different batch of the lamp waste and the adsorption experiment was performed for these two solutions.

The next experimental procedures were applied for all DSPE:

- 1) Composition of leaching solution was analyzed by ICP OES/MS;
- 2) The adsorbent was immersed to leaching solution with desired pH (2.5 for SiO₂-PdCA and 2.0 for SiO₂-AdMPA) and the composition of supernatant solution was analyzed;

- 3) The adsorbent was removed by centrifugation, washed with water and immersed in desorbing solution (2 mol L⁻¹ solution of HNO₃).

Concentration of metal in desorbing solution was finally determined.

Such configuration of adsorption experiment allows to calculate adsorption of metals from multicomponent solutions, desorption degree to selected eluent and overall recovery. The results of the analysis are presented in Table 17. Adsorption properties of SiO₂-AdMPA are slightly different from SiO₂-PdCA, particularly in selectivity toward color metals. The SiO₂-AdMPA has less affinity to transitional metals that could allow better separation of REEs from such elements as Cu, Zn, Fe, Cr, Ni, and Pb. To verify this, recovery of REEs from leaching solution #2 was studied for SiO₂-AdMPA. The results presented in Table 19 indeed demonstrate lower adsorption of Cr (84% vs. 45%), Ni (56% vs 0%), Cu (100% vs. 0%) and Pb (77% vs. 27%) on SiO₂-AdMPA comparatively with SiO₂-PdCA (Table 18). But, at the same time, SiO₂-AdMPA has higher affinity towards Al (19% vs. 81%), Fe (34% vs. 48%), Ti (2% vs. 40%). High concentration the latter ones in the leaching solution decrease overall concentration of REEs to 13% while easily hydrolyzed ions, such as Al and Ti consist of 66% of total metal content in desorbing solution, Figure 53. Also, incomplete desorption of Y (30%) change distribution of REEs, increasing content of Eu in the concentrate up to 52%. This effect can be used in the process where selective adsorption of f-elements is desirable.

For better understanding, the results of metal recovery from leaching solutions on SiO₂-PdCA and SiO₂-AdMPA have been divided into four groups: a) recovery of macro-components (ion concentration, C_M > 1.0 mg L⁻¹), b) recovery of micro-components (C_M < 0.2 mg L⁻¹) that demonstrated no essential adsorption on SiO₂-PdCA, c) recovery of micro-components (except REEs) that adsorbed on SiO₂-PdCA (SiO₂-AdMPA) and d) recovery of REEs.

Recovery of REEs on SiO₂-PdCA from leaching solution #1

The results of metal adsorption on SiO₂-PdCA from leaching solution #1 have been presented in Table 17. From data presented it can be seen that no one from macro-component of the leaching solution #1 (except Zn) essentially adsorbed on SiO₂-PdCA. This allows utilization of small amount of the adsorbent to be used for REE recycling since during the adsorbent application it will not be saturated with unwanted ions. At the selected experimental conditions about 35% of Zn ions can be removed from the leaching solution and about 62% from the adsorbed amount of the metal is released to desorbing solution. This constitutes about 22% of overall

Zn recovery. All other macro-components of leaching solution (including Na, Mg, Ca, Sr and Ba; Mn and Sb have negligible recovery, Table 17.

Table 17. Composition of the leaching solution #1, supernatant and desorbing solutions received after DSPE with SiO₂-PdCA, and corresponding adsorption, desorption, and overall recovery degrees.

Metal ion	C _M in leaching solution, mg L ⁻¹	C _M in supernatant solution, mg L ⁻¹	Adsorption, R, %	C _M in desorption solution, mg L ⁻¹	Desorption E, %	Recovery R _{ov} , %
a) Macro-components						
Na	263.00	283.00	0.00	20.63	7.83	0.00
Mg	7.66	10.30	0.00	0.05	0.64	0.00
Al	253.00	337.77	0.00	0.41	0.16	0.00
K	6.76	10.34	0.00	0.39	5.75	0.00
Ca	3888.00	5476.63	0.00	0.36	0.01	0.00
Ti	1.81	2.42	0.00	0.02	1.08	0.00
Mn	70.90	91.76	0.00	0.14	0.19	0.00
Fe	12.10	16.02	0.00	0.16	1.30	0.00
Zn	2.44	1.59	34.91	1.51	61.89	21.61
Sr	6.15	8.55	0.00	0.00	0.06	0.00
Sb	79.70	90.73	0.00	0.85	1.07	0.00
Ba	7.18	7.73	0.00	0.02	0.23	0.00
b) Micro-components						
Li	0.024	0.033	0.0	<0.005	2	0.0
Sc	0.011	0.017	0.0	<0.005	0	0.0
V	0.099	0.113	0.0	<0.005	8	0.0
Cr	0.23	0.304	0.0	<0.005	0	0.0
Co	0.027	0.033	0.0	<0.005	10	0.0
Ga	0.17	0.228	0.0	<0.005	1	0.0
As	0.11	0.145	0.0	<0.005	0	0.0
Rb	0.011	0.014	0.0	<0.005	4	0.0
Sn	0.050	0.082	0.0	0.002	8	0.0
Hg	0.21	0.410	0.0	0.003	2	0.0
Ni	0.16	0.126	23	0.081	50	11
Cu	0.100	0.023	77	0.048	48	37
Ag	0.096	0.022	77	<0.005	0	0
Pb	0.37	0.161	57	0.152	41	23
c) REEs						
Y	0.39	0.015	96.3	0.325	83.5	80
La	0.014	0.005	67.1	0.011	76.9	52
Ce	0.023	0.003	86.4	0.022	95.6	83
Pr	0.002	<0.001	91.3	0.002	99.0	90
Nd	0.028	0.002	92.3	0.027	96.9	89
Sm	0.051	0.002	96.8	0.046	89.9	87
Eu	0.17	0.006	96.2	0.150	88.0	85
Gd	0.077	0.002	97.6	0.067	86.7	85
Tb	0.15	0.003	98.2	0.124	80.4	79
Dy	0.005	<0.001	98.1	0.004	82.8	81
Ho	0.001	<0.001	96.9	0.001	67.3	65
Er	0.022	<0.001	98.3	0.015	68.2	67
Tm	0.002	<0.001	97.8	0.001	69.7	68
Yb	0.12	0.002	98.2	0.085	68.7	67
Lu	0.003	<0.001	97.6	0.002	70.4	69

Among micro-components on the leaching solution only some d- (Ni, Cu) and p- (Pb) metals demonstrated essential affinity towards SiO₂-PdCA with no more than 37% (Cu) of recovery, while such ions as Cr, Ga and Hg have about zero recovery. This fact assures low content of unwanted metals in desorbing solution. SiO₂-PdCA demonstrated very high affinity to REE ions, with 86-98% of adsorption. Similar to earlier presented data, light REEs have lower adsorption degree than heavy REE. This resulted in incomplete desorption of the heavy REEs from SiO₂-PdCA under experimental conditions, Table 17.

Utilization of SiO₂-PdCA allows essentially improved sustainability of the REEs recovery process. Firstly, total salinity of REEs concentrate after SiO₂-PdCA is about 1000 times lower than in the leaching solution (6.1 mg L⁻¹ vs. 5.6 g L⁻¹). Secondly, compositions of leaching and desorbing solutions are drastically different, Figure 50. Leaching solution for more than 99% consists of unwanted metal ions and has only 0.02 % of REEs, while the solution obtained eluting of metals adsorbed on SiO₂-PdCA consist of more than 15% of REE (REE relative enrichment is 750) and this amount can be easily increased by further optimization of the DSPE washing procedure.

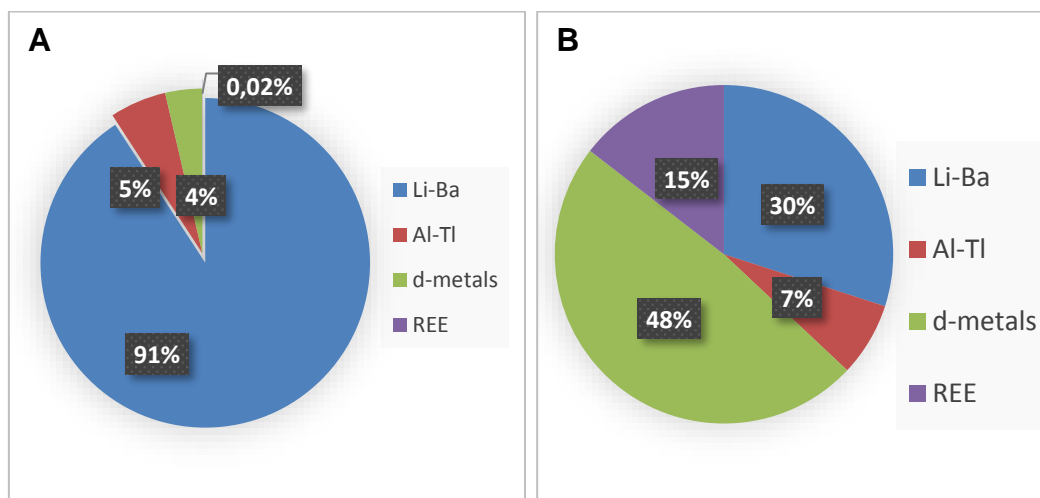


Figure 50. Composition of leaching solution #1 (A) and the concentrate obtained after desorption of metals from SiO₂-PdCA (B).

As it is also can be seen that utilization of the adsorbent does not essentially change internal distribution of REEs in the leaching solution and in the concentrate (Figure 51).

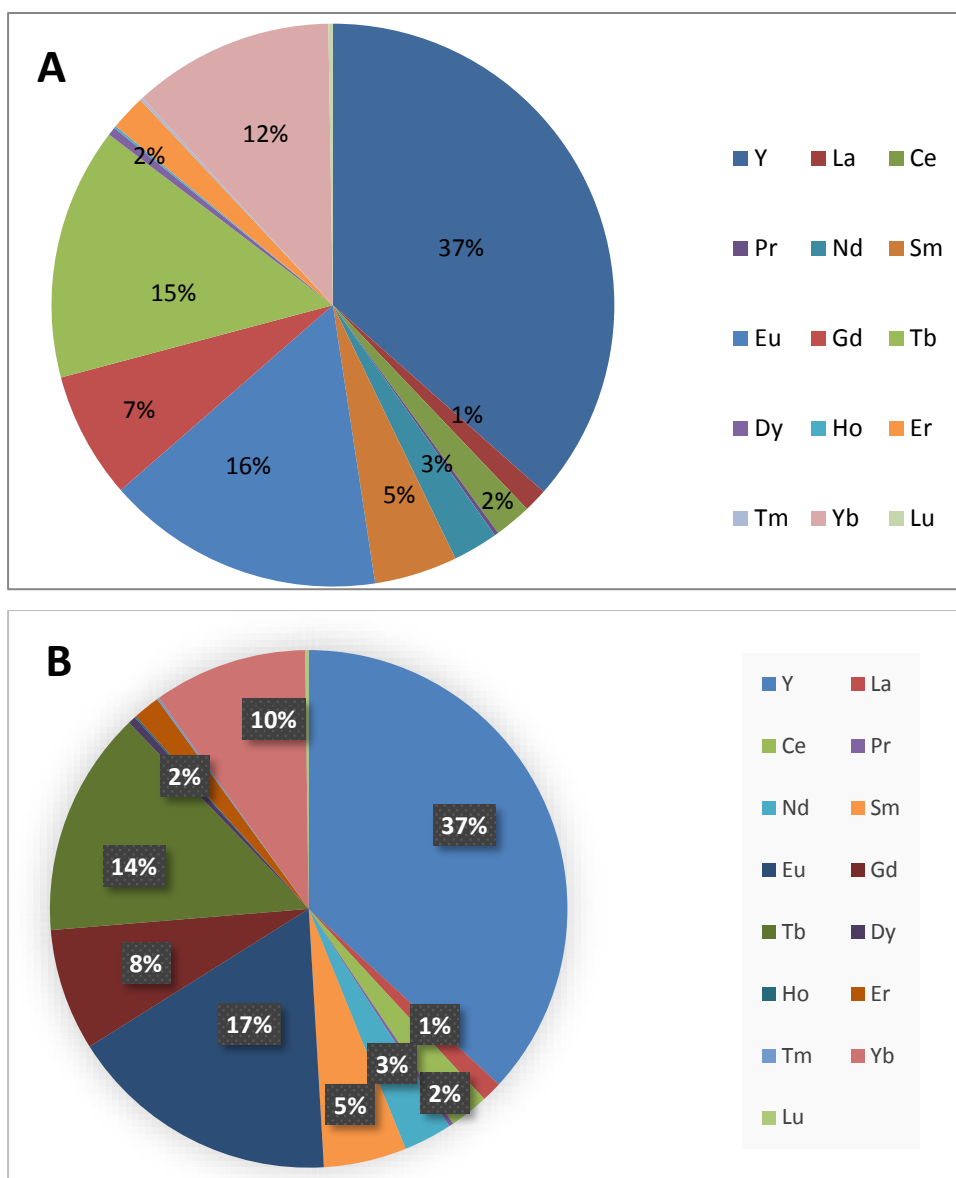


Figure 51. Distribution (%) of REEs in the leaching solution #1 (A) and in the concentrate (B) obtained after desorption of metals from SiO₂-PdCA.

Recovery of REEs on SiO₂-PdCA from leaching solution #2

In order to prove the robustness of the proposed method of adsorptive recovery of REEs on SiO₂-PdCA, the adsorbent has been used in DSPE of the metals from the leaching solution #2, having different composition (Table 18). From the comparison of the data presented in Table 17 and Table 18, it can be seen that salinity of the leaching solution #2 is much higher (17 g L⁻¹) than for the solution #1 with essentially higher (7 times) content of REEs (0.14%), Figure 52a. Nevertheless, treatment of leaching solution with SiO₂-PdCA in DSPE mode allows selectively extracts all REE with enrichment coefficient of 1350. After eluting of the adsorbed metal from SiO₂-PdCA, the solution consists of 32% of REEs, Figure 52b.

In contrast to leaching solution #1, solution #2 contains only two REEs: Y (60%) and Eu (36%). This distribution of REEs does not change in the eluting solution, which has about 64% of Y and 32% of Eu, Figure 53.

Thus, it can be seen, that SiO₂-PdCA selectively adsorbs of REEs from the lamp waste independently from the waste composition. Distribution of REES before and after DSPE on SiO₂-PdCA essentially does not change.

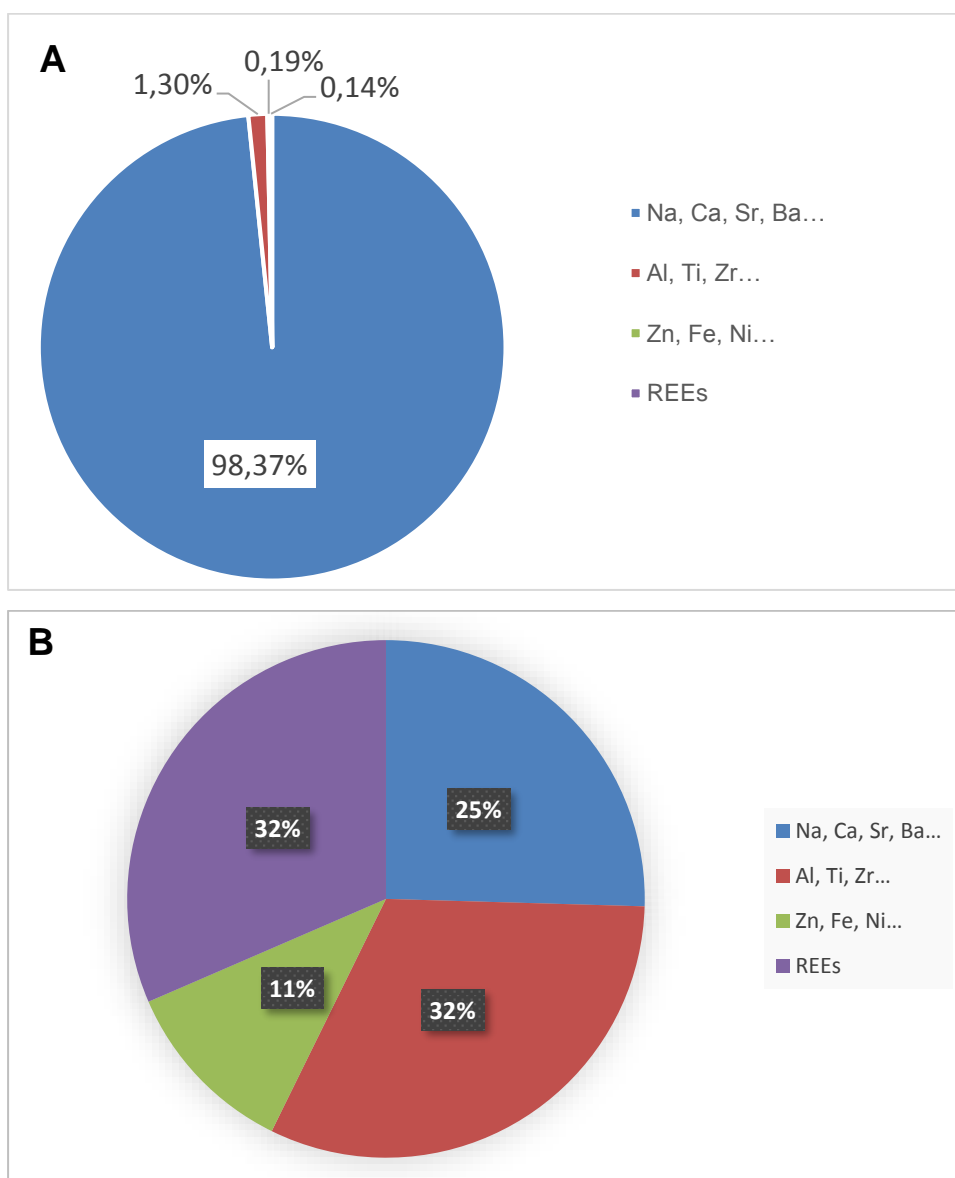


Figure 52. Composition of leaching solution #2 (A) and the concentrate (B) obtained after desorption of metals from SiO₂-PdCA.

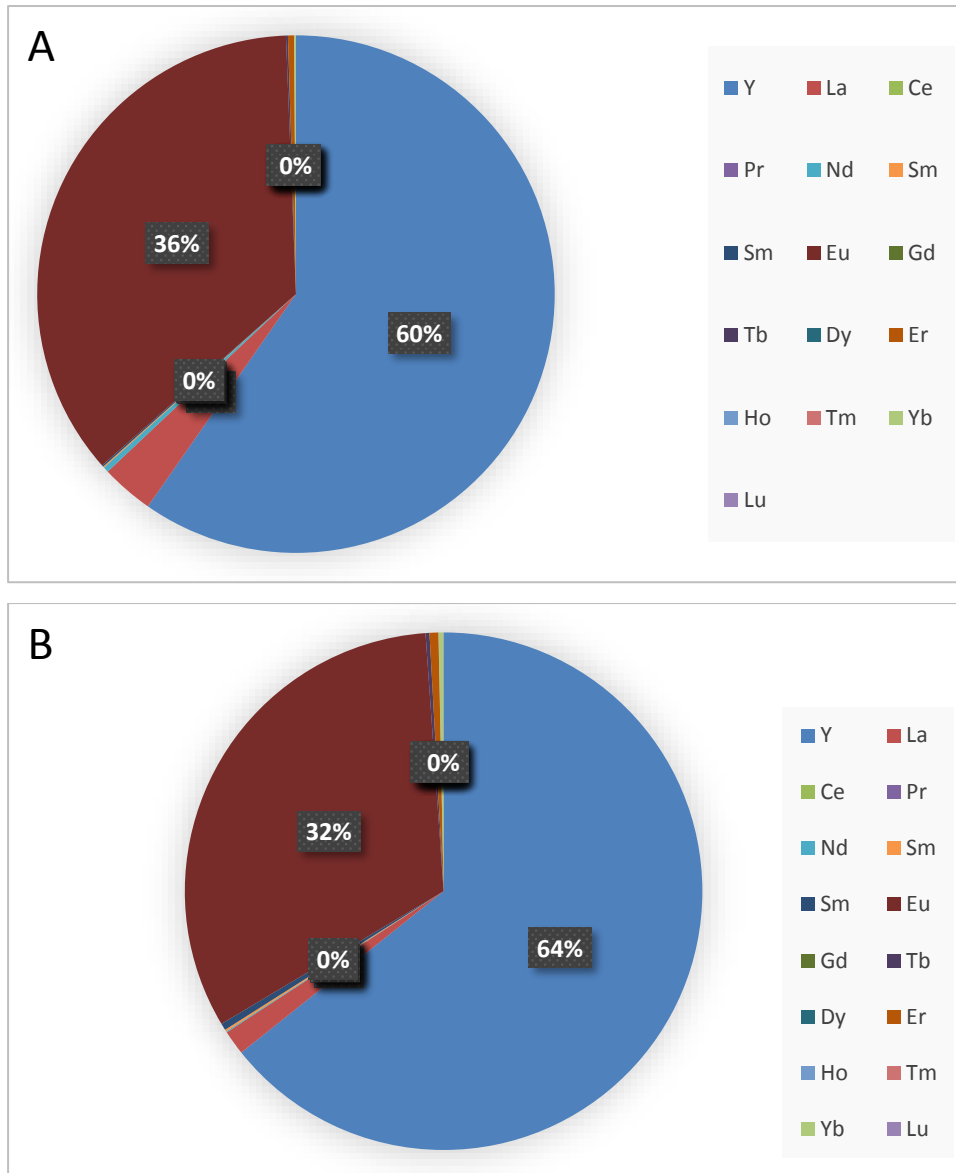


Figure 53. Distribution (%) of REEs in the leaching solution #2 (A) and in the concentrate (B) obtained after desorption of metals from SiO₂-PdCA.

Table 18. Composition of the leaching solution #2, supernatant and desorbing solutions received after DSPE with SiO₂-PdCA, and corresponding adsorption, desorption, and overall recovery degrees.

Metal ion	C _M in leaching solution, mg L ⁻¹	C _M in supernatant solution, mg L ⁻¹	Adsorption, R, %	C _M in desorption solution, mg L ⁻¹	Desorption E, %	Recovery R _{ov} , %
a) Macro-components						
Na	12940	10703	17	12.8	1	0
Ca	3650	3325	9	<0.005	0	0
Al	218	176	19	16.5	39	8
Mn	84.4	83.5	1	2.34	100	1
Zn	22.2	15.2	32	4.53	65	20
Ba	8.94	9.03	0	0.32	100	0
Sr	7.26	6.21	14	0.08	8	1
Fe	6.62	4.38	34	<0.005	0	0
Ti	1.89	1.86	2	<0.005	0	0
b) Micro-components						
V	0.45	0.30	33	0.12	80	27
Cr	0.80	0.13	84	0.42	62	52
Ni	0.41	0.18	56	0.16	70	39
Cu	0.05	<0.005	100	0.05	96	96
Ga	0.34	0.34	1	<0.005	100	1
Ag	0.15	0.17	0	<0.005	100	0
Hg	0.32	0.31	0	0.02	100	0
Pb	0.26	0.06	77	0.24	100	77
c) REEs						
Y	14.5	3.62	75	10.5	97	72
La	0.80	0.030	96	0.25	33	31
Ce	0.00	<0.001	0	<0.001	-	-
Pr	0.00	<0.001	0	<0.001	-	-
Nd	0.08	0.01	88	0.01	15	13
Sm	0.02	0.002	89	0.02	100	89
Eu	8.72	0.87	90	7.6	100	87
Gd	<0.001	<0.001	91	<0.001	-	-
Tb	0.03	0.010	66	0.04	100	66
Dy	<0.001	<0.001	0	<0.001	-	-
Er	0.09	<0.001	100	0.09	98	98
Ho	<0.001	<0.001	0	<0.001	100	0
Tm	<0.001	<0.001	100	0.002	100	100
Yb	0.03	<0.001	100	0.048	100	100
Lu	<0.001	<0.001	67	0.002	100	67

Adsorption properties of SiO₂-AdMPA are slightly different from SiO₂-PdCA, particularly in selectivity toward color metals. The SiO₂-AdMPA has less affinity to transitional metals that could allow better separation of REEs from such elements as Cu, Zn, Fe, Cr, Ni, and Pb. To verify this, recovery of REEs from leaching solution #2 was studied for SiO₂-AdMPA. The results presented in Table 19 indeed demonstrate lower adsorption of Cr (84% vs. 45%), Ni (56% vs 0%), Cu (100% vs. 0%) and Pb (77% vs. 27%) on SiO₂-AdMPA comparatively with SiO₂-PdCA (Table 18). But, at the same time, SiO₂-AdMPA has higher affinity towards Al (19% vs. 81%), Fe (34% vs. 48), Ti (2% vs. 40). High concentration the last ones in the

leaching solution decrease overall concentration of REEs to 13% while easily hydrolyzed ions, such as Al and Ti, consist of 66% of total metal content in desorbing solution (Figure 53). Also, incomplete desorption of Y (30%) change distribution of REEs, increasing content of Eu in the concentrate up to 52%, Figure 54. This effect can be used in the process where selective adsorption of f-elements is desirable.

Table 19. Composition of the leaching solution #2, supernatant and desorbing solutions received after DSPE with SiO₂-AdMPA, and corresponding adsorption, desorption, and overall recovery degrees.

Metal ion	C _M in leaching solution, mg L ⁻¹	C _M in supernatant solution, mg L ⁻¹	Adsorption, R, %	C _M in desorption solution, mg L ⁻¹	Desorption E, %	Recovery R _{ov} , %
a) Macro-components						
Ca	3646	3703	0.0	241	-	-
Al	217	40.6	81.4	73.9	42	34
Mn	84.4	84.6	0.0	8.04	-	-
Zn	22.2	12.9	41.9	11.8	100	42
Ba	8.94	8.8	1.6	1.53	100	2
Sr	7.26	7.34	0.0	2.11	-	-
Fe	6.62	3.42	48.3	1.94	61	29
Ti	1.89	1.13	40.2	0.15	20	8
b) Micro-components						
V	0.45	0.45	0.0	0.01	-	-
Cr	0.80	0.44	45.1	0.42	100	45
Ni	0.41	0.41	0.0	0.37	-	-
Cu	0.05	0.05	0.0	0.13	-	-
Ga	0.34	0.47	0.0	0.05	-	-
Ag	0.15	0.12	20.0	0	100	20
Hg	0.32	0.37	0.0	0	-	-
Pb	0.26	0.19	26.9	0.011	16	4
c) REEs						
Y	14.50	1.03	92.9	4.08	30	28
La	0.80	0.07	91.2	0.6	83	75
Ce	<0.001	<0.001	0.0	<0.001	-	-
Pr	<0.001	<0.001	0.0	<0.001	-	-
Nd	0.08	<0.001	100.0	0.06	72	72
Sm	0.02	0.002	89.0	0.05	100	89
Sm	0.02	<0.001	0.0	<0.001	-	-
Eu	8.72	0.53	94	7.4	100	94
Gd	0.29	0.041	85.8	0.37	150	128
Tb	0.03	0.01	66.2	0.03	153	101
Dy	<0.001	<0.001	0.0	<0.001	-	-
Er	0.09	0.01	89.1	0.08	98	87
Ho	<0.001	<0.001	0.0	<0.001	-	-
Tm	<0.001	0.001	0.0	<0.001	-	-
Yb	0.03	0.007	73.1	0.02	105	77

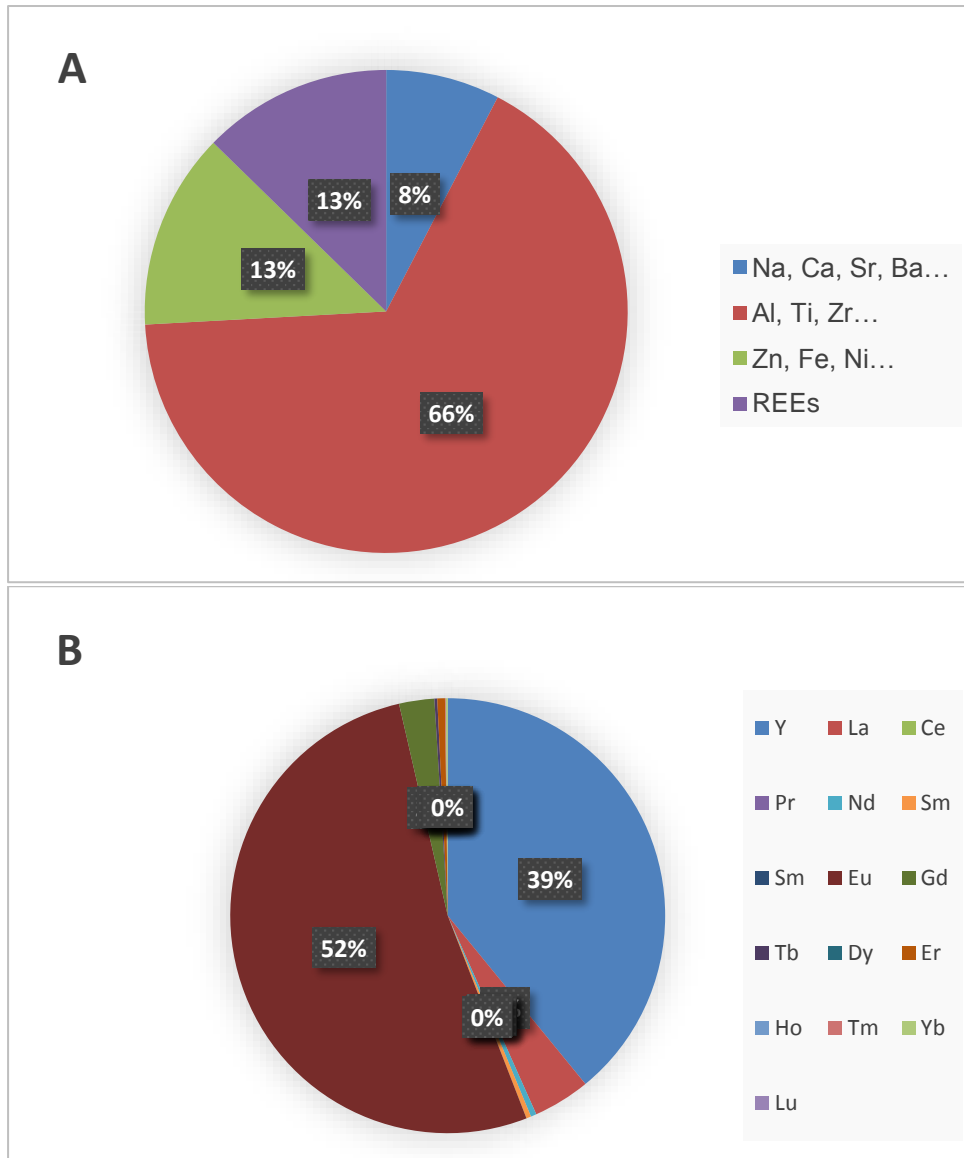


Figure 54. Distribution (%) of REEs in the leaching solution #2 (A) and in the concentrate (B) obtained after desorption of metals from SiO₂-AdMPA.

5 Conclusion

In agreement with the objectives of the thesis, three organo-silica adsorbents being covalently immobilized by derivatives of aminodiphosphonic ($\text{SiO}_2\text{-AdMPA}$), hydroxamic ($\text{SiO}_2\text{-BPHA}$) and pyridinecarboxylic ($\text{SiO}_2\text{-PdCA}$) acids have been successfully obtained. The materials were characterized by SEM, FTIR, high-resolution XPS, solid-state NMR. Porous characteristics of the silica support were determined from BET measurements. Functional analysis of immobilized organic fragments together with quantitative chemical analysis of the organo-silicas, such as pH- and conductometric titrations, elemental and thermogravimetric analysis allowed to determine concentration of binding sites on silica support as 0.21 – 0.36 mmol/g. It was demonstrated that the obtained materials adsorb metal ions due to formation of metal complex with immobilized ligands.

Adsorption properties of $\text{SiO}_2\text{-AdMPA}$, $\text{SiO}_2\text{-BPHA}$ and $\text{SiO}_2\text{-PdCA}$ towards REEs ions were studied in model (single-element) and real (multielement) solutions. It was demonstrated that pseudo-2nd-order kinetic model, which is frequently associated with the mechanism of chemical sorption, give better fit for the adsorption data for the adsorbents. The adsorption isotherms fit Langmuir model, which indicates high affinity of the sorbent to the metal ions due to formation of stable complexes immobilized ligands.

Metal complexation mechanism of metal adsorption determines strong correlation between recovery of metals and pH of adsorption media. It was demonstrated that SiO_2 and $\text{SiO}_2\text{-NH}_2$ have very low affinity towards REEs with less than 30% recovery from solution with $\text{pH} < 5$. Contrary $\text{SiO}_2\text{-PdCA}$ and $\text{SiO}_2\text{-AdMPA}$ quantitatively remove all REEs from water solution with $\text{pH} > 2$ and $\text{SiO}_2\text{-BPHA}$ from water solution with $\text{pH} > 4.5$. Therefore, the first two adsorbents are suitable for removing of REEs from acidic waters.

It was demonstrated that distribution coefficient of REEs on $\text{SiO}_2\text{-BPHA}$ is essentially increased (up to 80 times) with atomic number of REE, that allows REE separation. For other adsorbents equally high (9000-12000) for all REE allowing selective group pre-concentration of all the target metals.

Because of high affinity of REEs to $\text{SiO}_2\text{-PdCA}$ and $\text{SiO}_2\text{-AdMPA}$ their desorption is incomplete and difficult. The condition of the REEs desorption was

exhaustively studied using strong mineral acids and common chelating ligands. For both adsorbents application of 0.01 mol L⁻¹ water solution of EDTA with pH=8.0 as well as 2 mol L⁻¹ HNO₃ allow quantitative desorption of REEs to solution. EDTA solution is more suitable for desorption of heavy lanthanides, while HNO₃ solution is better to use for extraction of light elements. In optimal conditions, both adsorbents remain their adsorption properties in full after five adsorption/desorption cycles and allow complete (80-100%) recovery of all REEs from multicomponent solutions.

The adsorbents were used for separation of REEs from complex multielement solution. The results indicate that up to 200-fold excess of Fe³⁺ and Cu²⁺ ions for SiO₂-PdCA and 400-fold for SiO₂-AdMPA do not cause significant interference to adsorption of REEs. Interference effect of 22 metal ions on REEs recovery is insignificant up to 200-fold excess for both adsorbents. Recovery of REEs on SiO₂-BPHA is more sensible to interferences ions. It was demonstrated that up to 200-fold excess of each ion Na⁺, K⁺, Ca²⁺, Mg²⁺ do not cause significant interference to adsorption of REEs.

SiO₂-PdCA and SiO₂-AdMPA were applied for REE recovery from the phosphors of loose fluorescent lamps. It was demonstrated that application of SiO₂-PdCA allows essentially improve sustainability of the REEs recovery process. Firstly, total salinity of the concentrate after metal desorption from SiO₂-PdCA is about 1000 times lower than in the leaching solution (6.1 mg L⁻¹ vs. 17 g L⁻¹). Secondly, compositions of leaching and desorbing solutions drastically differed. The leaching solution for more than 99% consists of unwanted metal ions (mainly Na and Ca) and has only 0.02-0.14 % of REEs, while the solution obtained after eluting of metals from SiO₂-PdCA consist of more than 15-30% of REEs. Application of the adsorbent does not essentially change internal distribution of REEs indicating recovering of whole sets of REEs. SiO₂-AdMPA demonstrates less affinity to transitional metals than SiO₂-PdCA but higher affinity towards Al (19% vs. 81%), Fe (34% vs. 48%) and Ti (2% vs. 40%).

6 Perspectives

As it has been proved during the investigation of the present work, obtained silica-based adsorbents are very promising for efficient and selective extraction and separation of REEs from complex multielement matrixes. There are some possibilities of applications of the proposed materials were raised that can be suggested as a continuation of this study:

- As it was shown, SiO_2 -PdCA uptakes Eu and Tb ions from acidic solution giving strong red (for Eu) and green (for Tb) luminescent of the solids, which is very common of REE complexed with 2,6-pyridinedicarboxylic acid derivatives. Silica gel with immobilized fragments of hydroxamic acid (SiO_2 -BPHA) in the presence of Fe(III) ions in solution, became red, which proofs formation of Fe(III) complexes with derivatives of hydroxamic acid. These properties can be used as luminescent probes for monitoring of REE ions in water samples and for fast analysis of Fe(III) ions content in drinking and industrial water. Studies on the development of sensitive sensors based on silica-based adsorbents can be conducted.
- Adsorbent preparation procedure could be optimized in order to increase adsorption capacity of the adsorbents. It can be achieved by increasing the surface area of the support, using mesoporous material with a hierarchical structure or hybrid organo-mineral carriers.
- Further studies of REEs recovery from real industrial leachates of REEs containing waste products can be carried out.

7 References

AIROLDI, C.; ALCANTARA, E. F. C. Chemisorption of Divalent-Cations on N-(2-Pyridyl)Acetamide Immobilized on Silica-Gel - a Thermodynamic Study. **Journal of Chemical Thermodynamics**, v. 27, n. 6, p. 623–632, 1995.

ALI, S. H. Social and environmental impact of the rare earth industries. **Resources**, v. 3, n. 1, p. 123–134, 2014.

ARTIUSHENKO, O.; PEREIRA ÁVILA, E.; NAZARKOVSKY, M.; ZAITSEV, V. Reusable Hydroxamate Immobilized Silica Adsorbent for Dispersive Solid Phase Extraction and Separation of Rare Earth Metal Ions. **Separation and Purification Technology**, p. 115934, 2019.

ARTIUSHENKO, O.; ZAITSEV, V.; SANDOVAL, W.; PIERRE, T. D. SAINT. Recovery of Lanthanide Ions on Silica Adsorbent with Covalently Immobilized Derivative of 2,6-Pyridinedicarboxylic acid. **Methods and objects of chemical analysis**, v. 13, n. 4, p. 192–199, 2018.

ASHOUR, R. M.; ABDEL-MAGIED, A. F.; ABDEL-KHALEK, A. A.; HELALY, O. S.; ALI, M. M. Preparation and characterization of magnetic iron oxide nanoparticles functionalized by L-cysteine: Adsorption and desorption behavior for rare earth metal ions. **Journal of Environmental Chemical Engineering**, v. 4, n. 3, p. 3114–3121, 2016.

ASHOUR, R. M.; EL-SAYED, R.; ABDEL-MAGIED, A. F.; ABDEL-KHALEK, A. A.; ALI, M. M.; FORSBERG, K.; UHEIDA, A.; MUHAMMED, M.; DUTTA, J. Selective separation of rare earth ions from aqueous solution using functionalized magnetite nanoparticles: kinetic and thermodynamic studies. **Chemical Engineering Journal**, v. 327, p. 286–296, 2017.

ASHOUR, R. M.; SAMOUHOS, M.; POLIDO LEGARIA, E.; SVÄRD, M.; HÖGBLOM, J.; FORSBERG, K.; PALMLÖF, M.; KESSLER, V. G.; SEISENBAEVA, G. A.; RASMUSON, Å. C. DTPA-Functionalized Silica Nano- and Microparticles for Adsorption and Chromatographic Separation of Rare Earth Elements. **ACS Sustainable Chemistry and Engineering**, v. 6, n. 5, p. 6889–6900, 2018.

BABA, K.; HIROSHIGE, Y.; NEMOTO, T. Rare-earth magnet recycling. **Hitachi Review**, v. 62, n. 8, p. 452–455, 2013.

BAI, R.; YANG, F.; ZHANG, Y.; ZHAO, Z.; LIAO, Q.; CHEN, P.; ZHAO, P.; GUO, W.; CAI, C. Preparation of elastic diglycolamic-acid modified chitosan sponges and their application to recycling of rare-earth from waste phosphor powder. **Carbohydrate Polymers**, v. 190, n. November 2017, p. 255–261, jun. 2018.

BARJA, B. C.; BARI, S. E.; MARCHI, M. C.; IGLESIAS, F. L.; BERNARDI, M. Luminescent Eu(III) hybrid sensors for in situ copper detection. **Sensors and Actuators, B: Chemical**, v. 158, n. 1, p. 214–222, 2011.

BERNAL, J. P.; SAN MIGUEL, E. R. DE; AGUILAR, J. C.; SALAZAR, G.; GYVES, J. DE. Adsorption of metallic cations on silica gel-immobilized 8-hydroxyquinoline. **Separation Science and Technology**, v. 35, n. 10, p. 1661–1679, 2000.

BINNEMANS, K.; JONES, P. T. Rare Earths and the Balance Problem. **Journal of Sustainable Metallurgy**, v. 1, n. 1, p. 29–38, 2015.

BINNEMANS, K.; JONES, P. T.; BLANPAIN, B.; GERVEN, T. VAN; YANG, Y.; WALTON, A.; BUCHERT, M. Recycling of rare earths: A critical review. **Journal of Cleaner Production**, v. 51, p. 1–22, jul. 2013.

BINNEMANS, K.; PONTIKES, Y.; JONES, P. T.; VAN, T.; BLANPAIN, B. Recovery of Rare Earths From Industrial Waste Residues: a Concise Review. **3rd International Slag Valorisation Symposium**, p. 191–205, 2013.

BUCHERT, M.; MANHART, A.; BLEHER, D.; PINGEL, D. Recycling critical raw materials from waste electronic equipment. **Freiburg Öko-Institut**, v. 49, p. 30–40, 2012.

CALLURA, J. C.; PERKINS, K. M.; NOACK, C. W.; WASHBURN, N. R.; DZOMBAK, D. A.; KARAMALIDIS, A. K. Selective adsorption of rare earth elements onto functionalized silica particles. **Green Chemistry**, v. 20, n. 7, p. 1515–1526, 2018.

ÇELİK, I.; KARA, D.; KARADAŞ, C.; FISHER, A.; HILL, S. J. A novel ligandless-dispersive liquid-liquid microextraction method for matrix elimination and the preconcentration of rare earth elements from natural waters. **Talanta**, v. 134, p. 476–481, 2015.

CHARALAMPIDES, G.; VATALIS, K. I.; APOSTOPLOS, B.; PLOUTARCHNIKOLAS, B. Rare Earth Elements: Industrial Applications and Economic Dependency of Europe. **Procedia Economics and Finance**, v. 24, p. 126–135, 2015.

CHEN, L.; CHU, C. I.; LIU, R. S. Improvement of emission efficiency and color rendering of high-power LED by controlling size of phosphor particles and utilization of different phosphors. **Microelectronics Reliability**, v. 52, n. 5, p. 900–904, 2012.

CHEN, S.; CHENG, X.; HE, Y.; ZHU, S.; LU, D. Determination of the rare earth elements La, Eu, and Yb using solidified floating organic drop microextraction and electrothermal vaporization ICP-MS. **Microchimica Acta**, v. 180, n. 15–16, p. 1479–1486, 2013.

CHEN, Z. Global rare earth resources and scenarios of future rare earth industry. **Journal of Rare Earths**, v. 29, n. 1, p. 1–6, 2011.

CHO, J.; CHUNG, K. W.; CHOI, M. S.; KIM, H. J. Analysis of rare earth elements in seawater by inductively coupled plasma mass spectrometry after pre-concentration using TSK™-HD-MW-CNTs (highly dispersive multi-walled carbon nanotubes). **Talanta**, v. 99, p. 369–374, 2012.

COEY, J. M. D. Permanent magnets: Plugging the gap. **Scripta Materialia**, v. 67, n. 6, p. 524–529, 2012.

DAVE, S. R.; KAUR, H.; MENON, S. K. Selective solid-phase extraction of rare earth elements by the chemically modified Amberlite XAD-4 resin with azacrown ether. **Reactive and Functional Polymers**, v. 70, n. 9, p. 692–698, set. 2010.

DOLAK, I.; KEÇILI, R.; HÜR, D.; ERSÖZ, A.; SAY, R. Ion-imprinted polymers for selective recognition of neodymium(III) in environmental samples. **Industrial and Engineering Chemistry Research**, v. 54, n. 19, p. 5328–5335, 2015.

DUPONT, D.; BRULLOT, W.; BLOEMEN, M.; VERBIEST, T.; BINNEMANS, K. Selective Uptake of Rare Earths from Aqueous Solutions by EDTA-Functionalized Magnetic and Nonmagnetic Nanoparticles. **ACS Applied Materials & Interfaces**, v. 6, n. 7, p. 4980–4988, 9 abr. 2014.

DUTTA, T.; KIM, K.-H.; UCHIMIYA, M.; KWON, E. E.; JEON, B.-H.; DEEP, A.; YUN, S.-T. Global demand for rare earth resources and strategies for green

mining. **Environmental Research**, v. 150, p. 182–190, out. 2016.

EKAMBARAM, S.; PATIL, K. C. Synthesis and properties of rare earth doped lamp phosphors. **Bulletin of Materials Science**, v. 18, n. 7, p. 921–930, 1995.

EL-TAHER, A. Rare-earth elements in Egyptian granite by instrumental neutron activation analysis. **Applied Radiation and Isotopes**, v. 65, n. 4, p. 458–464, 2007.

_____. Elemental analysis of granite by instrumental neutron activation analysis (INAA) and X-ray fluorescence analysis (XRF). **Applied Radiation and Isotopes**, v. 70, n. 1, p. 350–354, jan. 2012.

ERDEM, A.; SHAHWAN, T.; ÇAĞIR, A.; EROĞLU, A. E. Synthesis of aminopropyl triethoxysilane-functionalized silica and its application in speciation studies of vanadium(IV) and vanadium(V). **Chemical Engineering Journal**, v. 174, n. 1, p. 76–85, 2011.

ESSER, B. K.; VOLPE, A.; KENNEALLY, J. M.; SMITH, D. K. Preconcentration and Purification of Rare Earth Elements in Natural Waters Using Silica-Immobilized 8-Hydroxyquinoline and a Supported Organophosphorus Extractant. **Analytical Chemistry**, v. 66, n. 10, p. 1736–1742, 1994.

ETTEHADI, J.; SID, H.; SHAKERI, A.; KHANCHI, A. Synthesis and characterization of Silica/polyvinyl imidazole/H₂PO₄-core-shell nanoparticles as recyclable adsorbent for efficient scavenging of Sm(III) and Dy(III) from water. **Journal of Colloid and Interface Science**, v. 505, p. 745–755, 2017.

EUROPEAN COMMISSION. Report lists 14 critical mineral raw materials. **MEMO/10/263**, n. June, 2010.

FALCONNET, P. The economics of rare earths. **Journal of The Less-Common Metals**, v. 111, n. 1–2, p. 9–15, 1985.

FAZAEI, Y.; GHOLAMREZA SHAHHOSSEINI, G.; SAMIRA SHAHBAZI, S.; FEIZI, S. An Investigation on the Pharmacological Profile of Titanium (IV) and Aluminum (III) 8-Hydroxyquinoline Derivatives Grafted on MCM-41 Mesoporous Silica. **International Journal of Basic Science in Medicine**, v. 3, n. 3, p. 120–126, 2019.

FIFAREK, B. J.; VELOSO, F. M.; DAVIDSON, C. I. Offshoring technology innovation: A case study of rare-earth technology. **Journal of Operations Management**, v. 26, n. 2, p. 222–238, 2008.

FISHER, A.; KARA, D. Determination of rare earth elements in natural water samples – A review of sample separation, preconcentration and direct methodologies. **Analytica Chimica Acta**, v. 935, p. 1–29, 2016.

FLOREK, J.; CHALIFOUR, F.; BILODEAU, F.; LARIVIÈRE, D.; KLEITZ, F. Nanostructured hybrid materials for the selective recovery and enrichment of rare earth elements. **Advanced Functional Materials**, v. 24, n. 18, p. 2668–2676, 2014.

FLOREK, J.; MUSHTAQ, A.; LARIVIÈRE, D.; CANTIN, G.; FONTAINE, F. G.; KLEITZ, F. Selective recovery of rare earth elements using chelating ligands grafted on mesoporous surfaces. **RSC Advances**, v. 5, n. 126, p. 103782–103789, 2015.

G.B. HAXEL, J.B. HEDRICK, G. J. O. Rare Earth Elements — Critical Resources for High Technology. **Climate Change 2013 - The Physical Science Basis**, p. 1–30, 2010.

GAMBOGI, J. RARE EARTHS [ADVANCE RELEASE]. **U.S. Geological Survey Minerals Yearbook-2014**, 2016.

GÁSQUEZ, J. A.; DELIMA, E.; OLSINA, R. A.; MARTINEZ, L. D.; LA GUARDIA, M. DE. A fast method for apatite selective leaching from granitic rocks followed through rare earth elements and phosphorus determination by inductively coupled plasma optical emission spectrometry. **Talanta**, v. 67, n. 4, p. 824–828, 2005.

GOONAN, T. G. Rare Earth Elements — End Use and Recyclability, U.S. Geological Survey. **Scientific Investigations Report 2011-5094**, p. 1–15, 2011.

GUTFLEISCH, O.; BOLLERO, A.; HANDSTEIN, A.; HINZ, D.; KIRCHNER, A.; YAN, A.; MÜLLER, K. H.; SCHULTZ, L. Nanocrystalline high performance permanent magnets. **Journal of Magnetism and Magnetic Materials**, v. 242–245, n. PART II, p. 1277–1283, 2002.

HAO, H.; LU, H.; AO, G.; SONG, Y.; WANG, Y.; ZHANG, X. Tunable emission color of $Gd_2(MoO_4)_3:Yb^{3+}$, Ho^{3+} , Tm^{3+} phosphors via different excitation condition. **Dyes and Pigments**, v. 148, p. 298–305, 2018.

HE, G.; YAN, H. Optimal spectra of the phosphor-coated white LEDs with excellent color rendering property and high luminous efficacy of radiation. **Optics Express**, v. 19, n. 3, p. 2519, 2011.

HENNEBRÜDER, K.; WENNRICH, R.; MATTUSCH, J.; STÄRK, H. J.; ENGEWALD, W. Determination of gadolinium in river water by SPE preconcentration and ICP-MS. **Talanta**, v. 63, n. 2, p. 309–316, 2004.

HOOGERSTRAETE, T. VANDER; ONGHENA, B.; BINNEMANS, K. Homogeneous liquid-liquid extraction of metal ions with a functionalized ionic liquid. **Journal of Physical Chemistry Letters**, v. 4, n. 10, p. 1659–1663, 2013.

HOOGERSTRAETE, T. VANDER; ONGHENA, B.; BINNEMANS, K. Homogeneous liquid-liquid extraction of rare earths with the betaine-betainium bis(trifluoromethylsulfonyl)imide ionic liquid system. **International Journal of Molecular Sciences**, v. 14, n. 11, p. 21353–21377, 2013.

HOOGERSTRAETE, T. VANDER; WELLENS, S.; VERACHTERT, K.; BINNEMANS, K. Removal of transition metals from rare earths by solvent extraction with an undiluted phosphonium ionic liquid: Separations relevant to rare-earth magnet recycling. **Green Chemistry**, v. 15, n. 4, p. 919–927, 2013.

HU, Y.; DROUIN, E.; LARIVIÈRE, D.; KLEITZ, F.; FONTAINE, F.-G. Highly Efficient and Selective Recovery of Rare Earth Elements Using Mesoporous Silica Functionalized by Preorganized Chelating Ligands. **ACS Applied Materials & Interfaces**, v. 9, n. 44, p. 38584–38593, 8 nov. 2017.

HUMPHRIES, M. Rare earth elements: The global supply chain. *In: Critical Materials Strategy for Clean Energy Technologies*. [s.l.: s.n.]. p. 143–158.

İÇHEDEF, Ç.; ŞİŞMANOĞLU, T.; TEKSÖZ, S. Hydrolytic Behavior of La^{3+} and Sm^{3+} at Various Temperatures. **Journal of Solution Chemistry**, v. 47, n. 2, p. 220–230, 2018.

IFTEKHAR, S.; SRIVASTAVA, V.; CASAS, A.; SILLANPÄÄ, M. Synthesis of novel GA-g-PAM/SiO₂ nanocomposite for the recovery of rare earth elements (REE) ions from aqueous solution. **Journal of Cleaner Production**, v. 170, p. 251–259, 2018.

IFTEKHAR, S.; SRIVASTAVA, V.; SILLANPÄÄ, M. Enrichment of lanthanides in aqueous system by cellulose based silica nanocomposite. **Chemical Engineering Journal**, v. 320, p. 151–159, 2017a.

_____. Synthesis and application of LDH intercalated cellulose nanocomposite for separation of rare earth elements (REEs). **Chemical Engineering Journal**, v. 309, p. 130–139, 2017b.

IWASHITA, M.; SAITO, A.; ARAI, M.; FURUSHO, Y.; SHIMAMURA, T. Determination of rare earth elements in rainwater collected in suburban Tokyo. **Geochemical Journal**, v. 45, n. 3, p. 187–197, 2011.

IZATT, S. R.; MCKENZIE, J. S.; IZATT, N. E.; BRUENING, R. L.; KRAKOWIAK, K. E.; IZATT, R. M. Molecular Recognition Technology: A Green chemistry process for separation of individual Rare Earth Metals. **White Paper on Separation of Rare Earth Elements (American Chemical Society National Historic Chemical Landmarks)**, v. 2, n. 1, p. 1–12, 2016.

JEREZ, J.; ISAGUIRRE, A. C.; BAZÁN, C.; MARTINEZ, L. D.; CERUTTI, S. Determination of scandium in acid mine drainage by ICP-OES with flow injection on-line preconcentration using oxidized multiwalled carbon nanotubes. **Talanta**, v. 124, p. 89–94, 2014.

JEZOREK, J. R.; FREISER, H. Metal-Ion Chelation Chromatography on Silica-Immobilized 8-Hydroxyquinoline. **Analytical Chemistry**, v. 51, n. 3, p. 366–373, 1979.

JIA, D.; HUNTER, D. N. Long persistent light emitting diode. **Journal of Applied Physics**, v. 100, n. 11, 2006.

JIANG, Y.; SHIBAYAMA, A.; LIU, K.; FUJITA, T. A hydrometallurgical process for extraction of lanthanum, yttrium and gadolinium from spent optical glass. **Hydrometallurgy**, v. 76, n. 1–2, p. 1–9, 2005.

JORDENS, A.; CHENG, Y. P.; WATERS, K. E. A review of the beneficiation of rare earth element bearing minerals. **Minerals Engineering**, v. 41, p. 97–114, fev. 2013.

JOWITT, S. M.; WERNER, T. T.; WENG, Z.; MUDD, G. M. Recycling of the rare earth elements. **Current Opinion in Green and Sustainable Chemistry**, v. 13, p. 1–7, 2018.

KANAZAWA, Y.; KAMITANI, M. Rare earth minerals and resources in the world. **Journal of Alloys and Compounds**, v. 408–412, p. 1339–1343, 2006.

KANO, N.; PANG, M.; DENG, Y.; IMAIZUMI, H. Adsorption of Rare Earth Elements (REEs) onto Activated Carbon Modified with Potassium Permanganate (KMnO₄). **Journal of Applied Solution Chemistry and Modeling**, v. 6, p. 51–61, 2017.

KHOLIN, Y.; ZAITSEV, V. Quantitative physicochemical analysis of equilibria on chemically modified silica surfaces. **Pure and Applied Chemistry**, v. 80, n. 7, p. 1561–1592, jan. 2008.

KIM, D.; POWELL, L. E.; DELMAU, L. H.; PETERSON, E. S.; HERCHENROEDER, J.; BHAVE, R. R. Selective Extraction of Rare Earth Elements from Permanent Magnet Scraps with Membrane Solvent Extraction. **Environmental Science and Technology**, v. 49, n. 16, p. 9452–9459, 2015.

KINGDOM, U.; ROAD, S. P.; ZAITSEV, V. N. N.; VASILIK, L. S. S.; EVANS, J.; BROUGH, A. Synthesis and structure of the grafted layer on silicas chemically modified by aminophosphonic acids. **Russian Chemical Bulletin**, v. 48, n. 12, p. 2315–2320, dez. 1999.

KNEPPER, T. P. Synthetic chelating agents and compounds exhibiting complexing properties in the aquatic environment. **TrAC - Trends in Analytical Chemistry**, v. 22, n. 10, p. 708–724, 2003.

KOSTENKO, L. S.; S.A. AHMEDOV; V.N. ZAITSEV. Chemical analytical properties of silica gel modified with amino diphosphonic acid. **Methods and objects of chemical analysis**, n. li, p. 116–122, 2006.

KOTLYAR, S. S.; YANISHPOL'SKII, V. V.; TERTYKH, V. A. Properties of 8-

hydroxyquinoline immobilized on a silica surface. **Theoretical and Experimental Chemistry**, v. 25, n. 1, p. 97–101, 1989.

LAI, X.; HU, Y.; FU, Y.; WANG, L.; XIONG, J. Synthesis and Characterization of Lu(III) Ion Imprinted Polymer. **Journal of Inorganic and Organometallic Polymers and Materials**, v. 22, n. 1, p. 112–118, 2012.

LEE, B. B. M. Rare Earth and Radioactive Waste. **National Toxics Network**, n. SEPTEMBER 2011, p. 30, 2012.

LEE, S.; SEO, S. Y. Optimization of Yttrium Aluminum Garnet:Ce³⁺ Phosphors for White Light-Emitting Diodes by Combinatorial Chemistry Method. **Journal of The Electrochemical Society**, v. 149, n. 11, p. J85, 2002.

LEME, F. O.; LIMA, L. C.; PAPAI, R.; AKIBA, N.; BATISTA, B. L.; GAUBEUR, I. A novel vortex-assisted dispersive liquid-phase microextraction procedure for preconcentration of europium, gadolinium, lanthanum, neodymium, and ytterbium from water combined with ICP techniques. **Journal of Analytical Atomic Spectrometry**, v. 33, n. 11, p. 2000–2007, 2018.

LESKELÄ, M.; NIINISTÖ, L. Applications of rare earths in full-colour EL displays. **Materials Chemistry and Physics**, v. 31, n. 1–2, p. 7–11, 1992.

LI, C.; ZHUANG, Z.; HUANG, F.; WU, Z.; HONG, Y.; LIN, Z. Recycling rare earth elements from industrial wastewater with flowerlike nano-Mg(OH)₂. **ACS Applied Materials and Interfaces**, v. 5, n. 19, p. 9719–9725, 2013.

LI, F. K.; GONG, A. J.; QIU, L. N.; ZHANG, W. W.; LI, J. R.; LIU, Y.; LIU, Y. N.; YUAN, H. T. Simultaneous determination of trace rare-earth elements in simulated water samples using ICP-OES with TODGA extraction/back-extraction. **PLoS ONE**, v. 12, n. 9, p. 1–16, 2017.

LI, W.; WANG, C.; GAO, B.; WANG, Y.; JIN, X.; ZHANG, L.; SAKYI, P. A. Determination of multi-element concentrations at ultra-low levels in alternating magnetite and pyrite by HR-ICP-MS using matrix removal and preconcentration. **Microchemical Journal**, v. 127, p. 237–246, 2016.

LI, X.; SONG, N.; FENG, W.; JIA, Q. Cloud point extraction of rare earths and zinc using 1,10-phenanthroline and Triton X-114 coupled with microwave plasma torch-atomic emission spectrometry. **Analytical Methods**, v. 9, n. 36, p. 5333–5338, 2017.

LI, Y.; HU, B. Cloud point extraction with/without chelating agent on-line coupled with inductively coupled plasma optical emission spectrometry for the determination of trace rare earth elements in biological samples. **Journal of Hazardous Materials**, v. 174, n. 1–3, p. 534–540, 2010.

LI, Y.; YU, H.; ZHENG, S.; MIAO, Y.; YIN, S.; LI, P.; BIAN, Y. Direct quantification of rare earth elements concentrations in urine of workers manufacturing cerium, lanthanum oxide ultrafine and nanoparticles by a developed and validated ICP-MS. **International Journal of Environmental Research and Public Health**, v. 13, n. 3, 2016.

LIAN, Y.; ZHEN, W.; TAI, Z.; YANG, Y.; SONG, J.; LI, Z. Cloud point extraction and flame atomic absorption spectrometry analysis of palladium, platinum, and gold ions from industrial polluted soil. **Rare Metals**, v. 31, n. 5, p. 512–516, 2012.

LIANG, P.; LIU, Y.; GUO, L. Determination of trace rare earth elements by inductively coupled plasma atomic emission spectrometry after preconcentration with multiwalled carbon nanotubes. **Spectrochimica Acta - Part B Atomic Spectroscopy**, v. 60, n. 1, p. 125–129, 2005.

LIU, J.; YANG, X.; CHENG, X.; PENG, Y.; CHEN, H. Synthesis and application of

ion-imprinted polymer particles for solid-phase extraction and determination of trace scandium by ICP-MS in different matrices. **Analytical Methods**, v. 5, n. 7, p. 1811–1817, 2013.

LUCAS, J.; LUCAS, P.; MERCIER, T. LE; ROLLAT, A.; DAVENPORT, W. Rare Earths in Rechargeable Batteries. *In: Rare Earths*. [s.l: s.n.]. p. 167–180.

LÜHRMANN, M.; STELTER, N.; KETTRUP, A. Synthesis and properties of metal collecting phases with silica immobilized 8-Hydroxyquinoline. **Fresenius' Zeitschrift für Analytische Chemie**, v. 322, n. 1, p. 47–52, 1985.

LUO, X. XIAN; CAO, W. HE. Upconversion luminescence of holmium and ytterbium co-doped yttrium oxysulfide phosphor. **Materials Letters**, v. 61, n. 17, p. 3696–3700, 2007.

MACHACEK, E.; RICHTER, J. L.; HABIB, K.; KLOSSEK, P. Recycling of rare earths from fluorescent lamps: Value analysis of closing-the-loop under demand and supply uncertainties. **Resources, Conservation and Recycling**, v. 104, n. 2015, p. 76–93, 2015.

MINOWA, H.; TAKEDA, M.; EBIHARA, M. Sequential determination of ultra-trace highly siderophile elements and rare earth elements by radiochemical neutron activation analysis: Application to pallasite meteorites. **Journal of Radioanalytical and Nuclear Chemistry**, v. 272, n. 2, p. 321–325, maio 2007.

MOUSSA, M.; NDIAYE, M. M.; PINTA, T.; PICHON, V.; VERCOUTER, T.; DELAUNAY, N. Selective solid phase extraction of lanthanides from tap and river waters with ion imprinted polymers. **Analytica Chimica Acta**, v. 963, p. 44–52, 2017.

MÜLLER, T.; FRIEDRICH, B. Development of a recycling process for nickel-metal hydride batteries. **Journal of Power Sources**, v. 158, n. 2 SPEC. ISS., p. 1498–1509, 2006.

NEGREA, A.; GABOR, A.; DAVIDESCU, C. M.; CIOPEC, M.; NEGREA, P.; DUTEANU, N.; BARBULESCU, A. Rare Earth Elements Removal from Water Using Natural Polymers. **Scientific Reports**, v. 8, n. 1, p. 1–11, 2018.

NOACK, C. W.; PERKINS, K. M.; CALLURA, J. C.; WASHBURN, N. R.; DZOMBAK, D. A.; KARAMALIDIS, A. K. Effects of ligand chemistry and geometry on rare earth element partitioning from saline solutions to functionalized adsorbents. **ACS Sustainable Chemistry and Engineering**, v. 4, n. 11, p. 6115–6124, 2016.

OGATA, T.; NARITA, H.; TANAKA, M. Adsorption behavior of rare earth elements on silica gel modified with diglycol amic acid. **Hydrometallurgy**, v. 152, p. 178–182, 2015.

OHSHIMA, K.; WATANABE, H.; HARAGUCHI, K. Preconcentration of Trace Metal Ions by Complexation with Ethylenediaminetriacetate-Bonded Silica Gel. **Analytical Sciences**, v. 2, n. 2, p. 131–135, 1986.

OLIVER KAMM. b-PHENYLHYDROXYLAMINE. **Organic Syntheses**, v. 4, p. 57, 1925.

PATRA, S.; ROY, E.; MADHURI, R.; SHARMA, P. K. Removal and Recycling of Precious Rare Earth Element from Wastewater Samples Using Imprinted Magnetic Ordered Mesoporous Carbon. **ACS Sustainable Chemistry and Engineering**, v. 5, n. 8, p. 6910–6923, 2017.

PAVÓN, S.; FORTUNY, A.; COLL, M. T.; SASTRE, A. M. Rare earths separation from fluorescent lamp wastes using ionic liquids as extractant agents. **Waste Management**, v. 82, p. 241–248, 2018.

PAVÓN, S.; FORTUNY, A.; COLL, M. T.; SASTRE, A. M. Improved rare earth elements recovery from fluorescent lamp wastes applying supported liquid membranes to the leaching solutions. **Separation and Purification Technology**, v. 224, p. 332–339, out. 2019.

PEDREIRA, W. R.; SILVA QUEIROZ, C. A. DA; ABRÃO, A.; PIMENTEL, M. M. Quantification of trace amounts of rare earth elements in high purity gadolinium oxide by sector field inductively coupled plasma mass spectrometry (ICP-MS). **Journal of Alloys and Compounds**, v. 374, n. 1–2, p. 129–132, 2004.

POPOV, V.; KOPTYUG, A.; RADULOV, I.; MACCARI, F.; MULLER, G. Prospects of additive manufacturing of rare-earth and non-rare-earth permanent magnets. **Procedia Manufacturing**, v. 21, p. 100–108, 2018.

PYRZYNSKA, K.; KUBIAK, A.; WYSOCKA, I. Application of solid phase extraction procedures for rare earth elements determination in environmental samples. **Talanta**, v. 154, p. 15–22, 2016.

QUEFFÉLEC, C.; PETIT, M.; JANVIER, P.; KNIGHT, D. A.; BUJOLI, B. Surface Modification Using Phosphonic Acids and Esters. **Chemical Reviews**, v. 112, n. 7, p. 3777–3807, 2012.

RADHIKA, S.; NAGARAJU, V.; NAGAPHANI KUMAR, B.; KANTAM, M. L.; REDDY, B. R. Solid-liquid extraction of Gd(III) and separation possibilities of rare earths from phosphoric acid solutions using Tulsion CH-93 and Tulsion CH-90 resins. **Journal of Rare Earths**, v. 30, n. 12, p. 1270–1275, dez. 2012.

RAHMAN, M. L.; BISWAS, T. K.; SARKAR, S. M.; YUSOFF, M. M.; SARJADI, M. S.; ARSHAD, S. E.; MUSTA, B. Adsorption of rare earth metals from water using a kenaf cellulose-based poly(hydroxamic acid) ligand. **Journal of Molecular Liquids**, v. 243, p. 616–623, 2017.

RAHMI, D.; ZHU, Y.; FUJIMORI, E.; UMEMURA, T.; HARAGUCHI, H. Multielement determination of trace metals in seawater by ICP-MS with aid of down-sized chelating resin-packed minicolumn for preconcentration. **Talanta**, v. 72, n. 2, p. 600–606, 2007.

RAMASAMY, D. L.; KHAN, S.; REPO, E.; SILLANPÄÄ, M. Synthesis of mesoporous and microporous amine and non-amine functionalized silica gels for the application of rare earth elements (REE) recovery from the waste water- understanding the role of pH, temperature, calcination and mechanism in Light REE and Hea. **Chemical Engineering Journal**, v. 322, p. 56–65, ago. 2017.

RAMASAMY, D. L.; REPO, E.; SRIVASTAVA, V.; SILLANPÄÄ, M. Chemically immobilized and physically adsorbed PAN/acetylacetone modified mesoporous silica for the recovery of rare earth elements from the waste water- comparative and optimization study. **Water Research**, v. 114, n. 17, p. 264–276, 2017.

RAMASAMY, D. L.; WOJTUŚ, A.; REPO, E.; KALLIOLA, S.; SRIVASTAVA, V.; SILLANPÄÄ, M. Ligand immobilized novel hybrid adsorbents for rare earth elements (REE) re- moval from waste water: Assessing the feasibility of using APTES functional- ized silica in the hybridization process with chitosan Ligand immobilized novel hybrid adsorbents for. **Chemical Engineering Journal**, v. 330, n. August, p. 1370–1379, 2017.

REPO, E.; KURNIAWAN, T. A.; WARCHOL, J. K.; SILLANPÄÄ, M. E. T. Removal of Co(II) and Ni(II) ions from contaminated water using silica gel functionalized with EDTA and/or DTPA as chelating agents. **Journal of Hazardous Materials**, v. 171, n. 1–3, p. 1071–1080, 2009.

REPO, E.; KURNIAWAN, T. A.; WARCHOL, J. K.; SILLANPÄÄ, M. E. T. Removal of Co(II) and Ni(II) ions from contaminated water using silica gel functionalized with

EDTA and/or DTPA as chelating agents. **Journal of Hazardous Materials**, v. 171, n. 1–3, p. 1071–1080, 2009.

RIBEIRO, C.; RIBEIRO, A. R.; MAIA, A. S.; GONCALVES, V. M. F.; TIRITAN, M. E. New Trends in Sample Preparation Techniques for Environmental Analysis. **Critical Reviews In Analytical Chemistry**, v. 44, n. 2, p. 142–185, 2014.

ROBINSON, P.; TOWNSEND, A. T.; YU, Z.; MÜNKER, C. Determination of scandium, yttrium and rare earth elements in rocks by high resolution inductively coupled plasma-mass spectrometry. **Geostandards Newsletter**, v. 23, n. 1, p. 31–46, 1999.

RONDA, C. R.; JÜSTEL, T.; NIKOL, H. Rare earth phosphors: Fundamentals and applications. **Journal of Alloys and Compounds**, v. 275–277, p. 669–676, 1998.

ROUT, A.; BINNEMANS, K. Liquid-liquid extraction of europium(iii) and other trivalent rare-earth ions using a non-fluorinated functionalized ionic liquid. **Dalton Transactions**, v. 43, n. 4, p. 1862–1872, 2014.

RYABCHENKO, E. V.; YANOVSKAYA, E. S.; TERTYKH, V. A.; KICHKIRUK, O. Y. Complexation of transition metals with 8-hydroxyquinoline chemically immobilized on the surface of a silica gel-polyaniline composite. **Russian Journal of Inorganic Chemistry**, v. 58, n. 3, p. 361–366, 2013.

SADEGHI, O.; TAVASSOLI, N.; AMINI, M. M.; EBRAHIMZADEH, H.; DAEI, N. Pyridine-functionalized mesoporous silica as an adsorbent material for the determination of nickel and lead in vegetables grown in close proximity by electrothermal atomic adsorption spectroscopy. **Food Chemistry**, v. 127, n. 1, p. 364–368, 2011.

SAHA, D.; AKKOYUNLU, S. D.; THORPE, R.; HENSLEY, D. K.; CHEN, J. Adsorptive recovery of neodymium and dysprosium in phosphorous functionalized nanoporous carbon. **Journal of Environmental Chemical Engineering**, v. 5, n. 5, p. 4684–4692, 2017.

SANCHEZ-CASTILLO, M. A.; MADON, R. J.; DUMESIC, J. A. Role of rare earth cations in Y zeolite for hydrocarbon cracking. **Journal of Physical Chemistry B**, v. 109, n. 6, p. 2164–2175, 2005.

SERGO, V.; SCHMID, C.; MERIANI, S. Rare earths in ceramic materials technology. **Materials Chemistry and Physics**, v. 31, n. 1–2, p. 37–43, 1992.

SHIRAIISHI, Y.; NISHIMURA, G.; HIRAI, T.; KOMASAWA, I. Separation of Transition Metals Using Inorganic Adsorbents Modified with Chelating Ligands. **Industrial & Engineering Chemistry Research**, v. 41, n. 20, p. 5065–5070, 2002.

SHU, Q.; KHAYAMBASHI, A.; WANG, X.; WEI, Y. Studies on adsorption of rare earth elements from nitric acid solution with macroporous silica-based bis(2-ethylhexyl)phosphoric acid impregnated polymeric adsorbent. **Adsorption Science and Technology**, v. 36, n. 3–4, p. 1049–1065, 2018.

SLEBIODA, M.; WODECKI, Z.; KOLODZIEJCZYK, A. M.; NOWICKI, W. Chromatographic Separation of Some Transition Metal Ions on Chelating Ccolumn Bearing Acetylacetone Moiety. **Chemia Analityczna**, v. 39, n. 2, p. 149–152, 1994.

SONG, X.; CHANG, M.-H.; PECHT, M. Rare-Earth Elements in Lighting and Optical Applications and Their Recycling. **JOM**, v. 65, n. 10, p. 1276–1282, out. 2013.

SONG, X.; ZHANG, S.; LI, T. A novel method for PAHs in aqueous samples based on ultrasound-assisted solidified floating organic drop microextraction. **IOP Conference Series: Earth and Environmental Science**, v. 121, p. 022017, fev. 2018.

STURGEON, R. E.; BERMAN, S. S.; WILLIE, S.; DESAULNIERS, J. A. H.; RUSSELL, D. S. Preconcentration of trace metals from seawater using silica immobilized 8-hydroxyquinoline. **Marine Chemistry**, v. 12, n. 2–3, p. 219, 1983.

STURGEON, R. E.; BERMAN, S. S.; WILLIE, S. N.; DESAULNIERS, J. A. H. Preconcentration of Trace Elements from Seawater with Silica-Immobilized 8-Hydroxyquinoline. **Analytical Chemistry**, v. 53, n. 14, p. 2337–2340, 1981.

SU, S.; CHEN, B.; HE, M.; HU, B.; XIAO, Z. Determination of trace/ultra-trace rare earth elements in environmental samples by ICP-MS after magnetic solid phase extraction with Fe₃O₄@SiO₂@polyaniline-graphene oxide composite. **Talanta**, v. 119, p. 458–466, 2014.

SUN, X.; LUO, H.; MAHURIN, S. M.; LIU, R.; HOU, X.; DAI, S. Adsorption of rare earth ions using carbonized polydopamine nano carbon shells. **Journal of Rare Earths**, v. 34, n. 1, p. 77–82, 2016.

SUN, Y.; WANG, Q.; CHEN, C.; TAN, X.; WANG, X. Interaction between Eu(III) and graphene oxide nanosheets investigated by batch and extended X-ray absorption fine structure spectroscopy and by modeling techniques. **Environmental Science and Technology**, v. 46, n. 11, p. 6020–6027, 2012.

SUTRA, P.; BRUNEL, D.; LENTZ, P.; DAELLEN, G.; NAGY, B. Si and ¹³C MAS-NMR characterization of surface modification of micelle-templated silicas during the grafting of organic moieties and end-capping. **Colloids and Surfaces A: Physicochemical and Engineering Aspects**, v. 158, p. 21–27, 1999.

TAJABADI, F.; YAMINI, Y.; SOVIZI, M. R. Carbon-based magnetic nanocomposites in solid phase dispersion for the preconcentration of some lanthanides, followed by their quantitation via ICP-OES. **Microchimica Acta**, v. 180, n. 1–2, p. 65–73, 2013.

TAN, Q.; DENG, C.; LI, J. Enhanced recovery of rare earth elements from waste phosphors by mechanical activation. **Journal of Cleaner Production**, v. 142, p. 2187–2191, 2017.

TAN, Q.; LI, J.; ZENG, X. Rare Earth Elements Recovery from Waste Fluorescent Lamps: A Review. **Critical Reviews in Environmental Science and Technology**, v. 45, n. 7, p. 749–776, abr. 2015.

TANAKA, T.; KUZUHARA, M.; WATADA, M.; OSHITANI, M. Effect of rare earth oxide additives on the performance of NiMH batteries. **Journal of Alloys and Compounds**, v. 408–412, p. 323–326, 2006.

TANG, Z. L.; ZHANG, X. P. Effect of Rare Earth on 30CrMnSi Steel Investment Castings Cracking. **Advanced Materials Research**, v. 160–162, p. 692–697, 2010.

TONG, A.; AKAMA, Y.; TANAKA, S. Selective preconcentration of Au(III), Pt(IV) and Pd(II) on silica gel modified with γ -aminopropyltriethoxysilane. **Analytica Chimica Acta**, v. 230, n. C, p. 179–181, 1990.

TOPEL, S. D.; LEGARIA, E. P.; TISEANU, C.; ROCHA, J.; NEDELEC, J.-M.; KESSLER, V. G.; SEISENBAEVA, G. A. Hybrid silica nanoparticles for sequestration and luminescence detection of trivalent rare-earth ions (Dy³⁺ and Nd³⁺) in solution. **Journal of Nanoparticle Research**, v. 16, n. 12, p. 2783, 4 dez. 2014.

TSAKANIKI, L. V.; OCHSENKÜHN-PETROPOULOU, M. T.; MENDRINOS, L. N. Investigation of the separation of scandium and rare earth elements from red mud by use of reversed-phase HPLC. **Analytical and Bioanalytical Chemistry**, 2004.

TU, Z.; HU, Z.; CHANG, X.; ZHANG, L.; HE, Q.; SHI, J.; GAO, R. Silica gel modified

with 1-(2-aminoethyl)-3-phenylurea for selective solid-phase extraction and preconcentration of Sc(III) from environmental samples. **Talanta**, v. 80, n. 3, p. 1205–1209, 2010.

TUNSU, C. Hydrometallurgy in the recycling of spent NdFeB permanent magnets. *In: Waste Electrical and Electronic Equipment Recycling*. [s.l.] Elsevier, 2018. p. 175–211.

U.S. GEOLOGICAL SURVEY. Mineral Commodity Summaries 2018: U.S. Geological Survey. **U.S. Geological Survey**, 2018.

____. Mineral Commodity Summaries. **U.S. Geological Survey**, 2019.

VARBANOVA, E. K.; ANGELOV, P. A.; SIMITCHIEV, K. K.; KAYNAROVA, L. I.; STEFANOVA, V. M. Cloud Point Extraction of lanthanides with 3-ethylamino-but-2-enoic acid phenylamide from water samples prior to ICP-MS determination. **Bulgarian Chemical Communications**, v. 49, n. Special Issue G, p. 49–54, 2017.

VIORNERY, C.; CHEVOLOT, Y.; LÉONARD, D.; ARONSSON, B.-O.; PÉCHY, P.; MATHIEU, H. J.; DESCOUTS, P.; GRÄTZEL, M. Surface Modification of Titanium with Phosphonic Acid To Improve Bone Bonding: Characterization by XPS and ToF-SIMS. **Langmuir**, v. 18, n. 7, p. 2582–2589, abr. 2002.

VITO, I. E. DE; OLSINA, R. A.; MASI, A. N. Enrichment method for trace amounts of rare earth elements using chemofiltration and XRF determination. **Fresenius' Journal of Analytical Chemistry**, v. 368, n. 4, p. 392–396, 2000.

VLADIMIR N. ZAITSEV. Complexing silicas: preparation, structure of bonded layer, surface chemistry. **Folio**, n. May, p. 240, 1997.

VOOLAPALLI, R. K.; THOTA, C.; GOKAK, D. T.; CHOUDARY, N. V.; SIDDIQUI, M. A. Fluid Catalytic Cracking. *In: Petroleum Refining and Natural Gas Processing*. [s.l.: s.n.]. p. 127–158.

WANHALA, A. K.; DOUGHTY, B.; BRYANTSEV, V. S.; WU, L.; MAHURIN, S. M.; JANSONE-POPOVA, S.; CHESHIRE, M. C.; NAVROTSKY, A.; STACK, A. G. Adsorption mechanism of alkyl hydroxamic acid onto bastnäsite: Fundamental steps toward rational collector design for rare earth elements. **Journal of Colloid and Interface Science**, v. 553, p. 210–219, out. 2019.

WILLIE, S. N.; STURGEON, R. E. Determination of transition and rare earth elements in seawater by flow injection inductively coupled plasma time-of-flight mass spectrometry. **Spectrochimica Acta - Part B Atomic Spectroscopy**, v. 56, n. 9, p. 1707–1716, 2001.

WU, D.; SUN, Y.; WANG, Q. Adsorption of lanthanum (III) from aqueous solution using 2-ethylhexyl phosphonic acid mono-2-ethylhexyl ester-grafted magnetic silica nanocomposites. **Journal of Hazardous Materials**, v. 260, p. 409–419, set. 2013.

XUEJUAN, L.; ZHEFENG, F. Liquid–Liquid–Liquid Micro Extraction Combined with CE for the Determination of Rare Earth Elements in Water Samples. **Chromatographia**, v. 70, n. 3–4, p. 481–487, ago. 2009.

YAN, P.; HE, M.; CHEN, B.; HU, B. Fast preconcentration of trace rare earth elements from environmental samples by di(2-ethylhexyl)phosphoric acid grafted magnetic nanoparticles followed by inductively coupled plasma mass spectrometry detection. **Spectrochimica Acta - Part B Atomic Spectroscopy**, v. 136, p. 73–80, 2017.

YANG, R.-Z.; WANG, J.-H.; WANG, M.-L.; ZHANG, R.; LU, X.-Y.; LIU, W.-H. Dispersive solid-phase extraction cleanup combined with accelerated solvent extraction for the determination of carbamate pesticide residues in radix

glycyrrhizae samples by UPLC-MS-MS. **Journal of Chromatographic Science**, v. 49, n. 9, p. 702–708, 2011.

YANOVSKA, E. S.; GLUSHCHENKO, O. V.; KARMANOV, V. I.; KICHKIRUK, O. Y.; TERTYKH, V. A. Adsorption of Toxic Metal Ions onto Silica with Covalently Bound 8-Hydroxyquinoline. **Adsorption Science & Technology**, v. 24, n. 3, p. 229–238, 2006.

YENISOY-KARAKAŞ, S.; GAGA, E. O.; DOĞANGÜN, A.; TUNCEL, S. G. Determination of major and rare earth elements in bastnasite ores by ICP-AES. **Analytical Letters**, v. 37, n. 13, p. 2701–2709, 2004.

YEO, B. E.; CHO, Y. S.; HUH, Y. D. Synthesis and photoluminescence properties of a red-emitting phosphor, $K_2SiF_6:Mn^{4+}$, for use in three-band white LED applications. **Optical Materials**, v. 51, p. 50–55, 2016.

ZAITSEV, V. N.; KHOLIN, Y. V.; YU GORLOVA, E.; KHRISTENKO, I. V. Silica chemically modified with N-benzoyl-N-phenylhydroxylamine in chemisorption of hydrogen and metal ions. **Analytica Chimica Acta**, v. 379, n. 1–2, p. 11–21, 1999.

ZAITSEV, V. N.; KOSTENKO, L. S.; KOBYLINSKAYA, N. G. Acid–base properties of silica-based ion-exchanger having covalently bonded aminodi(methylphosphonic) acid. **Analytica Chimica Acta**, v. 565, n. 2, p. 157–162, abr. 2006.

ZAITSEV, V. N.; VASSILIK, L. S. A New Class of Silica-Bonded Ion Exchangers. *In: Fundamental and Applied Aspects of Chemically Modified Surfaces*. [s.l.: s.n.]. p. 361–368.

ZAR, J. H. Biostatistical Analysis, Fifth Edition. **Pearson**, 2009.

ZAWISZA, B.; PYTLAKOWSKA, K.; FEIST, B.; POLOWNIAK, M.; KITA, A.; SITKO, R. Determination of rare earth elements by spectroscopic techniques : a review. **J. Anal. At. Spectrom.**, p. 2373–2390, 2011a.

_____. Determination of rare earth elements by spectroscopic techniques: A review. **Journal of Analytical Atomic Spectrometry**, v. 26, n. 12, p. 2373–2390, 2011b.

ZEPF, V. Rare Earth Elements: What and Where They Are. *In: [s.l.: s.n.].* p. 11–39.

ZHANG, H.; MCDOWELL, ROCKLAN G.; MARTIN, L. R.; QIANG, Y. Selective Extraction of Heavy and Light Lanthanides from Aqueous Solution by Advanced Magnetic Nanosorbents. **ACS Applied Materials & Interfaces**, v. 8, n. 14, p. 9523–9531, 13 abr. 2016.

ZHANG, H.; MCDOWELL, ROCKLAN G.; MARTIN, L. R.; QIANG, Y. Selective Extraction of Heavy and Light Lanthanides from Aqueous Solution by Advanced Magnetic Nanosorbents. **ACS Applied Materials & Interfaces**, v. 8, n. 14, p. 9523–9531, 13 abr. 2016.

ZHANG, J.; CHENG, R.; TONG, S.; GU, X.; QUAN, X.; LIU, Y.; JIA, Q.; JIA, J. Microwave plasma torch-atomic emission spectrometry for the on-line determination of rare earth elements based on flow injection preconcentration by TiO₂-graphene composite. **Talanta**, v. 86, n. 1, p. 114–120, 2011.

ZHANG, L.; CHANG, X.; ZHAI, Y.; HE, Q.; HUANG, X.; HU, Z.; JIANG, N. Selective solid phase extraction of trace Sc(III) from environmental samples using silica gel modified with 4-(2-morinyldiazonyl)-N-(3-(trimethylsilyl)propyl)benzamide. **Analytica Chimica Acta**, v. 629, n. 1–2, p. 84–91, 2008.

ZHANG, LINA; CHANG, X.; HU, Z.; ZHANG, LIJUN; SHI, J.; GAO, R. Selective solid phase extraction and preconcentration of mercury(II) from environmental and biological samples using nanometer silica functionalized by 2,6-pyridine dicarboxylic acid. **Microchimica Acta**, v. 168, n. 1–2, p. 79–85, 2010.

ZHANG, Q.; HE, M.; CHEN, B.; HU, B. Preparation, characterization and application of *Saussurea tridactyla* Sch-Bip as green adsorbents for preconcentration of rare earth elements in environmental water samples. **Spectrochimica Acta - Part B Atomic Spectroscopy**, v. 121, p. 1–10, 2016.

ZHANG, X.; LIU, J.; YI, Y.; LIU, Y.; LI, X.; SU, Y.; LIN, P. Determination of rare earth impurities in high purity samarium oxide using inductively coupled plasma mass spectrometry after extraction chromatographic separation. **International Journal of Mass Spectrometry**, v. 260, n. 1, p. 57–66, 2007.

ZHANG, Z.; WU, C. Effect of fluid flow in the weld pool on the numerical simulation accuracy of the thermal field in hybrid welding. **Journal of Manufacturing Processes**, v. 20, p. 215–223, out. 2015.

ZHAO, F.; REPO, E.; MENG, Y.; WANG, X.; YIN, D.; SILLANPÄÄ, M. An EDTA- β -cyclodextrin material for the adsorption of rare earth elements and its application in preconcentration of rare earth elements in seawater. **Journal of Colloid and Interface Science**, v. 465, p. 215–224, 2016.

ZHAO, Z.; QIU, Z.; YANG, J.; LU, S.; CAO, L.; ZHANG, W.; XU, Y. Recovery of rare earth elements from spent fluid catalytic cracking catalysts using leaching and solvent extraction techniques. **Hydrometallurgy**, v. 167, p. 183–188, jan. 2017.

ZHU, Y.; ZHENG, Y.; WANG, A. A simple approach to fabricate granular adsorbent for adsorption of rare elements. **International Journal of Biological Macromolecules**, v. 72, p. 410–420, 2015.

ZHUANG, W.; HUANG, X.; ZHANG, S.; FANG, Y.; HU, Y.; HE, H. Rare earth phosphors for white LEDs. **Institute of Physics Conference Series**, v. 182, p. 167–168, 2004.

ZOLFONOUN, E.; YOUSEFI, S. R. Simultaneous determination of rare earth elements by ICP OES after on-line enrichment using multi-walled carbon nanotubes coated cellulose acetate membrane. **Journal of the Brazilian Chemical Society**, v. 27, n. 12, p. 2348–2353, 2016.

ZOUGAGH, M.; CANO PAVÓN, J. M.; GARCIA DE TORRES, A. Chelating sorbents based on silica gel and their application in atomic spectrometry. **Analytical and Bioanalytical Chemistry**, v. 381, n. 6, p. 1103–1113, 2005.